TE/TM BASED INTEGRATED OPTICAL SENSING PLATFORMS

ISBN - 90-36515238

TE/TM BASED INTEGRATED OPTICAL SENSING PLATFORMS

PROEFSCHRIFT

ter verkrijging van
de graad van doctor aan de Universiteit Twente,
op gezag van de rector magnificus,
prof. dr. F.A. van Vught,
volgens besluit van het College voor Promoties
in het openbaar te verdedigen
op vrijdag 8 december 2000 te 16.45 uur.

door

Tonnis Meindert Koster

geboren op 4 oktober 1970
te Veendam

Dit proefschrift is goedgekeurd door:
de promotor: Prof. Dr. Th.J.A. Popma
de assistent promotor: Dr. P.V. Lambeck

Table of Contents

Chapter 1 : Introduction **1**
1.1 Once upon a time... 1
1.2 Integrated chemo-optical sensors 3
1.3 Evanescent field sensing 4
1.4 Matching of the sensing platform - transduction layer 6
1.5 Outline of this thesis 8

Chapter 2 : Passive polarisation converter in SiON technology **11**
2.1 Introduction 11
2.2 Structure and design 12
2.3 Fabrication 18
2.4 Experimental results 19
2.5 Discussion 23
2.6 Summary 25

Chapter 3 : Thermally tunable polarisation converter **27**
3.1 Introduction 27
3.2 Analysis 28
3.3 Design 31
3.4 Demonstrator device 37
3.5 Summary 38

Chapter 4 : Mode selective waveguide-detector couplers **40**
4.1 Introduction 40
4.2 Analysis and design 42
4.3 Fabrication 47
4.4 Experimental results 48
4.5 Summary 50

Chapter 5 : An integrated optical platform for absorptive sensing of chemical concentrations using chemo-optical monolayers **52**
5.1 Introduction 52
5.2 Absorptive sensing 55
5.3 Functional design of the circuit 58
5.4 Physical design of the sensor 61
5.5 Device fabrication 66
5.6 Experimental results and discussion 67
5.7 Summary 69

Chapter 6 : Fully integrated optical polarimeter **72**
6.1 Introduction 72
6.2 Functional design of the polarimeter 75
6.3 Physical design of the polarimeter 87
6.4 Device fabrication 93
6.5 Experimental results 93
6.6 Summary 95

Chapter 7 : Epilogue **98**
7.1 Summary of the individual chapters 98
7.2 Matching of the sensing platform-transduction layer 99
7.3 General evaluation 100

Appendix : Absorption induced real refractive index changes **103**

Samenvatting **107**

Thanx **110**

Bibliography **112**

I. Introduction

1. Once upon a time...

a joint research proposal entitled 'Integrated optical sensors for the detection of heavy metal ions' was submitted to STW (Stichting Technische Wetenschappen) by two of the research groups of the $MESA^+$ research institute, the Supra Molecular Engineering Group (SMCT) and the Lightwave Devices Group (LDG). The aim of the research project was to investigate and develop an integrated optical absorption sensor consisting of a sensing platform on which chemo-optical transducer layers are bonded which could selectively detect heavy metal ions such as Pb^{2+}, Hg^{2+} and Cd^{2+} in an aqueous environment.

In the proposal, the research was divided into two sub-projects. The first sub-project (SMCT group) aimed at the realisation of chemo optical transduction layers, which should be selective to a given heavy metal ion, sensitive to concentration changes in the desired range, stable in time, etcetera. As a final demand, they had to be bonded on top of an integrated optical channel waveguide in order to be interrogated by means of absorptive evanescent field sensing. The second sub-project (LDG) concerned the realisation of an integrated optical sensing platform (optical sensing chip), with which the absorption changes in the transduction layers could be read out. In this sensing platform, optical functionalities had to be implemented for eliminating or compensating for various kinds of disturbing effects. Seeing the potential of the proposed research, STW decided that the project was worth funding, a decision finally resulting amongst others in this PhD thesis.

This PhD thesis deals with the integrated optical part of the project; ie. the development and optimisation of absorptive integrated optical sensing platforms. In the beginning of the project, it was decided to use multiple interrogation modes enabling the compensation or elimination of several disturbances. As a consequence, several integrated optical functionalities had to be developed in order to generate and manipulate the interrogation modes. In figure 1, the functional design of the platform is shown. In this platform, the following integrated optical functionalities are incorporated:

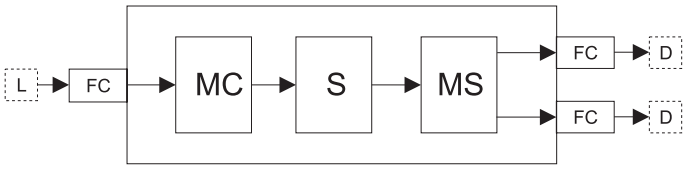

Figure 1. The functional design of the sensing circuit. MC=mode converter, S=sensing function, MS=mode splitter, FC=fiber chip coupler, L=lightsource, D=detector.

- In order to enable the insertion of the optical chip into fibre networks, fibre to chip couplers are required. As fibre to chip couplers have already been developed mainly by other members of LDG [1], our contribution to optimisation of the coupler fabrication has not been included in this thesis.
- For on-chip generation of the desired interrogation modi, a mode generator was needed, and it has been developed within the project (Chapter two).
- A sensing region was needed with a large difference of the modal sensitivities to changes in the absorption coefficient of the transduction layer while simultaneously the differential sensitivity to changes of the background absorption should be zero. Such a sensing region has been developed (Chapter five).
- After sensing, the optical powers carried by both interrogation modes have to be separately detected, for which mode splitters and mode selective waveguide-detector couplers have been developed (Chapter four).
- In order to cope with possible deviations in the value of one of the key parameters of the mode generator, a facility for tuning this parameter has been developed (Chapter three).

During the development of these optical functionalities, other applications of them were investigated as spin-off projects, one of which ended up in this PhD thesis: a differential sensing platform for detecting chemically induced changes in the real part of the refractive index of a transduction layer. As changes in the real part of the refractive index are related to changes in the imaginary part of the refractive index, this platform is also suited for reading out the chemically induced effects of transduction layers primary developed for absorptive sensing.

The title of this thesis, **'TE/TM based integrated optical sensing platforms'**, can be explained as follows:

- **'TE/TM based'** : Both sensing platforms presented in this thesis use the lowest order TE and TM polarised modes as interrogation modes. Also, all the developed sub-functionalities manipulate these modes in one way or another.
- **'integrated optical'** : All devices presented in this thesis are planar waveguide devices, ie. integrated optical structures. In the case of the sensing platforms, 'integrated' also reflects the aim at implementing all required optical functionalities in a single optical chip.
- **'sensing platform'** : The term 'sensing platform' indicates that the same integrated optical circuits can be used for the determination of many types of measurands provided that the platforms are supplied with the appropriate transduction layer. A boundary condition is the operating wavelength, as due to the implemented functionalities the platform is wavelength dependent.

The title is considered to cover all the work presented in this thesis properly and to reflect the general applicability of the final optical circuits.

2. Integrated chemo-optical sensors

A chemical sensor is a system which translates the concentration of a chemical entity into a signal, of which the strength expresses the specific value of that concentration. That signal can be perceived by an observer or can be used for further processing. Generally, this translation is a complex process which may involve several physical domains and may require the implementation of many functionalities in the various domains. As shown in figure 2, for a chemical sensor (at least) three distinct domains can be discerned : the chemical domain, the domain corresponding to the interrogation signals and the domain of the representation signals. If the output signals of the sensor are used for further processing, with the current state of electrical signal processing and the widespread use of computers, they are generally required to be in the electrical domain. If perceived by a human being, they are required in the optical (for example a pH indicator strip) or acoustical (for example an alarm) domain.

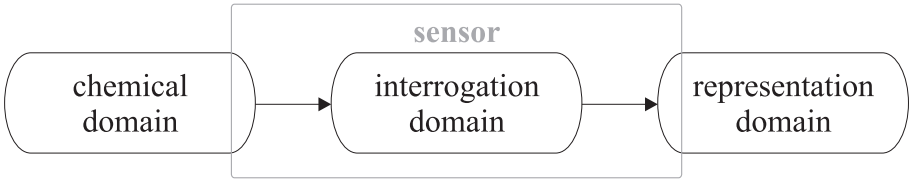

Figure 2. The chemical domain, the domain of the interrogation signals and the domain of the representation signals.

There are many possible paths leading from information within the chemical domain, e.g. the concentration of the measurand, to the representation signal. For example, the paths can differ as to the physical domain of the interrogation signals (for example electrical or optical), the type of physical effects used (for example optical absorption or refractometry) and the complexity or level of integration of the sensing system (for example μTAS systems [2] or a pH paper strip containing cellulose immobilised colour indicators [3]).

There is no 'ultimate sensor' like a tricorder [4]. Each specific application has a multitude of demands regarding the resolution, the range, reproducibility, alarming or monitoring function, working environment, lifetime, operating power, compatibility with other units, desired output signal, size, weight, maintenance, required side equipment, reliability, available patents, user friendliness, financial aspects and many more, which determines which interrogation domain, which physical implementation and which level of integration is most suited. As this thesis deals with integrated optical planar waveguide sensors, in figure 3 some considerations are shown which would lead towards the use of optical interrogation signals and the use of planar waveguide technology for the physical implementation of the sensor [5].

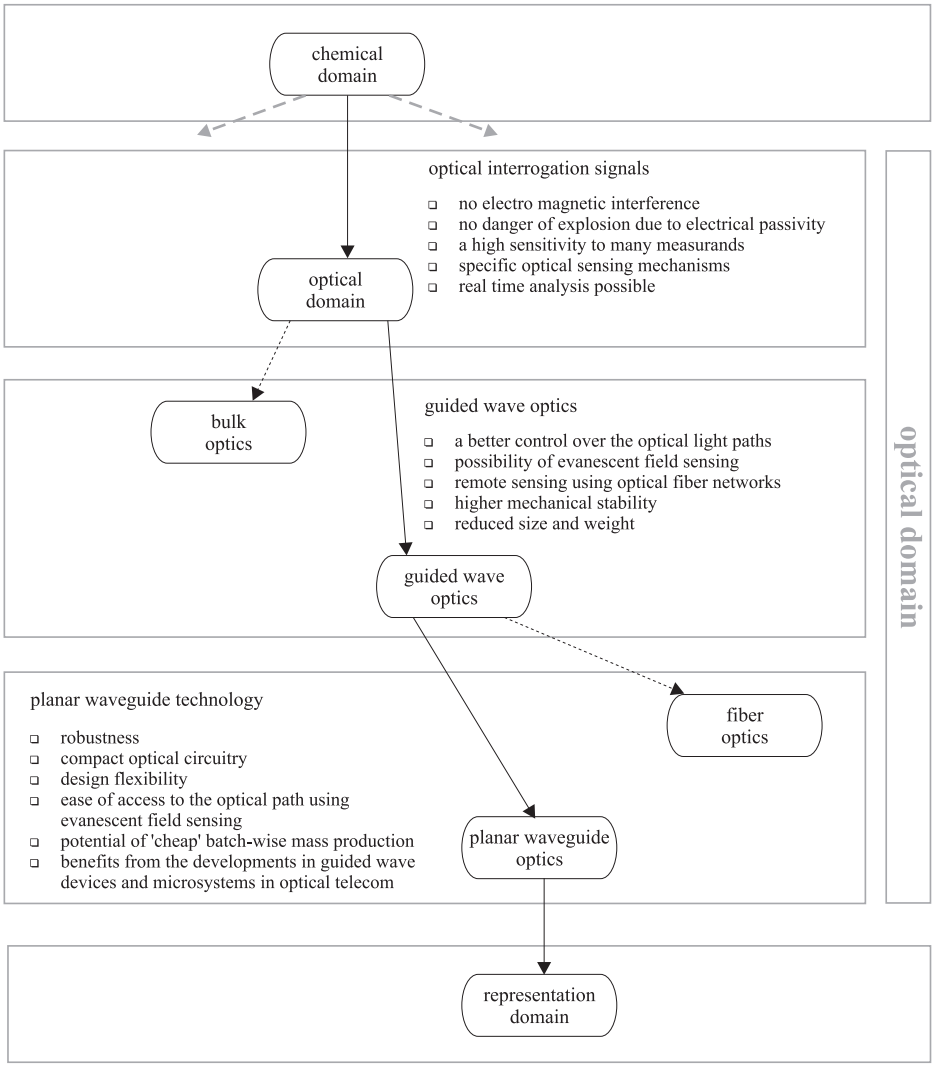

FIGURE 3. Some considerations leading towards integrated chemo-optical planar waveguide sensors.

3. EVANESCENT FIELD SENSING

The sensing principle used in the here presented sensing platforms is evanescent field sensing. Here, due to interaction of the evanescent field with the measurand, the propagation properties of the guided mode are influenced by the measurand. If the optical properties of the measurand itself are directly measured, it is called *direct sensing* (figure 4a). However, often too low concentrations and/or too small

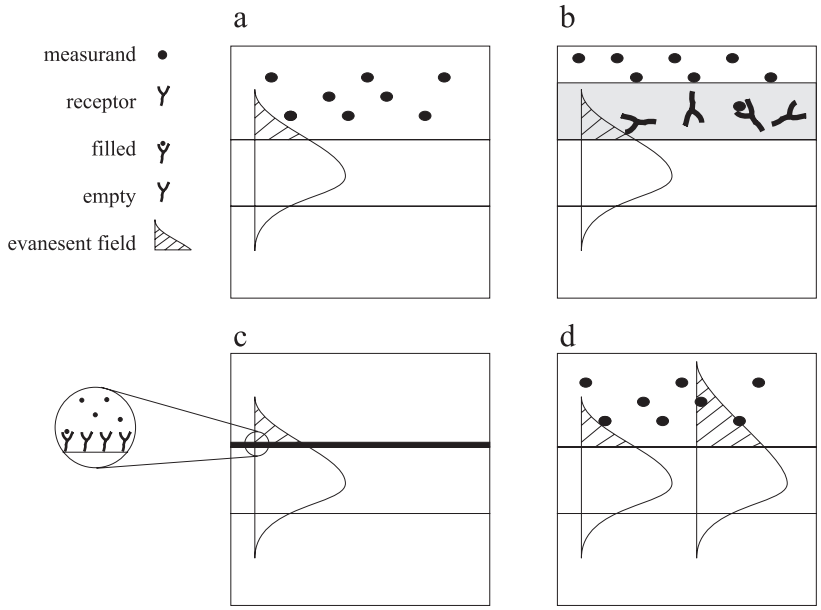

FIGURE 4. Evanescent field sensing : a) direct sensing, b) transduction layer based bulk sensing c) transduction layer based surface sensing d) bimodal sensing.

interactions with the individual measurand entities do not afford for direct sensing. Also, often lack of selectivity might cause insuperable problems. In order to cope with these problems, chemo-optical transduction layers [6] can be used, which contain receptor molecules being selective to the measurand and which may enhance the optical interaction per molecule. Depending on the thickness of the transduction layer, two types of sensing can be discerned. *Bulk sensing* (figure 4b) implies that the evanescent field is completely confined in the transduction layer. In the case of *surface sensing* (figure 4c), however the evanescent field also penetrates significantly into the outer medium adjacent to the thin transduction layer. This implies that the sensor will also show an undesired sensitivity to optical changes of the environment. In the sensor platforms presented in this PhD thesis the medium is interrogated by two modes, see figure 4d. In the case of absorptive sensing, this double interrogation is useful for eliminating the effects of disturbing background absorption on the output signal. In the differential sensing platform, the measurement principle is based on the differential sensitivity of both interrogation modes to the measurement.

4. Matching of the sensing platform - transduction layer

In the case of absorption sensing, the concentration of the measurand, C, directly influences the optical power carried by a mode i, $P_{i,opt}$,

$$P_{i,opt}(\lambda) = P_0(\lambda) e^{-\frac{4\pi}{\lambda} S_i(\lambda) L_{int} \Delta n"(C,\lambda)} e^{-\alpha_{bg}(\lambda)}, \tag{1}$$

where λ is the wavelength, L_{int} is the interaction length, $S_i(\lambda)$ the sensitivity of mode i to changes in $\Delta n"(C)$, which is the measurand induced change in the imaginary part of the refractive index, and α_{bg} represents the background losses. With direct sensing,

$$\Delta n"(C) = \frac{\ln(10)\epsilon(\lambda) C \lambda}{4\pi}, \tag{2}$$

with $\epsilon(\lambda)$ the molar extinction coefficient of the measurand. In the case of using a transduction layer,

$$\Delta n"(C) = \frac{\ln(10)\lambda}{4\pi} \left[f_{co}(C)\epsilon_{co} + (1 - f_{co}(C))\epsilon_{un} \right] [I], \tag{3}$$

with ϵ_{co} and ϵ_{un} the molar extinction coefficients of the filled and empty receptor molecules, respectively, $f_{co}(C)$ the fraction of the receptor molecules that is filled, often an S-shaped function of the concentration C, and $[I]$ the concentration of receptor molecules in the transduction layer.

With these equations, specifications regarding the transduction layer and optical platform can be given. These specifications are directed by the desired application, and in generally be stated in the following form: in a concentration range $[C_{min}, C_{max}]$ around the relevant concentration C_{rel} a resolution ΔC is required.

Combining (1) and (3), the optical power can be written as

$$\begin{aligned} P_{i,opt}(\lambda) &= P_0(\lambda) 10^{-\{\alpha_{bg}(\lambda) + S_i(\lambda) L_{int} \epsilon_{un}(\lambda)[I]\} - S_i(\lambda) L_{int} f_{co} \{\epsilon_{co}(\lambda) - \epsilon_{un}(\lambda)\}[I]} \\ P_{i,opt}(\lambda) &= P_0(\lambda) 10^{-\{A_{back} + \Delta A(C)\}} = P_0(\lambda) 10^{-A_{total}(C)}, \end{aligned} \tag{4}$$

In figure 5, the general shape of the absorbance $A_{total}(C)$ of a transduction layer containing receptor molecules is given as a function of the concentration C. Here it is assumed that at the operational wavelength the extinction coefficient of filled receptors exceeds that of the empty ones. $pK_a = -10 \log K_a$, the association constant. A high resolution is obtained if $\frac{\partial A_{total}}{\partial C}$ is large. Therefore, the design of the transduction layer should aim at obtaining $pK_a =^{10} \log C_{rel}$. As, there is a minimum detectable optical power P_{min}, there is a maximum $A_{total}(C)$. Therefore, the concentration independent term A_{back} should be minimised, meaning α_{bg} (optical platform) and $\epsilon_{un}(\lambda)$ (transduction layer) should be zero. $\Delta A(C)$ should

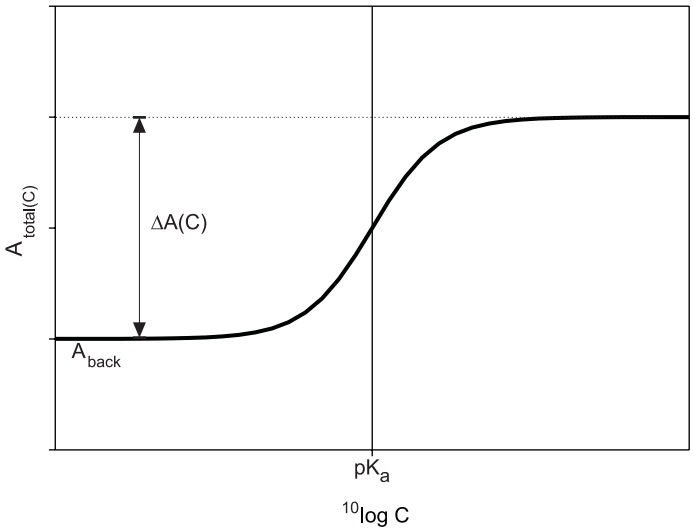

FIGURE 5. The general relation of the absorbance $A_{total}(C)$ as a function of the concentration C, when using receptor molecules.

be matched to the available optical power budget $[P_{min}, P_0]$, which can be done by a careful choice of $S_i L_{int}$ (optical platform) and $\{\epsilon_{co}(\lambda) - \epsilon_{un}(\lambda)\}[I]$ (transduction layer).

As is indicated in (4), there is a wavelength dependence of the output signal as amongst others the optical sensitivity of the waveguide and the molar extinction coefficients are wavelength dependent. For the optical sensing platform, operating wavelengths larger than 650 nm are preferred as cheap lightsources are available in this region. Also, generally the background losses $\alpha_{bg}(\lambda)$ are lower for higher wavelength. Unfortunately, receptor molecules which show large changes in their absorption spectra at higher wavelengths are more difficult to synthesise, and therefore from a chemical point of view lower wavelengths are preferred [7].
A solution to these conflicting wavelength demands might be a refractometric interrogation of absorptive transduction layers. In the appendix, it is shown that transduction layers which show absorption changes in the near ultra-violet (easy synthesis) might be interrogated using near infrared wavelengths (cheap lightsources). An additional advantage of this method is that it can be expected that there are fewer chemicals with absorption bands in this region, resulting in less interfering background absorption.

Other specifications to the transduction layer can be stated. It should be selective only to the measurand and chemically and physically stable. Regarding the stability, there are conflicting wishes regarding the optical powers used. From the optical point of view, high optical powers are preferred as they increasing the optical range $[P_{min}, P_0]$. However, for the transduction layer high optical powers may

cause photo bleaching of the receptor molecules. Response times, dependent on the internal structure and geometry of the transduction layer have to match the requirements of specific applications. Finally, the transduction layer must be bondable to the optical platform, which may put demands on the chemical composition of both the transduction layer and the (surface) of the optical waveguide.

Because within the project, no design specifications, which could immediately be converted into requirements to the optical readout system, were given, we defined the following objectives, most of them directed to a versatile usability of the optical platform:

- The sensing functions have to be optimised for obtaining the highest sensitivity.
- The use of two interrogation modes in order to compensate for disturbing effects will be investigated. Using two modes, the effects of environmental absorption on the output signal can be eliminated.
- The background losses α_{bg} have to be minimised.
- All purely optical functionalities will be integrated on one optical chip.
- Because a priori the operating wavelength could not be defined, we have decided to optimise all sensing functions for an operating wavelength of 655 nm, being in the lower wavelength region of available, cheap solid state lightsources.
- The SiON technology as developed in the LDG will be used for the realisation of the sensing platforms. With this technology, materials with refractive indices inbetween 1.45 and 2.01 are available. An additional advantage is that the OH-groups in general present on the surfaces are very appropriate for covalent bonding of organic groups, using e.g. silanisation methods.

5. Outline of this thesis

In figure 6, an overview of all research and the relations between the different parts of the research are shown. The research resulted in two *differential sensing platforms*, one for detecting changes of the imaginary part of the refractive index (absorptive sensor)and one for detecting changes in the real part (refractive sensor). Both of the sensing platforms are realised by an *integration of multiple integrated optical functionalities*.

Several optical functionalities needed for the platforms are newly developed: the *polarisation converter*, later extended to a *tunable polarisation converter*, needed for a well controlled partial power transfer from a launched TE_{00} mode into a TM_{00} mode and *coupling structures* for coupling light whether or not mode selectively into monolithically integrated detectors. Other functions such as the sensing region and a mode splitter are principally known, but optimised for the specific application. In this thesis, the chapters two to six correspond to submitted papers, and are therefore self consistent. Chapter seven summarises and evaluates the conclusions

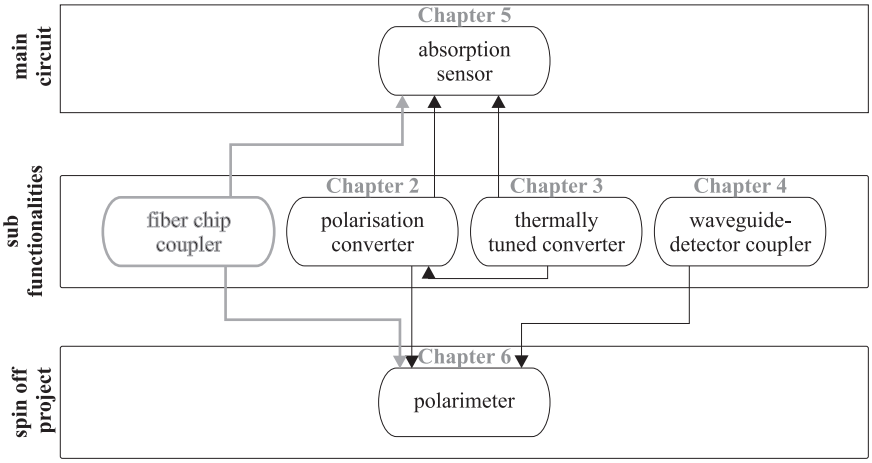

FIGURE 6. An overview of the research presented in this thesis showing the connections between the different chapters.

drawn in the previous chapters. In some more detail, this thesis is organised as follows:

- First, in *chapter 2*, the polarisation converter is presented, as this is one of the key components for both sensing platforms. The polarisation converter has two functions: it is used to obtain from one launched mode both interrogation modes with a well known power ratio. In the case of the fully integrated optical polarimeter, it is also applied for obtaining the required interference of both interrogation modes after being modified in the sensing function.
- One of the conclusions, drawn in chapter two, was that it can not be guaranteed that the polarisation converter shows exactly the intended amount of conversion. In *chapter 3* it is presented how the converter can be externally tuned to obtain its intended performance.
- In both sensing platforms, after having passed the sensing function the powers of both interrogation modes have to be separately detected in order to obtain the information carried by each of the modes. In order to achieve this mode splitting, coupling structures were developed, which are able to transfer mode selectively the optical power carried by a certain mode into a photo detector which is monolithically integrated in the substrate wafer. The research concerning these coupling structures is presented in *chapter 4*.
- In *chapter 5*, the sensing platform for absorption sensing is presented, in which all purely optical functionalities are implemented in a single integrated optical circuit. In this sensing platform, the perturbing effect of environmental absorption present when using monomolecular transduction layers in combination with evanescent field sensing is addressed to. A functional analysis

and the physical design of the circuit, its fabrication and the characterisation of the individual subfunctions and the nearly complete sensor are presented.

- In *chapter 6* the refractive sensing platform, the fully integrated optical polarimeter, is presented. As with the sensor described in chapter five, here all purely optical functionalities are implemented as a single integrated optical circuit. The functional design and an analysis,followed by the physical design of the sensor are presented. After a summary of the fabrication of the device, experimental results regarding the characterisation of the individual integrated optical functionalities and the complete sensor are presented.
- A summary and evaluation of the work presented in this thesis are given in *chapter 7*.
- In the *Appendix*, the effect of absorption changes on index changes, as given by the Kramers-Kronig relations, is investigated. Here, using a realistic example, it is shown that refractometric interrogation of absorptive transduction layers is very well feasible.

References

[1] R.G. Heideman and P.V. Lambeck. Simple and reusable fibre-to-chip interconnect with adjustable coupling efficiency. *SPIE*, 3099:238–247, 1997.

[2] edt. A. van den Berg. Micro total analysis systems 2000. In *proceeding of the Mutas 2000 Symposium, 14-18 May, Enschede, The Netherlands*, 2000.

[3] edt. O.S. Wolfbeis. *Fibre optic chemical sensors and biosensors*. CRC press.

[4] http://www.startrek.com/library/techno.asp?id=70294&dockingbay=equipment.

[5] P.V. Lambeck. Integrated chemo-optical sensors. *Sensors and Actuators B*, 8:103–116, 1992.

[6] K. Seiler and W. Simon. Theoretical aspects of bulk optode memranes. *Analytica Chimica Acta*, 226:73–87, 1992.

[7] Niels van der Veen, private communications.

II. Passive polarisation converter in SiON technology

Abstract- A passive polarisation converter has been realised in Silicon Oxynitride technology. The device is a grating assisted co-directional coupler consisting of segments of asymmetrically etched ridge waveguides. By using a double masking technique, the fabrication of the device is tolerant with respect to the alignment of the required masks. Conversion efficiencies up to 0.98 (TE->TM and TM->TE) and insertion losses of 3dB/cm have been measured. Using 2D BPM simulations, an observed beat pattern in the converter could be explained to be due to a leaky mode which is captured in the grating structure.

1. Introduction

The existence of two states of polarisation propagating through monomodal integrated optical waveguides poses problems to some integrated optical circuits and is exploited in others. An example of the former is an add drop multiplexer [1], of which the peformance must be polarisation independent due to the unknown state of polarisation coming out of the input fiber. An example of the latter is a polarimeter [2], which is a sensor based on the different sensitivities of modes of both polarisations to the measurand. If the existence of modes of both polarisations poses a problem to a given integrated optical device, there are two ways to eliminate it. One is the realisation of polarisation independent devices [3], thereby posing severe limitation/requirements to both the design and technology. Another is is the implementation of polarisation manipulating functionalities in the devices, such as a polarisation converter [4], which enables transfer of optical power from one state of polarisation to the other and vice versa. For many devices exploiting the TE/TM behaviour of light, such as the polarimeter, the polarisation converter is an essential basic building block.

Both active [3] and passive [4] converters have been reported in literature. Here, active refers to the use of physical cross effects for inducing the grating that is needed for obtaining polarisation conversion. Active converters have the advantage that the amount of conversion can be controlled by changing the driving power, while in the opto-acoustic case also the grating period can be adjusted [3]. However, the use of most of the active converters reported up to now [3],[5] is limited by the need for (expensive) materials which should show physical cross effects (such as electro-optical or acousto-optical) and should have a crystal structure with a symmetry that permits coupling between both types of polarisation. In the case of acousto-optical devices, an additional drawback is the use of high frequency control electronics [3] which limits low cost commercial application of these devices. Contrary to active converters, in passive converters there are fewer restrictions with respect to the

materials used and in general a much simpler fabrication technology is possible. If required by the application, wavelength tunability can be added using the thermo optical effect [6], [7] which, as opposed to the electro and acousto optical effect, does not require any expensive material or technology.

In 1990, the first paper on a passive polarisation converter was published by Shani et al. [4]. Since then, various groups have published results about passive polarisation converters based mainly on two different principles. One uses waveguides with strongly hybrid modes in order to obtain polarisation conversion without using periodic structures, for example the converters in [8],[9]. The other principle implies the use of asymmetrical grating structures in grating assisted couplers such as reported in [10],[11]. The converter presented here is based on such a grating structure.

In this paper we present a passive converter realised in Silicon Oxynitride technology. The waveguide system consists of a high index Si_3N_4 core layer in between two low index SiO_2 layers. In this layer system, the ridge type channel modes are nearly similar to slab modes, in sofar that they show very small non-dominant field components. Hence, converters based on strongly hybrid modes cannot be implemented in this material system, and grating type polarisation structures have to be used. The converter reported here is the first realisation [12] of a converter based on segments of asymmetrical etched ridge waveguides, as proposed by [13]. The structure has been designed in order to minimise the effect of technological uncertainties on the conversion wavelength. Furthermore, by using a double masking technique, the fabrication can be made very tolerant with respect to the alignment of the converter mask to the waveguide mask. The device shows a narrow band wavelength response, offering the possibility of implementing it as a wavelength filter in devices such as add drop multiplexers.

In section 2, the structure and principle of the converter are explained. After a brief discussion of the device fabrication in section 3, experimental results are presented in section 4. In section 5, the obtained experimental results are compared to results obtained in literature. Also possible applications of the converter are shortly discussed. In section 6, a summary is given.

2. Structure and design

In this section, the device principle will be briefly discussed and the designing process, in which a tolerance analysis of the converter plays a main part, is presented. Due to the specific application, which is in our case an integrated optical sensor of specific type [14], the converter presented here is designed for a wavelength of 655 nm. However, the design methodology, based on an optimisation with respect to device reproducibility, can be generally applied for every operation wavelength.

The converter is a co-directional grating assisted coupler consisting of segments of asymmetrical etched ridge waveguides, as shown in figure 1. Due to the induced asymmetry, there is a slight tilt of the optical birefringence axis with respect to the

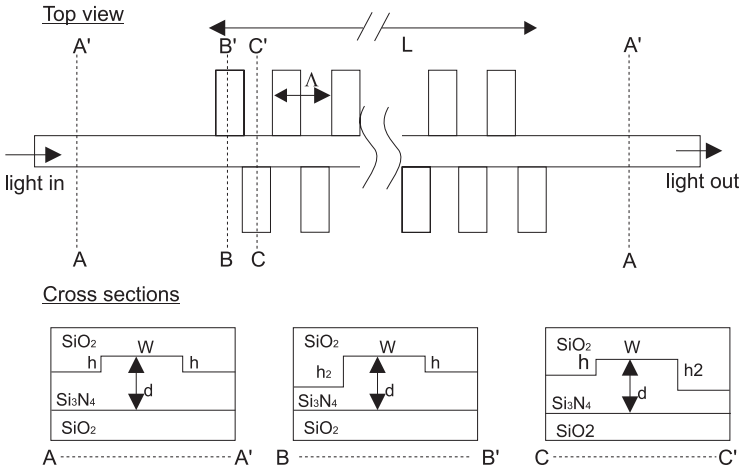

FIGURE 1. A topview and cross sections of the polarisation converter

symmetrical layer system. As a result, there is a non-zero field overlap between the TE and TM fields in adjacent grating segments. At each transition between adjacent segments, the polarisation angle is slightly rotated for the resonance wavelength λ_r given by

$$\lambda_r = \Lambda \left(N^c_{TE} - N^c_{TM}\right) \equiv \Lambda \Delta N^c_{TE-TM}. \tag{1}$$

Here, Λ is the grating period and N^c_{TE} and N^c_{TM} are the effective indices of the TE and TM channel mode, respectively. It should be noted that (1) is exact, as in our case both grating segments are each others mirror image with respect to the centre of the ridge waveguide, so the TE mode in both segments, just as the TM modes, have the same effective index.

The layer stack in which the converter is realised is shown in figure 1; it consists of a high index Si_3N_4 core layer in between two SiO_2 layers. This layer stack was chosen because of the intended application circuits in which the converter should be incorporated. However, the presented layer stack also has additional advantages for the converter. First, these layers can be grown/deposited very accurately with respect to their refractive indices and to the thickness of the Si_3N_4 layer, thereby increasing the reproducibility of the converter. Secondly, using this high refractive index contrast layer system, a large difference between the effective indices of the TE and TM mode is obtained, resulting in grating periods of acceptable length.

There are several boundary conditions to the design. First, the converter should be mono modal, allowing only the lowest order TE and TM to propagate through the structure. For the given operation wavelength and layer stack, this limits the core layer thickness to a maximum of 250 nm, as can be calculated by the mono

modal condition $V < \pi$, with V the normalised core thickness [15]. Using the effective index method (EIM) and ignoring in a first stage the asymmetry, the monomodal condition in the lateral direction can be expressed as

$$\frac{2}{\lambda}\sqrt{2N_i^s\frac{\partial N_i^s}{\partial d}}W\sqrt{h} < 1, \tag{2}$$

with N_i^s the effective index of the slab modes for TE or TM for a core thickness d, ridge height h and ridge width W. Second, the coupling to radiation modes must be absent for first order coupling, which puts a lower limit to the allowed grating period Λ,

$$\Lambda > \frac{\lambda_r}{N_{TM}^c - n_{SiO_2}}, \tag{3}$$

with n_{SiO_2} the refractive index of the SiO_2 layer. Third, the converter should be fabrication tolerant regarding its resonance wavelength and the coupling strength, ie. the design has to take technological uncertainties into account.

Most important is the control of the resonance wavelength, λ_r, which is a function of the effective index difference between the TE and TM mode. Using the EIM, it can easily be shown that the effective indices of the TE and TM channel modes, N_i^c lie in the interval

$$N_i^s(d) - \frac{\partial N_i^s(d)}{\partial d}h < N_i^c < N_i^s(d), \tag{4}$$

where i stands for TE or TM; here the higher order terms in the Taylor expansion have been neglected. The superscript 's' again refers to the slab modes in a core layer with thickness d and 'c' refers to the channel modes of the ridge waveguide.

As there is a high contrast layer system in the vertical direction, the ridge height h has to be very small (0-2 nm combined with a ridge width W in between 2 and 5 μm) in order to obtain a monomodal system, and hence the range in which the effective index difference lies is very narrow. From 4, it can be noted that if $\frac{\partial \Delta N_{TE-TM}^s(d)}{\partial d} = 0$, ΔN_{TE-TM}^c should be independent of h within the validity of our approximations.

Now, we will investigate the influence of h_2 on ΔN_{TE-TM}^c. In the EIM, the asymmetry manifests itself in the normalised a-parameter of the equivalent slab guides in the lateral direction. Because of the small lateral effective index contrast, this a-parameter is in good approximation identical for the TE and TM slab guides,

$$a = \frac{(N_{d-h}^s)^2 - (N_{d-h_2}^s)^2}{(N_d^s)^2 - (N_{d-h}^s)^2} \approx \frac{2N^s(d)\frac{\partial N^s}{\partial d}(h_2 - h)}{2N^s(d)\frac{\partial N^s}{\partial d}h} = \frac{h_2 - h}{h}. \tag{5}$$

The influence of h_2 on ΔN^c_{TE-TM} is generally much smaller than the influence of h on ΔN^c_{TE-TM}, especially in the case of a large asymmetry parameter (> 10) which, as will be seen later on, is the case with the presented converter.

Regarding all geometrical parameters, it can be concluded that the effective index difference, and hence the resonance wavelength, is mainly dependent on the core layer thickness. The design of the converter should aim at minimising the effect of variations in d on ΔN^c_{TE-TM}, in that way in the same time minimising the effects of uncertainties in h and h_2.

The effect of technological uncertainties on the coupling strength cannot be as easily analysed as their effect the resonance wavelength, as it requires the (full vectorial) calculation of overlap integrals between adjacent segments. It is clear that the overlap will strongly dependent on the asymmetry, as was also found by preliminary experiments. In the design study, we will vary h_2 within the range of 5-20 nm. With such h_2 values, it was experimentally found that acceptable coupling lengths of the order 10 mm can be obtained [12].

Now, the influence of the fabrication tolerances on the the resonance wavelength will be worked out more quantitatively. For small variations in the device geometry and in the refractive indices, the relative shift in the resonance wavelength λ_r can be written as

$$\frac{\Delta\lambda_r}{\lambda_r} = \frac{1}{\Delta N_{TE-TM}} \sum_{i=1}^{7} \frac{\partial \Delta N_{TE-TM}}{\partial x_i} \Delta x_i, \tag{6}$$

where higher order (cross) terms are neglected. x_i stands whether for a layer index or one of the geometrical parameters. In table 1, the maximum deviations in these parameters are given, using the technologies available in our laboratory [16]. If the deviations are relative, as in the case of the geometrical parameters, the absolute deviations for the final structure are given in between brackets.

Table 1 : technological parameters and the technological uncertainties therein.

parameter	**max.deviation**
Si_3N_4 thickness	1% (1.5 nm)
Si_3N_4 index	$5 * 10^{-4}$
cladding SiO_2 index	$2 * 10^{-3}$
substrate SiO_2 index	$1 * 10^{-4}$
h	10% (0.1 nm)
h_2	10% (2 nm)
W	0.2 μm

As the materials within the layer system are already chosen, the free parameters in the design are the Si_3N_4 core thickness d, the small etch step h, the deep etch step h_2 and the ridge width W. Above, it was already concluded that the resonance wavelength will be mainly dependent on the core layer thickness d. In figure 2,

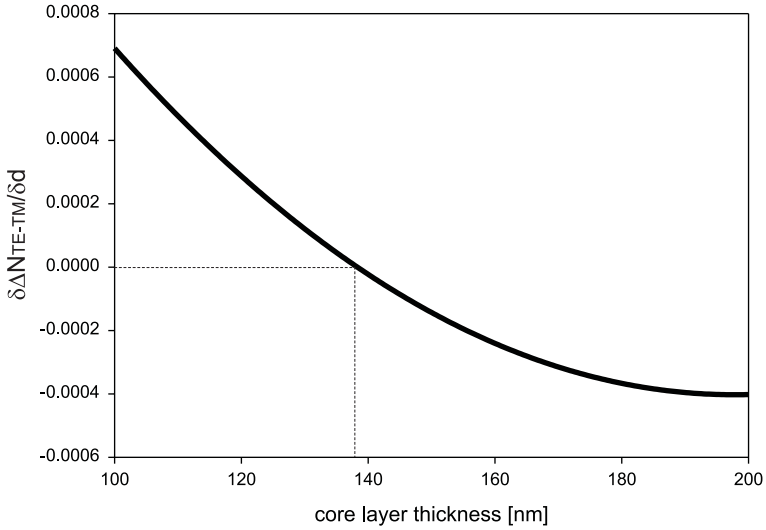

FIGURE 2. $\frac{\partial \Delta N^s_{TE-TM}}{\partial d}$ versus the core layer thickness.

$\frac{\partial \Delta N^s_{TE-TM}}{\partial d}$ is given as a function of the core thickness for a 3 layer slab system. A core thickness of 137nm results in the required $\frac{\partial \Delta N^s_{TE-TM}}{\partial d} = 0$.

Using a 2D mode solver [17], the influence of variations in the geometrical parameters on $\Delta\lambda_r/\lambda_r$ have been calculated.Using an iterative process for the minimisation of $\Delta\lambda_r/\lambda_r$, the optimum system appears to correspond with (d=137 nm,h=1 nm, W=4 μm and h_2=15 nm). For this system, in figure 3, $\Delta\lambda_r/\lambda_r$ is given as a function of these parameters.

In figure 3, in each graph the effect of a variation of one of the parameters on $\Delta\lambda_r/\lambda_r$ while keeping the others were kept constant is shown, and also as the expected maximum deviation in each parameter is indicated. As predicted, the influence of variations in d is orders of magnitude higher than the influence of variations in the other parameters. It can be seen that for both the d and W values, taken in the designed system, $\Delta\lambda_r/\lambda_r$ is at a maximum.

As expected, the influence of h_2 on $\Delta\lambda_r/\lambda_r$ can be neglected with respect to the other terms. This has the consequence that h_2-parameter can be used as a parameter to tune the coupling strength without any effective influence on the resonance wavelength, and hence the grating period required; this implies that, without altering the photolithographic masks, converters with different amounts of polarisation conversion can be obtained by varying the etching time for defining h_2 only.

Up to now, only the effect of deviations in the geometrical parameters of the layers have been taken into account. For the before mentioned waveguide system, the effects of deviations of the refractive indices on $\partial(\Delta\lambda_r/\lambda_r)/\partial n$ can be calculated

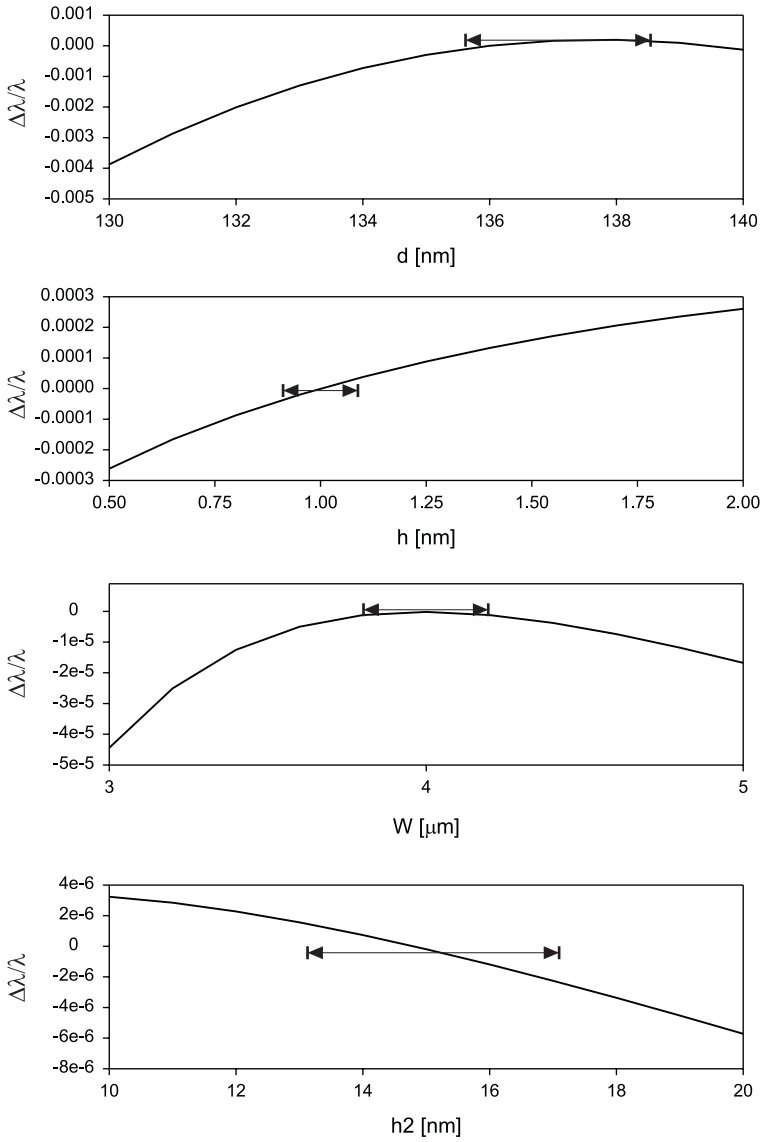

FIGURE 3. The effect of technological deviations on $\Delta\lambda_r/\lambda_r$.

to be -0.2 for the SiO_2 cladding layer, 0.32 for the Si_3N_4 core layer and -0.2 for the SiO_2 substrate layer.

Now, the maximum deviation (worst case analysis) in the resonance wavelength due to technological fluctuations can be calculated to be

(7) $$\Delta\lambda_r = 655 * 0.0038 = 3.8nm,$$

where the largest contribution to this deviation arises from variations in the cladding SiO_2 refractive index.

The full width half maximum (FWHM) bandwidth of a co-directional grating assisted coupler with a length of 10 mm is approximately fifteen times smaller than 3.8 nm. This implies that for proper performance a system with a strongly increased coupling strength, and thereby an increased FWHM, or adjustment by tuning the resonant wavelength or adjustment of the wavelength entering the converter is necessary. This is addressed too in the experimental section of this paper.

3. Fabrication

The devices are fabricated on 3" Silicon wafers. The substrate SiO_2 layer is grown by thermal oxidation of the Silicon wafer, the core layer deposited using Low Pressure Chemical Vapour Deposition (LPCVD) and the cladding layer deposited using Plasma Enhanced Chemical Vapour Deposition (PECVD) applying the processes as developed in our laboratory [16]. The 1 nm high ridge was defined using BHF etching (0.55 nm/min), the 15 nm deep etch step by Reactive Ion Etching (RIE).

In order to increase the fabrication tolerance with respect to mask alignment, a double masking technique [18] was used to define the deep etch step, see figure 4. After definition of the waveguide structure, the positive resist was given a heat treatment in order to make it insensitive to UV exposure, after which a second resist layer was spin coated on top of the old layer. Then, using a mask as shown in figure 4, the structure for the deep etch step was defined in the second resist layer. Using this double masking technique, there is an alignment tolerance equal to the width of the waveguide, here being 2 μm. Also, it is guaranteed that the etch step

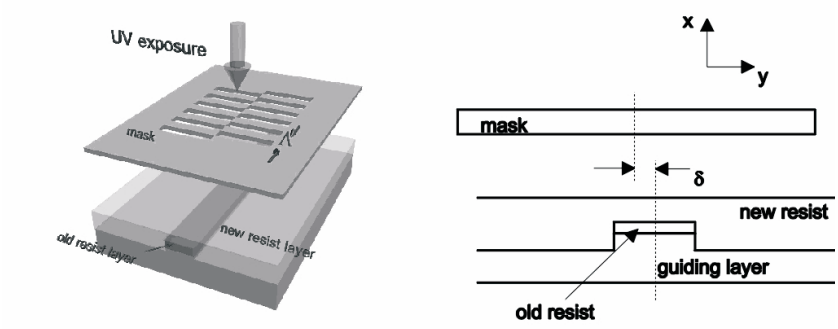

Figure 4. The double etch step technique for lowering the tolerances regarding the alignment of the grating mask to the waveguide mask.

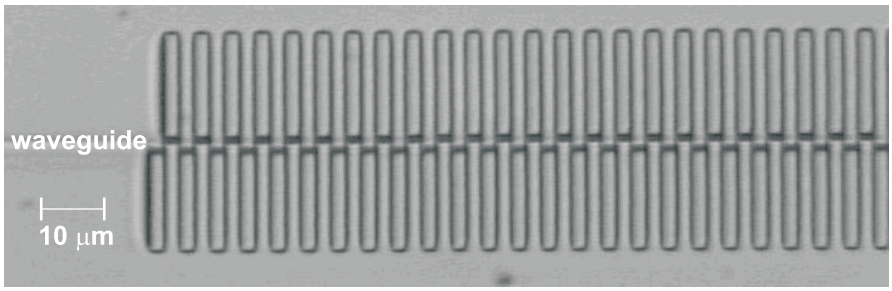

FIGURE 5. Micrograph of the waveguide and grating structure in the photoresist layers.

is only at the sides of the ridge. In figure 5, a micrograph of the converter structure after development of the second photo resist layer is shown.

4. EXPERIMENTAL RESULTS

The converters have been characterised using an Argon pumped (515 nm) dye laser (DCM dye, 620-680 nm, step size 0.03 nm) as shown in figure 6. Different wafers with several converters have been realised in order to investigate the reproducibility of the converter performance on single wafers and from wafer to wafer. The converters have been characterised with respect to the resonance wavelength, their FWHM, the channel and functional losses and the coupling strength.

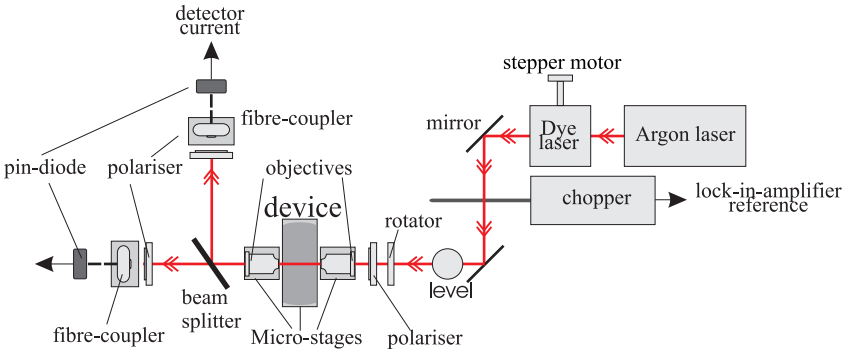

FIGURE 6. The experimental set up.

In figure 7, for a device length of 12 mm and (h=1 nm, h_2=15 nm, d=137 nm,W=4 μm), the conversion versus the wavelength is shown. It can be seen that the FWHM of the conversion peak is small, 0.25 nm. It can further be seen that the resonance wavelength is not 655 nm, but 657.4 nm. The asymmetry in the side lobs is caused by a position dependent effective index difference along the converter. The on-chip spread in the resonance wavelengths was determined to be smaller than

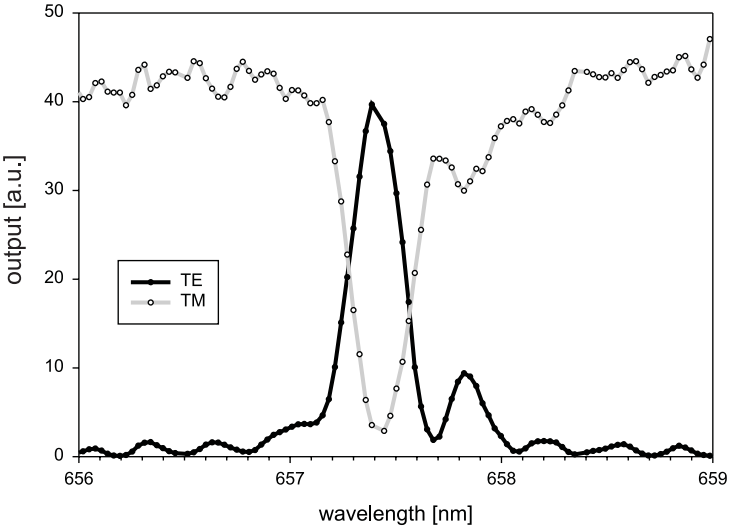

FIGURE 7. Typical measured wavelength response of the polarisation converter.

0.1nm. By performing measurements at converters on several samples from different batches, it was found that the resonance wavelength was 655.3 nm with deviations smaller than 4.3 nm, ie. a maximum shift $\Delta\lambda/\lambda = 0.007$, which corresponds well to the predicted value (655 $\pm$ 3.7 nm) for the resonance wavelength.

Next, loss measurements have been performed regarding the waveguides and the converter. By measuring the scattering on top of the waveguide with a CCD camera and by performing an exponential fit on the intensity versus length dependence, the propagation loss in the waveguide channels was determined to be 1.6 $\pm$ 0.1 dB/cm, for both the TE and the TM mode. By measuring the output signals of converters with different length, the functional losses of the converter were determined to be 3 $\pm$ 0.3 dB/cm both for TE and TM input light.

Now, with the propagation and functional losses known, the coupling strength of the converters can be determined. For converters on the same wafer having different lengths, the amount of polarisation conversion was determined. As for the resonance wavelength the device length and the amount of conversion, PC, are related by [19]

$$PC = sin^2(CL), \tag{8}$$

with PC ranging from 0 to 1, where 1 corresponds to a 90 degrees polarisation rotation, L is the converter length and C is the coupling strength. In figure 8, for converters with (h=1 nm, h_2=15 nm, d=137 nm,W=4 μm), the polarisation conversion (for TE and TM input light) is shown as a function of device length.

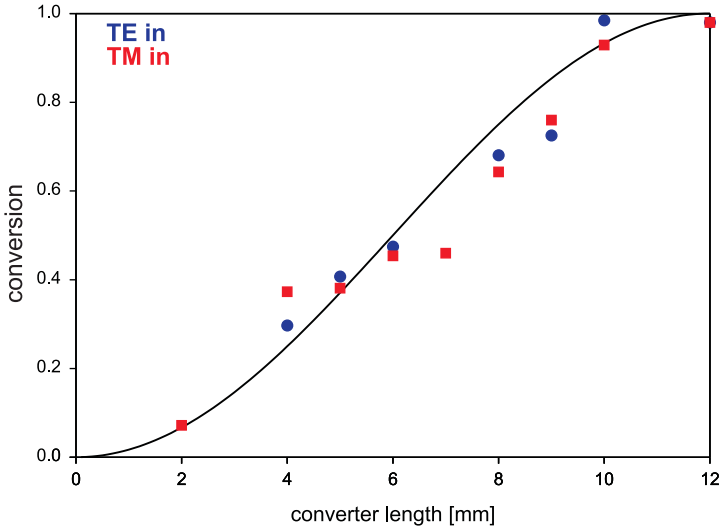

FIGURE 8. Device length versus the polarisation conversion PC.

Complete conversion is obtained at a device length of 12 mm, corresponding to a coupling strength of $6.5 * 10^{-5}$ μm^{-1}. This corresponds to a very small rotation of the polarisation axis of 0.011 degrees at each transition. Devices with an etch step of 8 nm showed complete conversion for a length of 16 mm, corresponding to a coupling strength of $4.9 * 10^{-5}$ μm^{-1}.

Devices with deeper etch steps have been realised in order to obtain converters with higher coupling strengths. However, it was found that for these devices the losses increased rapidly when increasing the depth of the etch step. Experimentally, it could not be discerned whether this was due to an increased scattering as a result of an increase in the surface roughness or as a result of an increased mode mismatch, eg. increased coupling losses between adjacent segments. However, from BPM simulations no significant increase in the losses at higher h_2 values were found, so most likely the experimentally found loss increase has to be ascribed to an increase of the effects of the surface roughness.

The maximum amount of polarisation conversion which was measured was 98% for both TE and TM light launched into the converter. Taking the FWHM of the converter response and the line width of the dye laser into account, this is the maximum conversion that can be obtained with our experimental set up. Therefore, as for several samples a conversion of 98% was measured, the conversion might even be higher for light with a smaller line width.

For the resonance wavelength, 655 ± 4.3 nm was found, while the FWHM was 0.25 nm. Therefore, it is not assured that for each converter, the desired amount of conversion is achieved for the desired operation wavelength. Several solutions to this problem can be considered. The first is to make the coupling strength C stronger, resulting in a widening of the FWHM approximately inversely proportional to C. However, in order to increase C, the asymmetry has to be increased, which was experimentally shown to have the drawback of a strong increase of the functional losses. A second solution would be the use of a broad band lightsource centred around λ_r having a spectral output wider than 8.6 nm, combined with a filter which can be tuned to the resonance wavelength of the polarisation converter, or even better, to the wavelength where the conversion shows its intended value. Alternatively, a tunable lightsource could be applied. The third option, which is currently being investigated, is thermally tuning the resonance wavelength of the converter itself. Preliminary calculations show that within a temperature range of approximately 70 degrees Celcius of the heater electrode, a tuning range of 10nm can be covered. A more quantitative analysis of the thermally tuned polarisation converter will be given elsewhere [7].

When launching TM polarised light into the converter and looking on top of the structure with a microscope, a beat pattern with a period of 63 ± 5 μm could be observed, see figure 9. This beat pattern corresponds to an effective index difference of 0.01 between the two beating modes. This beating was present not only for the resonance wavelength, but also for other wavelengths ranging from 620 to 680 nm, with a variation in the beat period of about 3 μm, so it is not specifically related to the polarisation conversion process. A 2D BPM simulation, using the EIM, of the converter structure showed a similar beat pattern with much the same period of 67 ± 2 μm over a wavelength range 620 to 680nm. For TE polarised light similar results were obtained. The simulation showed a fringe visibility of 0.08 between the modes, indicating a weak coupling of the zeroth order (TM) mode to another mode. As the beating is not only present for the resonance wavelength of the converter, the beating must be between two different TM modes. The question arises which other mode is involved in the beat pattern.

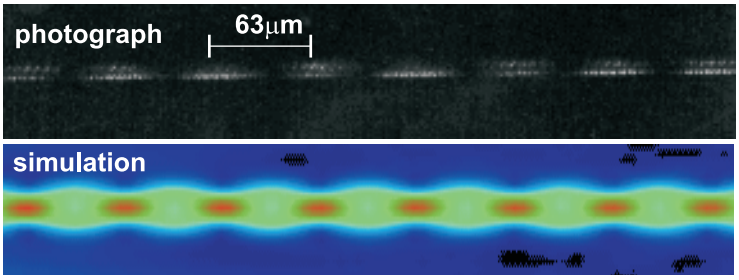

FIGURE 9. Micrograph of the beat pattern (top) and BPM simulation of the same structure (same scale).

The effective index difference between both modes is 0.01, so as the N_{eff} of the TM_{00} mode is 1.60, the effective index of the other mode must be 1.59. As the channel structure is mono modal, the second mode cannot be another channel mode. Therefore, the beat pattern must be between the lowest order TM mode and a leaky (radiation) mode in the lateral direction. Because the effective index of the zeroth order mode in a slab waveguide with a thickness of 136 nm (ie. the slab region defined by the d - h ridge step) is 1.5995 and in a slab waveguide with a thickness of 122 nm (ie. the slab region defined by the d - h_2 deep etch step) 1.5775, the unknown radiation mode may be a radiation mode launched into the 136 nm thick slabguide fragments, its propagation direction deviating approximately 6 degrees from the channel axis. The BPM simulations also show that the propagation losses increase rapidly with increasing grating period, which supports the idea of the existence of a radiation mode: for larger grating periods the radiation, generated at a certain transition is more distanced from the channel axis at the next transition, so at this transition the modal overlap with the guided mode decreases and less power is coupled back to the guided mode. Another indication pointing towards coupling with radiation modes is the following: calculations using a full vectorial mode solver [20] showed that the absolute square of the field overlap integral of TM modes in adjacent grating segments is low, namely 0.6 only, so if the radiation modes should not couple back to the guided mode, the functional losses would be $7 * 10^4$ dB/cm !!!. As the functional losses while propagating through a structure with 1500 periods are 3 dB only, most of the energy transferred to the radiation modes must be coupled back to the guided channel mode.
One can wonder whether this radiation mode might be involved in the polarisation conversion process in the same way as the higher order TE_{10} mode was in the systems, reported in [21]. However, because both the wavelength and device length dependence of the conversion correspond completely to the model of a simple co-directional grating assisted coupling between two guided modes, we expect only the zeroth order TE and TM mode to be involved in the conversion process.

5. Discussion

In table 2, the here presented converter is compared with other passive converters known from literature.

	thispaper	**Lang** [11]	**tol** [22]	**merthens** [8]
principle	grating	grating	grating	hybrid modes
material	SiO_xN_y	ion exchanged glass	InP	InP
technology	+	+	–	++
max. conv.	98%	99%	93%	93%
coupling length	12 mm	18mm	1 mm	0.25mm
losses	3 dB	0.4dB	10dB	?
ΔW_{FWHM}	0.25nm	"large"	$\approx$ 30 nm	?
$\Delta\lambda/\lambda_{res}$	0.007	?	?	?

From this table, the following observations can be made:

- The converter presented in [11] showed a slightly higher conversion for a longer length (18 mm), and the functional losses are lower due to graded index profiles obtained by using ion exchange technology instead of etching techniques. Similar to our converter, the realisation of this structure is also simple.
- Compared to the structure in [22], our structure shows a higher conversion, lower losses and is technologically simpler. However, the structure in [22] is much shorter ($< 1mm$) as, due to the high refractive index contrast the coupling can be made much stronger, also resulting into a much larger FWHM-value.
- The converter presented in [8] showed a conversion of 93% for the very short length of 0.25mm (converter losses were not mentioned) and could be realised in a single step. However, for this type of converter, a strongly hybrid character of the propagating modes is required. Also, for filtering applications this converter is not suited as the wavelength dependence is low.

The type of converter best suited for a specific application depends strongly on the required complexity of the optical circuitry and the tolerance with respect to optical losses. If the converters have to be implemented in a complicated optical circuit and high losses and costs are tolerable, InP devices are favoured, as due to the high index contrast not only small converters are obtained, but also small bending radii are feasible, thereby allowing for a large optical functionality per square mm. If the converters have to be implemented in simple low functionality circuits where large bending radii are tolerable and if low losses are required, the converters fabricated in ion exchanged glass technology are most promising. The here presented SiON type converter is most suited for moderately complicated circuits with moderate demands regarding losses, i.e. the 'middle-of-the-road' type of device, as SiON technology combines the possibility of relatively small bending radii with moderately low losses.

Our passive converter is based on a geometrically induced asymmetrical perturbation of the waveguide cross sections. For the realisation of these perturbations, no specific crystal structure is required, so this type of converter can be implemented into every material system. Tailoring the design to the technological tolerances results into small maximum deviations of the resonance wavelength from its design-value, allowing for matching both values by thermo-optical tuning. The small FWHM of the conversion versus wavelength makes it an interesting option as a wavelength selective component in filtering applications, especially in combination with the thermal tuning ability of a slightly modified device; the tuning range being about 10 nm [7].

Passive polarisation converters can be applied in either integrated optical sensors or in telecommunication circuits. Currently, in our laboratory the converter has been successfully implemented in several integrated optical sensing platforms, such

as a fully integrated optical polarimeter [14] and a differential absorption sensor [23]. In these circuits, the converters are used for partial conversion of a launched TE mode into a TM polarised mode and also for obtaining the interference of TE and TM polarised zeroth order modes. In both sensing systems the converter acts like wavelength specific $\lambda/4$ wave plates.

Due to the wavelength dependence of the conversion, in principle the polarisation converter can also be used as a wavelength selective component in telecommunication circuits. Using our polarisation converter with a thermo optical tuning facility [7], the Add Drop Multiplexer (ADM) described in [3] can be realised in a technologically simpler and cheaper way. The specific application of these ADMs depends on the width of the conversion response, which is related to the device length. In our converter, with a coupling length of 12 mm, around 1550 nm minimum channel separations of 2 to 3 nm are feasible, excluding its applicability in ADMs for dense wavelength multiplexing. However, it is useful in applications in which the channel spacing is wider, for example, in Local Area Networks (LAN) [24], where channel spacings up to 10 nm are used. Also in high speed systems where the channel spacing is relatively wide, an ADM based on the presented converter should be an option, provided that a flat band response can be obtained for the add and drop channel [25]. This is expected to be feasible by introducing apodisation and a phase shift in the grating [26].

6. Summary

A passive asymmetrical grating based $TE_{00} \leftrightarrow TM_{00}$ polarisation converter in SiON technology has been developed. An analysis of the system is given, in which much attention has been paid to minimising the effects of technological uncertainties in the fabrication process, that may degrade the system performance. Based on that analysis, the physical layout of the converter has been defined. By using a double masking technique, the fabrication of the device is very tolerant with respect to the alignment of the grating mask to the waveguide mask. Several converters have been realised, on different wafers and in different batches. The experimentally determined resonance wavelength was 655.3 ± 4.3 nm, matching well the theoretically predicted value of 655 ± 3.7 nm. The on-chip variation in the resonance wavelength was smaller than 0.1nm. The device losses of the converter are 3 ± 0.3dB/cm for both TE and TM polarisation. 98% conversion has been obtained for a converter with a length of 12 mm. An experimentally observed beat pattern in the converter could be explained (using 2D BPM simulations) as being due to a leaky mode which is captured in the grating structure. The converter has already been successfully applied in two types of sensors. Also, due to the narrow wavelength response, the converter offers the potential of implementation as a wavelength selective element in ADMs.

References

[1] K.Okamoto, K.Takiguchi, and Y.Ohmori. 16-channel optical add/drop multiplexer using silica-based arrayed-waveguide gratings. *Electronic Letters*, 31:723–724, 1995.

[2] C. Stamm and W. Lukosz. Integrated optical difference interferometer as immunosensor. *Sensors and Actuators B*, 31:203–207, 1996.

[3] F.Wehrmann, C.Harizi, H.Herrmann, U.Rust, W.Sohler, and S.Westenhofer. Integrated optical, wavelength selective acoustically tunable 2 x 2 switches (add-drop multiplexers) in $linbo_3$. *IEEE Journal of Selected Topics in Quantum Electronics*, 2:263–296, 1996.

[4] Y.Shani, R.Alferness, T.Koch, U.Koren, M.Oron, B.I.Miller, and M.G.Young. Polarisation rotation in asymmetric periodic loaded rib waveguides. *Applied Physics Letters*, 11:1278–1280, 1991.

[5] F. Heismann, L.L. Buhl, and R.C. Alferness. Electro-optically tunable, narrowband $ti : linbo_3$ wavelength filter. *Electronic Letters*, 23:572–574, 1987.

[6] Z. Tang, O.Eknoyan, H.F. Taylor, and V.P. Swenson. Tunable guided-wave optical polarisation converter in lithium tantalate. *Applied Physics Letters*, pages 1059–1061, 1993.

[7] T.M.Koster and P.V.Lambeck. Thermally tunable polarisation converter. *Submitted to Pure and Applied Optics*.

[8] K.Mertens, B.Opitz, R.Hovel, K.Heime, and H.J.Schmitt. First realised polarisation converter based on hybrid supermodes. *IEEE Photonics Technology Letters*, 10:388–390, 1998.

[9] V.P. Tzolov and Marie Fontaine. A passive polarisation converter free of longitudinally-periodic structure. *Optics Communications*, 127:7–13, 1996.

[10] J.J.G.M.van der Tol, F.Hakinzadeh, J.W.Pedersen, and H.van Brug D.li. A new short and low-loss passive polarisation converter on inp. *IEEE Photonics Technology Letters*, 7:32–34, 1995.

[11] T.Lang, F Bahnmuller, and P.Benech. New passive polarisation converter on glass substrate. *IEEE Photonics Technology Letters*, 10:1295–1297, 1998.

[12] T.M.Koster and P.V.Lambeck. Fabrication tolerant passive polarisation converter realised in SiON technology. In *Proc. LEOS Benelux Chapter, 26 november, Gent, Belgium, 1998*, pages 117–120, 1998.

[13] C.M. Weinert and H.Heidrich. Vectorial simulation of passive te/tm mode converter devices on inp. *IEEE Photonics Technology Letters*, pages 324–326, 1993.

[14] T.M.Koster, N.E.Posthuma, and P.V.Lambeck. Fully integrated optical polarimeter. In *Proceedings Europt(r)ode V, 16-19 April 2000 Lyon, France*, 2000.

[15] H. Kogelnik and V. Ramaswamy. Scaling rules for thin-film optical waveguides. *Applied Optics*, 13:1857–1862, 1974.

[16] K.Worhoff, A.Driessen, P.V.Lambeck, L.T.H.Hilderink, P.W.C.Linders, and T.J.A.Popma. Plasma enhanced chemical vapour deposition silicon oxynitride optimised for application in integrated optics. *Sensors and Actuators A*, 74:9–12, 1999.

[17] 2d mode solver selene, bbv software bv, Enschede, The Netherlands.

[18] E.C.M. Pennings. *Bends in optical ridge waveguides : modelling and experiments*. PhD thesis, University of Delft, Delft, The Netherlands, 1990.

[19] H.Berends. *Integrated optical bragg reflectors as narrowband wavelength filters*. PhD thesis, University of Twente, Enschede, The Netherlands, 1997.

[20] Fimmwave, 2d vectorial mode solver, photon design, Oxford, United Kingdom.

[21] K. Mertens, B. Scholl, and H.J. Schmitt. Strong polarisation conversion in periodically loaded strip waveguides. *IEEE Photonics Technology Letters*, 8:1133–1135, 1998.

[22] J.J.G.M.van der Tol, J.W.Pedersen, E.G.Metaal, Y.S.Oei, F.H.Groen, and I.Moerman. Efficient short polarisation converter. *Proceedings ECIO 1995, Delft, The Netherlands*, pages 319–322, 1995.

[23] T.M.Koster and P.V.Lambeck. Integrated optical platform for absorptive sensing of chemical concentrations using chemo-optical monolayers. *submitted to Sensors and Actuators B*.

[24] B.E.Lemoff, L.B.Aronson, and L.A.Buckman. A low cost multi wavelength local area network. *The Hewlett Packard Journal*, pages 42–52, 1997.

[25] C.K. Madsen and J.H. Zhao. *Optical filter design and analysis: a signal processing approach*. John Wiley and Sons, 1999.

[26] B.E. Little, C. Wu, and W.P. Huang. Synthesis of ideal window filter response in grating-assisted couplers. *Optics Letters*, 21:725–727, 1996.

III. Thermally tunable polarisation converter

Abstract- Polarisation converters based on grating structures generally show a small conversion bandwidth only. Therefore, due to technological uncertainties it cannot be guaranteed that the resonance wavelength of a fabricated converter coincides with its intended value. In this paper, we report the design of a polarisation converter, consisting of alternating segments of asymmetrically etched ridge waveguide segments, of which the resonance wavelength can be tuned thermo-optically to its intended value. The converter has been realised in SiON technology in combination with polymers. It has been calculated, that with an actuation power of maximally only 214 mW, the shift in the resonance wavelength due to technological uncertainties can be compensated for. A demonstrator device has been fabricated, showing a wavelength shift of 12 nm (@670nm) for a temperature increase of 100 K.

1. INTRODUCTION

During the fabrication of integrated optical devices, technological uncertainties may result in a deterioration of the performance of a fabricated device with respect to its intended one. Therefore, when optimising the device performance, during the design stage, these technological uncertainties also have to be taken into account as to minimise their effect on the degradation of the performance. This will result in a higher reproducibility upon fabrication and this into a higher yield.

For some integrated optical devices however, the requirements to these tolerances are too tight, and the desired performance of the circuit cannot be guaranteed. These fabrication intolerant devices can be dealt with in two ways. One is to accept that a certain fraction of the devices does not satisfy the performance requirements and discard them, thereby lowering the yield. Another approach is to implement a tuning facility into the device in order to adjust some critical device parameters to their intended value [1] [2].

Recently, in our group a polarisation converter was developed, which consists of an asymmetrical grating structure realised in SiON technology [3]. The converter is implemented in several integrated optical sensing platforms, one of which is a fully integrated optical polarimeter [4]. Here, the converter is used to obtain a 50:50 power splitting over the lowest order TE and TM mode before the light enters the sensing function. After sensing, a second converter is used to obtain interference of the TE and TM mode, with as an output two other TE and TM modes of which the powers are related to a measurand induced phase shift.

Although the device has been designed for minimising the effects of the technological tolerances, an analysis indicated that the spread in the resonance wavelengths of fabricated converters can be expected to be much larger than the full

width half maximum (FWHM) conversion bandwidth, being 8.6 nm and 0.25 nm, respectively. As a result, the obtained amount of conversion at the intended operating wavelength is far from the intended one. In our laboratory, this shift in the resonance wavelength causes no problem for the characterisation of the converter and the sensing platforms as a tunable lightsource was available, so the operating wavelength could be tuned to the resonance wavelength of a fabricated converter. However, for the commercialisation of the sensing platforms in which the converter is to be implemented, a cheap single line light source is a pre. Hence, the problem of the resonance wavelength shift has to be solved.

The deviation between the resonance wavelength of a realised converter and its intended value is mainly due to a shift in the effective index difference between the lowest order TE and TM mode, ΔN. In order to adjust the resonance wavelength, a thermo-optical tuning facility can be implemented for counterbalancing that shift.

In this paper, thermal tuning of a polarisation converter will be presented. First, the polarisation converter will be introduced. Next, thermal tuning of the converter will be treated, after which in section three the optimisation of the thermally tunable polarisation converter will be given. Experimental results obtained from a demonstrator-type device will be presented in section four. This paper closes with a summary of the main results.

2. Analysis

The polarisation converter which was developed [3] earlier is a co-directional grating assisted coupler with a grating period Λ, as shown in figure 1. The grating consists of alternating segments with an asymmetrical cross section. Due to this asymmetry at the transition between adjacent segments, there is a non-zero overlap

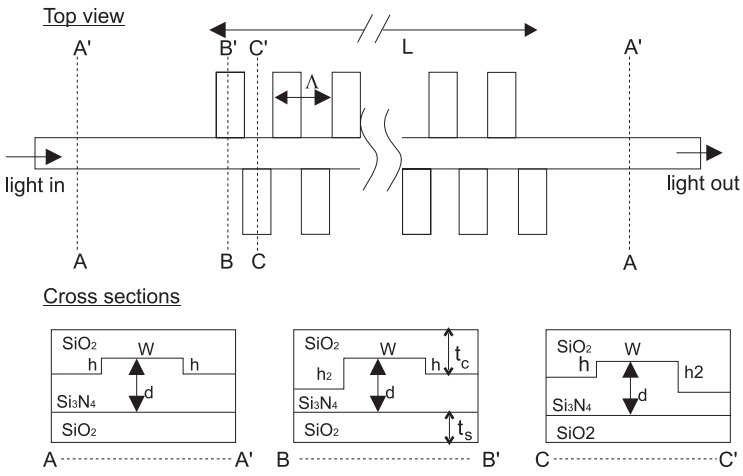

Figure 1. Structure (topview and sideview) of the polarisation converter.

between the TE and TM fields of these segments. As the converter is a grating structure, a significant amount of conversion is achieved only in a small wavelength region around the resonance wavelength, λ_r, which is given by the phase match relation [5]

$$\lambda_r = (N_{TE} - N_{TM})\Lambda \equiv \Delta N \Lambda. \tag{1}$$

where N_{TE} and N_{TM} are the effective refractive indices of the TE and the TM zeroth order mode, respectively. In figure 2, the typical wavelength response of a polarisation converter of this type is shown, as calculated for the design given in figure 1.

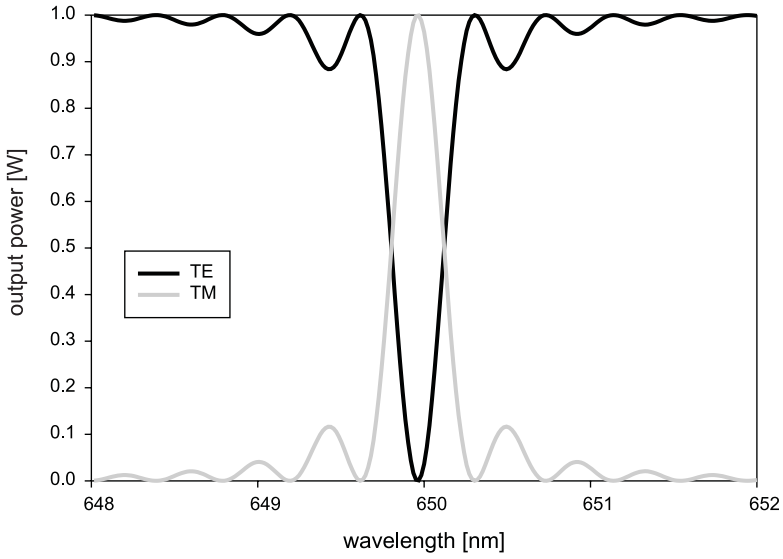

FIGURE 2. Typical (calculated) wavelength response of the polarisation converter.

Although the converter design had been optimised, amongst others by making it as insensitive as possible to technological uncertainties, the resonance wavelength λ_f of a fabricated converter always differs from its intended value λ_i. The deviation in the wavelength, $\Delta\lambda_f$, is mainly caused by the deviation $\delta\Delta N$ in the effective index difference ΔN.

$$\Delta\lambda_f = (\lambda_f - \lambda_i) = \left(\delta\Delta N|_{\lambda_i} + \frac{\partial \Delta N}{\partial \lambda}|_{\lambda_i}\Delta\lambda_f\right)\Lambda, \tag{2}$$

where the second term on the right hand side arises from the waveguide dispersion.

Now, assume an external tuning mechanism, controlled by a tuning parameter x, which induces small changes in the refractive index distribution of the optical layer system. By this tuning mechanism, a shift in the resonance wavelength $\Delta\lambda_t$ will be introduced, equal to

$$\Delta\lambda_t = (\lambda_t - \lambda_f) = \left(\frac{\partial \Delta N}{\partial x}|_{x=x_0} (x - x_0) + \frac{\partial \Delta N}{\partial \lambda}|_{\lambda_f} \Delta\lambda_f \right) \Lambda. \tag{3}$$

Assuming the derivatives in the dispersion terms in both (2) and (3) to be identical, which is a very good approximation for the small wavelength shifts in our devices, it can readily be seen that in order to have $\Delta\lambda_t = -\Delta\lambda_f$, the tuning parameter x has to be set to (see figure 3)

$$x = x_0 + \frac{\delta \Delta N}{\frac{\partial \Delta N}{\partial x}|_{x=x_0}}, \tag{4}$$

In order to induce changes in the refractive index distribution, physical cross effects can be exploited: electro-optical [6], magneto-optical [6], elasto-optical [7], mechano-optical [8] or thermo-optical [9]. The technologically simplest tuning method is the thermo-optical one using a heater electrode.

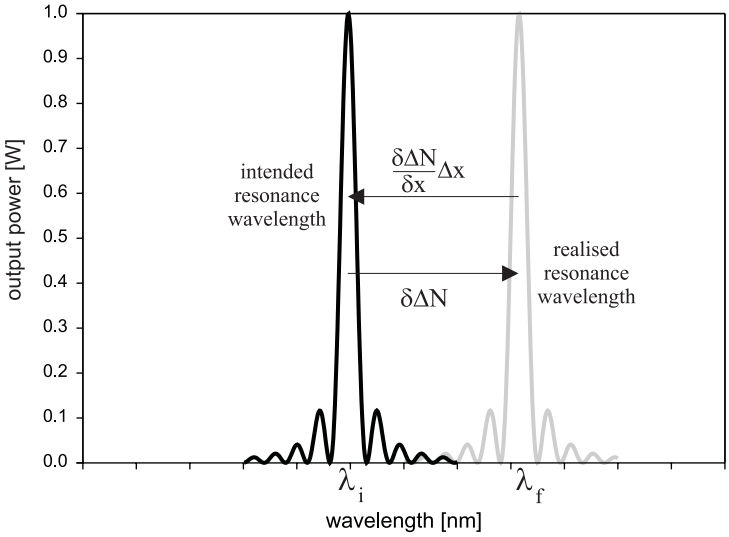

FIGURE 3. A tuning mechanism with tuning parameter x can be used to counterbalance the shift in ΔN due to technological uncertainties.

Then, (4) can be written as

$$T = T_0 + \frac{\delta\Delta N}{\frac{\partial\Delta N}{\partial T}|_{T=T_0}}, \tag{5}$$

$$P_e = P_0 + \frac{\delta\Delta N}{\frac{\partial\Delta N}{\partial P_e}|_{P_e=P_0}},$$

depending on whether the temperature T of the heater electrode or the electrical power P_e dissipated by the heater electrode is taken as the actuation parameter. Here, T_0 is the ambient temperature. In the remaining part of this paper, it will be assumed that this ambient temperature is constant and that $\Delta\lambda_f$ is defined at this temperature T_0.

From (1) it can be derived that the wavelength shift corresponding to a given temperature T of the heater electrode equals

$$\Delta\lambda_t = \frac{\frac{\partial\Delta N}{\partial T}|_{T=T_0}}{\frac{1}{\Lambda} - \frac{\partial\Delta N}{\partial\lambda}|_{\lambda=\lambda_i}}(T - T_0) \tag{6}$$

The denominator of the quotient on the right hand side is a function of the optical field distribution only. The numerator is a function of both the thermal and optical field distribution.

Note that, as the use of heater electrodes affords a wavelength shift in one direction only, the sign of $\frac{\partial\Delta N}{\partial T}$ determines whether $\frac{\partial\lambda}{\partial T}$ is positive or negative. Therefore, all possible λ_f must be on one side of λ_i.

From the analysis it follows that the main objectives of the design should be maximising $\frac{\partial\Delta N}{\partial T}$, while keeping a small $\Delta\lambda_{f,max}$.

3. Design of a thermo-optically tuned polarisation converter

First, the design objectives, the boundary conditions and the free design parameters will be stated. Next, the systematical design of the tunable converter, resulting in an optimised layer structure, will be discussed.

The main design objective is that the maximum expectable shift in the effective index difference $\delta\Delta N_{max}$ due to technological uncertainties can be compensated for by tuning. In addition, the electrical power required for obtaining a $-\delta\Delta N_{max}$ should be as low as possible.

We are starting from the design as given by figure 1. Because the function of the cladding material has to be extended from being protective only to being also thermo-optical, the choice of this material has to be reconsidered. Because this may imply a change in the refractive index of the material, also the optimal thickness of the core layer, i.e. the thickness where $\frac{\partial\Delta N}{\partial d} = 0$ [3] and the grating period have to be adapted. As a result of the introduction of temperature effects, also the temperature distribution in the system becomes relevant and therefore also

the thickness of the cladding and substrate layer come into play in an additional way. The heat will be generated in a metal Cr/Au electrode on top of the cladding layer, and the dimensions of this electrode have to be defined. In addition it has to be considered whether the system outside the optical field region can be modified in order to maximise $\frac{\partial \Delta N}{\partial T}$. For this, two options have been investigated; making grooves in the multi layer structure and removal of the Silicon underneath the converter. The free design parameters are given in figure 4.

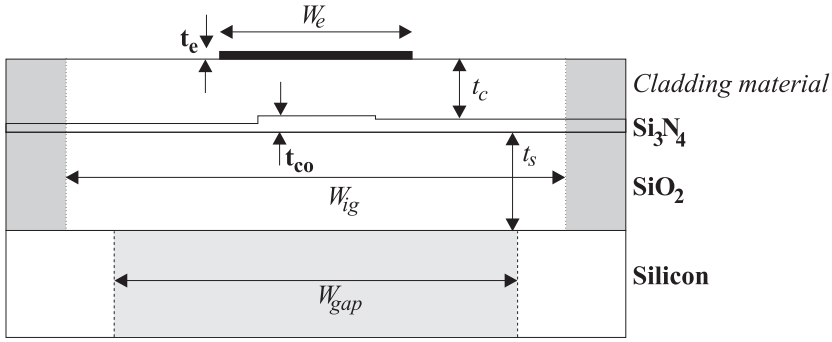

FIGURE 4. The free design parameters.

It appeared that the design process could be divided into a series of steps, ordered in such a way that in each step the optimum parameters found in previous steps could be well used in the calculations.

Because the substrate and core layer are SiON materials, practically the choice will be a SiON or a polymer cladding. In the table, the relevant material properties of SiON and polymers are given, i.e. the thermo optical coefficient $\frac{\partial n}{\partial T}$, the thermal conductivity κ, the maximum temperature the material can be exposed to, T_{max}, and the uncertainty δn in the refractive index of the material on deposition.

Material	$\frac{\partial n}{\partial T}$ [/K]	κ [W/m K]	T_{max} [^{0}C]	δn	n
SiON	$\approx 1 * 10^{-5}$	1.4	300	$2 * 10^{-3}$	1.46
polymer	$-1.1 * 10^{-4}$	0.2	100-150	$1 * 10^{-3}$	1.51

In the last column, the refractive index of the material around which this δn is achieved is given.

Considering the thermo-optical coefficient and the maximum temperature, it is clear that a the polymer allows for a larger changes in its refractive index (0.01-0.015) than the SiON-cladding (0.003), while in addition the uncertainty in its refractive index is lower.

$\frac{\partial \Delta N}{\partial T}$ is made up of contributions from the individual optical layers. From perturbation theory [10], it can be derived that

$$(7) \quad \frac{\partial \Delta N}{\partial T}\Delta T = \sum_{i=1}^{3} 8\epsilon_0 n_i c \iint_{t_i} \frac{\partial n_i}{\partial T}\Delta T(x,y)\left(\overline{\mathbf{E}}_{TE}\cdot\overline{\mathbf{E}}_{TE} - \overline{\mathbf{E}}_{TM}\cdot\overline{\mathbf{E}}_{TM}\right)dxdy,$$

with $\overline{\mathbf{E}}_{TE}$ and $\overline{\mathbf{E}}_{TM}$ the normalised electric field vectors of the TE and TM mode, respectively, ϵ_0 the dielectric permittivity of vacuum, c the light velocity in vacuum, the parameter 'i' refers the different layers and z is the propagation direction.

Due to the difference in the sign of the thermo-optical coefficients of SiON and the polymer, the contributions of index changes of the individual layers to the total effective index difference, might cancel out, resulting in a $\frac{\partial \Delta N}{\partial T} = 0$.

For the system we finally realise, for a temperature distribution which is homogeneous throughout the optical layer system, the contributions of the individual layers to $\frac{\partial \Delta N}{\partial T}$ have been calculated to be $+2.4 * 10^{-5}$/K (cladding), $+3.3 * 10^{-6}$/K (core) and $-1.6 * 10^{-6}$/K (substrate). It can be seen that in this example, the contribution from the cladding layer is an order of magnitude larger than the other contributions. Therefore, it can be concluded that for realistic temperature distributions, this difference in the sign of the thermo-optical coefficients will not be a problem.

Taken all considerations mentioned above into account, a polymer with a refractive index of 1.51 is used.

For the further design, two programs have been used. One is ATRguide, a 1-D slab mode solver developed within our group, the other is TempSelene [11], a commercially available 2-D mode solver designed to calculate effective indices of modes taking temperature induced refractive index distributions into account.

With the cladding material chosen, an optimum core layer thickness of 140 nm has been calculated using a tolerance analysis similar to that in [3]. With the materials used and taking their technological uncertainties into account, for this system a maximum deviation of ± 2.5 nm from the design wavelength can be expected. Now the first design aim can be quantified: in order to guarantee that the resonance wavelength can be set to the intended 655 nm, the converter has to be designed for a wavelength of 652.5 nm and a tuning range of 5 nm must be achieved.

Minimum cladding and substrate thicknesses arise from the requirement that optical losses originating from the electrode and Silicon substrate have to be lower than 0.01 dB/cm. These minimum thicknesses can be calculated to be 1.5 μm in both cases.

At this point, the optical structure is completely defined. All not yet defined parameter values influence the temperature distribution only and they have to be optimised to give a maximum $\frac{\partial \Delta N}{\partial P_e}$.

Now, the substrate layer thickness, which manifests itself in its effect on the temperature distribution through the optical layer system, and hence $\frac{\partial \Delta N}{\partial P_e}$, will be

optimised. In the discussion about the cladding material, it was shown that of all optical layers the largest contribution to $\frac{\partial \Delta N}{\partial T}$ will be from the polymer cladding layer. Therefore it is desired that in the polymer large temperature changes are induced. Under the approximations that the temperature distribution only has a transversal dependence (i.e. perpendicular to the optical layers), radiation into the air can be neglected and that the Silicon substrate acts as a heatsink with constant temperature T_0, in figure 5 for several SiO_2 cladding layer thicknesses the temperature distribution in the layer systems are given for a temperature of the heater electrode of $T_e = T_0 + 10^o$C. It can be seen that large SiO_2 thicknesses are favoured. The maximum thickness of the substrate layer depends on the deposition process of this layer. If standard wet thermal oxidation is used, due the the square root dependence of the oxide thickness versus the growth time, the fabrication of very thick layers takes a very long time. A substrate layer thickness of 10 μm will be taken, which is technologically well feasible using rapid thermal oxidation techniques.

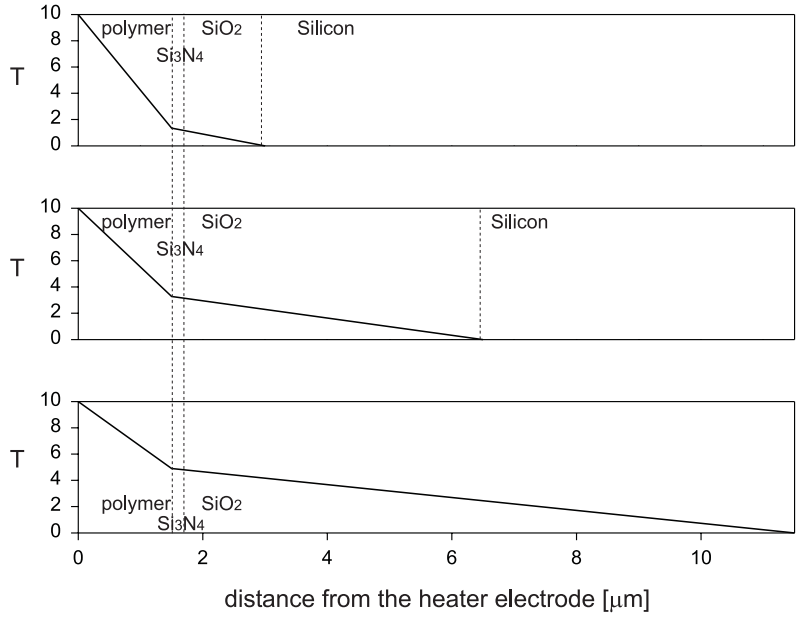

FIGURE 5. The one dimensional temperature distribution throughout the layer system for different SiO_2 layer thicknesses. The dashed lines indicate the interfaces between different layers.

A gold heater electrode will be used, of which the thickness and width have to be optimised. The electrode should be small in order to minimise the actuation power. A lower limit to the electrode width is given by the fact that for too small a width due to the negative thermo-optical coefficient the waveguide becomes non-guiding

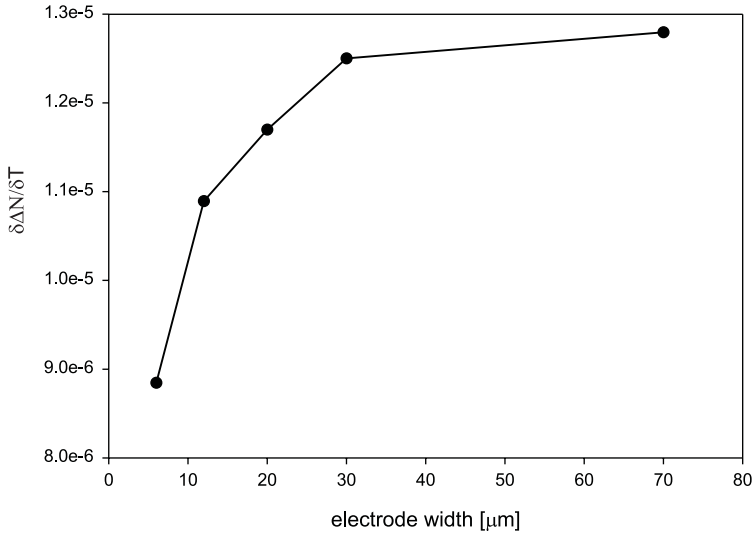

FIGURE 6. $\frac{\partial \Delta N}{\partial T}$ versus the electrode width.

in the lateral direction. In figure 6, $\frac{\partial \Delta N}{\partial T}$ is shown as a function of W_e. As expected, for larger widths of the electrode, the curve flattens, and here the 1-dimensional approximation used above is valid.

The thickness-width-length ($t_e - W_e - L_e$) combination of the electrode determines the voltage V required for a certain P_e,

$$V = \sqrt{\frac{P_e \rho L_e}{W_e t_e}}. \tag{8}$$

For a $W_e = 30\ \mu m$, $t_e = 0.5\ \mu m$, $L_e = 5$ mm and taking a ρ of $2.2 * 10^{-8}\ \Omega m$, $V = 2.7\sqrt{P_e}$.

In order to suppress the lateral heat flow, isolation grooves can be applied [9], see figure 4. However, in our case, due to the large lateral mode width ($1/e^2$ values of 15-20 μm), the minimum distance between the isolation grooves has to be 30-40 μm in order not to influence the modal propagation. Calculations showed that for these distances, the lateral heat flow is negligible and therefore the effect of isolation grooves is negligible. Hence, no isolation grooves will be applied.

The complete sensor is realised on top of a Silicon wafer, which acts as a heat sink. By partly removing the Silicon underneath the converter, the heat sink is placed further away from the heater. As a result, for a given electrode temperature larger refractive index changes are obtained and hence a larger $\frac{\partial \Delta N}{\partial T}$. In figure 7 for $W_e = 30\ \mu m$, $\frac{\partial \Delta N}{\partial T}$ is shown as a function of the gap width (see figure 4). A gap of

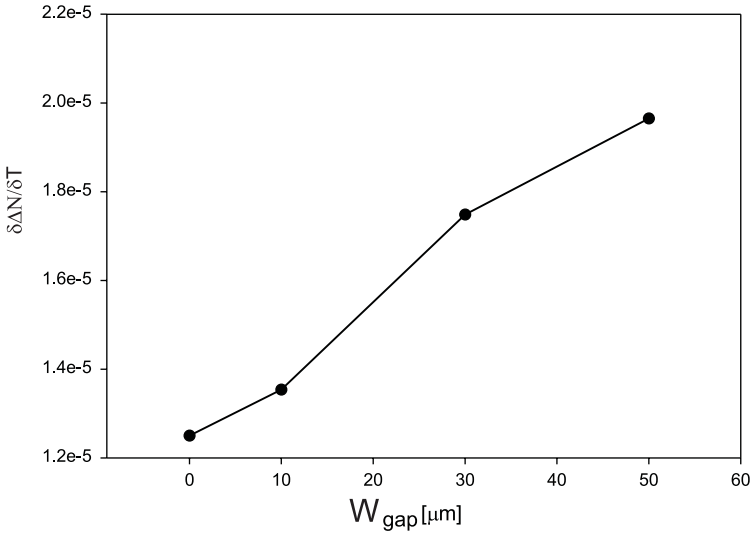

FIGURE 7. $\frac{\partial \Delta N}{\partial T}$ versus the width of the etched region, W_{gap}.

50 μm results in an increase in $\frac{\partial \Delta N}{\partial T}$ of nearly 1.5 times compared to the situation where no gap is present.

The optimised device structure is shown in figure 8. The wavelength shift as a function of the actuation power is

$$\Delta\lambda_t = \frac{\frac{\partial \Delta N}{\partial T}|_{T=T_0}}{\frac{1}{\Lambda} - \frac{\partial \Delta N}{\partial \lambda}|_{\lambda=\lambda_i}} \frac{\partial T_e}{\partial P_e}|_{P_e=0} P_e \tag{9}$$

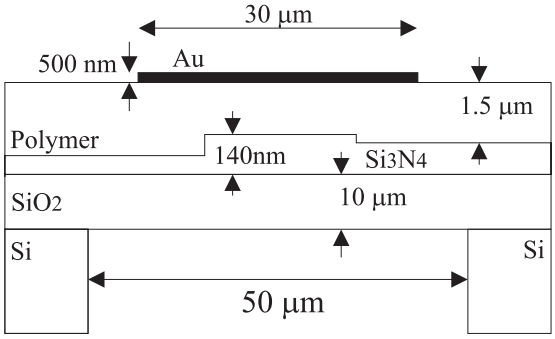

FIGURE 8. The optimised device with all optimised parameters.

For the optimised device structure with a W_e of 30 μm, $\frac{\partial \Delta N}{\partial T} = 1.96 * 10^{-5}$ /K, $\frac{1}{\Lambda} = 1.47 * 10^{-4}$, $\frac{\partial \Delta N}{\partial \lambda} = 4.6 * 10^{-6}$ and $\frac{\partial T_e}{\partial P_e} = 180$ (calculated using [11], for a converter length of 5 mm [4]). Expressed in terms of the required electrical actuation power P_e, the wavelength shift $\Delta\lambda_t$ then equals

$$\Delta\lambda_t[nm] = 23.3 P_e[W], \tag{10}$$

which means that for a $\Delta\lambda_{t,max}$ of 5 nm, a maximum electrical actuation power of 214 mW is required. With an electrode thickness of 0.5 μm, this $P_{e,max}$ corresponds to a maximum actuation voltage of 1.25 V. This power corresponds to a temperature of the heater electrode $T_e = T_0 + 36K$. If it is assumed that the device operates at room temperature (20-30 degrees Celcius), this T_e is well below the T_{max} of the polymer.

The maximum wavelength shift which can be achieved with the optimised device equals $\Delta\lambda_{t,max} = 0.13(T_{max} - T_0)$ nm. For a T_{max} of 100 degrees Celcius (assuming $T_0 = 20$ degrees Celcius), a $\Delta\lambda_{t,max}$ of 10.4 nm can be achieved for a $P_e = 472$ mW.

So it can concluded that for the designed structure, the resonance wavelength of a fabricated converter can be driven to its intended value, and therefore to the wavelength of the intended lightsource, by thermo-optical tuning. The calculated maximum wavelength shift, approximately 10 nm, is twice as large as the required 5 nm.

4. Demonstrator device

In order to prove the feasibility of the thermally tunable polarisation converter, the demonstrator-device shown in figure 9 was realised.

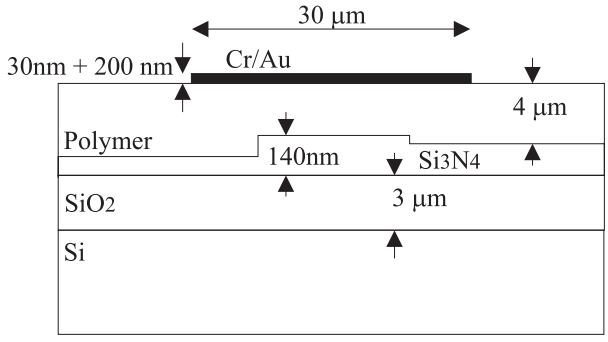

Figure 9. The realised demonstrator device.

In a first prototype, unfortunately there was no electrical contact between the bondpads and the heater electrode. To get an impression of the temperature effects,

now the complete wafer is heated. In figure 10, the the experimentally observed wavelength shift $\Delta\lambda_t$ as a function of the temperature of the wafer is shown. As expected, $\Delta\lambda_t$ is positive, i.e. the resonance wavelength increases with increasing temperature. Also, the relation between $\Delta\lambda_t$ and the temperature is linear. A wavelength shift of 12 nm was achieved for a temperature increase of 100 K, corresponding to a $\frac{\Delta\lambda}{\Delta T} = 0.12$. For a homogenous temperature distribution throughout the realised waveguide structure, a $\frac{\Delta\lambda}{\Delta T} = 0.17$ can be calculated, i.e. of the same order of magnitude as experimentally determined, indicating the applicability of the model.

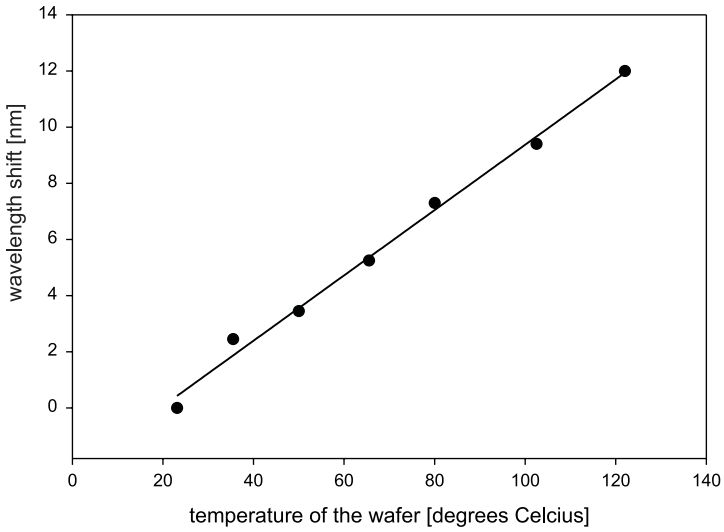

FIGURE 10. The measured wavelength shift as a function of the wafer temperature.

5. SUMMARY

In order to compensate for deviations in the resonance wavelength of a fabricated polarisation converter, which are due to deviations in the effective index difference ΔN between the TE_{00} and TM_{00} mode caused by technological uncertainties, a thermal tuning facility was investigated. With a heater electrode, a change in the refractive index distribution is generated which results in a shift in ΔN which counterbalances the shift due to technological uncertainties. A design is presented which requires an electrical actuation power of maximally 214 mW (actuation voltage 1.25 V) in order to compensate for wavelength shifts up to 5 nm. A demonstrator device, showing a 12 nm wavelength shift for a temperature increase of 100 K is presented.

References

[1] B.J. Offrein, F. Horst, G.L. Bona, R. Germann, H.W.M. Salemink, and R. Beyeler. Adaptive gain equaliser in high-index-contrast SiON technology. *IEEE Photonics Technology Letters*, 12:504–506, 2000.

[2] H. Toba, K. Oda, and K. Nosu. 16 channel optical fdm distribution/transmission experiment utilising multichannel frequency stabiliser and waveguide selection switch. *Electronic Letters*, pages 574–576, 1989.

[3] T.M.Koster and P.V.Lambeck. Fabrication tolerant passive polarisation converter realised in SiON technology. In *Proc. LEOS Benelux Chapter, 26 november, Gent, Belgium, 1998*, pages 117–120, 1998.

[4] T.M.Koster, N.E.Posthuma, and P.V.Lambeck. Fully integrated optical polarimeter. In *Proceedings Europt(r)ode V, 16-19 April 2000 Lyon, France*, 2000.

[5] Amon Yariv. *Optical waves in crystals*. John Wiley and Sons, New York.

[6] E. Hecht. *Optics*. Addison-Wesley.

[7] T.Lang, F Bahnmuller, and P.Benech. New passive polarisation converter on glass substrate. *IEEE Photonics Technology Letters*, 10:1295–1297, 1998.

[8] G.J. Veldhuis, C. Gui, T. Nauta, T.M. Koster, J.W. Berenschot, P.V. Lambeck, J.G.E. Gardeniers, and M. Elwenspoek. Mechano-optical waveguide on-off intensity modulator. *Otpics Letters*, 23:1532–1534, 1999.

[9] M. Hoffmann. Thermo-optical digital switches on silicon. *Proceedings ECIO*, pages 403–406, 1995.

[10] T. Tamir and R.C. Alferness. *Guided-wave optoelectronics*. Springer Verlag.

[11] 2d mode solver selene, bbv software bv, Enschede, The Netherlands.

IV. Mode selective waveguide-detector couplers

Abstract- The design, realisation and experimental results of coupling structures for partial or complete power transfer from an optical waveguide into a photo detector are presented. The coupling structures are based on thinning down the core layer at the position of the detector, resulting in a widening of the mode profile and leaky wave coupling into the detector. By an appropriate design of the layer system, the coupling structure can be made mode selective, allowing different modes to be coupled into different detectors. Experimental results show a controlled partial power transfer to the detector, which is in excellent agreement with the model. A mode selectivity of -13 dB (TM_{00} over TE_{00}) has been obtained.

1. Introduction

The use of Silicon wafers as platforms for integrated optical circuits offers the possibility of integrating optics and electronics in order to obtain cheap, compact and reliable optoelectronic devices [1],[2]. The fields of application of such devices are in either one of the rapidly growing areas of communication networks [3] or optical sensors [4].

Systems which consists of a waveguide circuit combined with photo detectors are a well known class of optoelectronic devices. Examples of these devices are optical taps [5], optoelectronic sensors [6] and coherent receiver front ends [7]. In these devices, efficient transfer of optical power from a waveguide into a photo detector is desired. This power transfer is achieved by using coupling structures, of which two types can be discerned: but coupling [1] and leaky wave (or evanescent field) coupling [8]. With the first type, the light is launched into the photo detector using end-fire coupling, a common technique in III-V materials [1]. In the latter type, optical power is coupled into a detector by means of penetration of the evanescent field of the guided mode into the detector. Both types permit for complete power transfer from a waveguide to a detector. However, only with leaky wave coupling structures, mode selective coupling [9] and tapping, ie. partial power transfer, is possible. Mode selective coupling means that different modes, be it of different order or polarisation, are coupled into different detectors. This way, mode specific information can be detected. By means of tapping, reference signals for intensity referencing or for feedback control loops [10] are obtained. Currently, in our group two bi-modal sensors (using the lowest order TE and TM modes) are developed [11], which both require mode selective coupling from a waveguide to a detector and tapping. Hence, our investigations have focussed on leaky wave coupling structures.

In literature, several Silicon based waveguide-detector coupling structures based on leaky wave coupling have been presented [2],[8],[12],[13]. In these structures, the

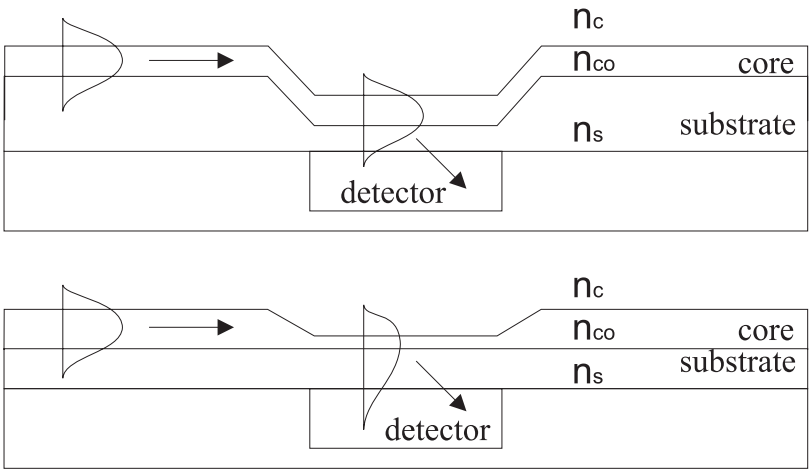

FIGURE 1. Waveguide-detector coupling structures with a thinned substrate layer(top) and with a thinned core layer (bottom).

(low index) substrate layer in between the high index core layer and the Si wafer is thinned down, thereby letting the evanescent field penetrate into the Silicon photo detector, see figure 1. In this paper, we present another type of coupling structure where instead of the buffer layer the high index core layer is thinned down [9], see figure 1. Due to this thinning down of the core layer, the width of the mode field increases [14] and it can penetrate into the photo detector.

Compared to the coupling structures where the substrate layer is thinned down, our coupling structure offers the adavantage of a much higher mode selectivity. Furthermore, the here presented coupling structure is simple to realise, as it requires only one additional etch step. In the case of thinning down the substrate layer typically a few hundred nanometer to a micrometer have to be etched off. With the here presented coupling structures, the core layer thickness has to be etched back 30-100 nm only. Also, the etching of our core layer (Si_3N_4) results into a more adiabatic tapering and hence the coupling to the photo detector should be more efficient than in the case of tapering a SiO_2 substrate layer.

By an appropriate design of the layer system, these coupling systems permit for mode dependent or independent coupling from a waveguide into a detector. However, as for our specific application circuits mode selectivity is desired, here the focus is on mode selective coupling structures. More specific, we will deal with mode selective coupling structures which are able to couple the lowest order TE and TM modes in separate detectors.

In section two, the analysis and the design of the coupling structures will be presented, after which in section three in short the fabrication of the coupling structures will be described. Experimental results and a discussion thereof are given in section four, after which, in section five, a summary is given.

2. Analysis and design

In this section, first a qualitative analysis of the coupling structure will be given. Next, within the boundary conditions dictated by the specific application circuits, the design of several coupling structures will be presented.

The coupling principle is based on locally, at the position of the detector, thinning down the core layer close to the cut-off thickness of the mode which has to be coupled into the detector. Due to this thinning, the mode profile widens [14] and can penetrate through the substrate layer into the detector, see figure 1. This way, a leaky mode coupling of the optical power into the detector is achieved. In order to suppress the mode widening at the cladding layer side, the layer system has to be asymmetric with $n_c < n_s$ and a high transversal index contrast is preferred. A large mode selectivity can be obtained if the modes propagate through a high index contrast waveguide, as there is a large difference between the cut-off thicknesses of the modes. If the modes have the same mode order but differ in their polarisation, it is especially the asymmetry which together with a high index contrast ensures a large difference in the cut-off thicknesses, and hence a large mode selectivity.

The detectors as presented in this paper are meant for implementation in several integrated optical sensor circuits. One of these circuits is the fully integrated optical polarimeter [11], as seen in figure 2, where separate detection of TE_{00} and TM_{00} modes is required for increasing the resolution of the sensor. In this monomodal circuit, three different coupling structures have to be implemented. The first one (1) is used to couple a small part of the (completely TE polarised) input light into a detector for intensity referencing. The second coupling structure (2) must couple all power carried by the TM_{00} mode into a detector. As there is also the TE_{00} mode propagating in the same channel, this coupling structure must be as mode selective as possible. Finally, a third coupling structure (3) is required to couple the power carried by the remaining TE_{00} mode into a detector. The first and last coupling structures do not have to be mode selective, as here only the TE_{00} mode is propagating through the structure. As in leaky wave coupling, the amount of optical power transferred to the detector is governed by the length of the coupling region, the first coupling structure can, except for its shorter length, be taken identical to the last one. The operating wavelength of the polarimeter is

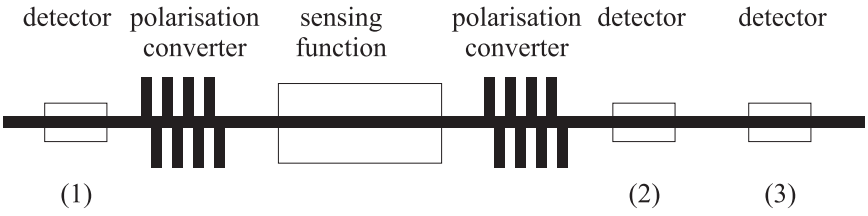

Figure 2. The fully integrated optical polarimeter, indicating the position of the different coupling structures.

655 nm, which will also be the wavelength for which the coupling structures will be designed.

The optimum layer stack with the largest asymmetry and hence largest difference in cutoff thickness can be derived using a normalised analysis based on the normalised parameters b, a and V given in [14]. The normalised cut-off thickness V of a mode in a three layer waveguide system equals

$$V_{co,m} = m\pi + \arctan\sqrt{a_{TEorTM}} \tag{1}$$

with m the mode number and a_{TEorTM} the asymmetry parameter for TE or TM,

$$a_{TEorTM} = (\frac{n_{co}}{n_c})^{4i} \frac{n_s^2 - n_c^2}{n_{co}^2 - n_s^2} \tag{2}$$

with $i = 0$ for TE and $i = 1$ for TM polarised light. n_{co}, n_s and n_c are the refractive indices of the core, substrate and cladding layer, respectively, with $n_{co} > n_s > n_c$. For any given three layer system, the difference in the normalised cut-off thickness between the n^{th} and $(n+1)^{th}$ order mode is π, independent of the specific asymmetry present in the layer system. For a symmetric three layer system, the cut-off thicknesses are identical for TE and TM modes of the same mode order. For an asymmetric three layer system they differ due to the $(\frac{n_{co}}{n_c})^{4i}$ factor in the asymmetry parameter.

In order to have a large mode selectivity between the TE_{00} and TM_{00} mode, the difference in the normalised cut-off thickness

$$\Delta V_{co} = V_{co,TM} - V_{co,TE} \tag{3}$$

should be as large as possible, as can be seen from the normalised mode width graph in [14].

In figure 3, iso-ΔV_{co} lines are given as a function of $\frac{n_c}{n_{co}}$ and $\frac{n_c}{n_s}$. Note that always $\frac{n_c}{n_s} > \frac{n_c}{n_{co}}$. For asymmetrical layer systems, for a constant $\frac{n_c}{n_s}$ the difference in the normalised cut-off thickness for TE and TM modes of the same order increases monotonously with decreasing $\frac{n_c}{n_{co}}$. With respect to $\frac{n_c}{n_s}$, there is an optimum value for a fixed $\frac{n_c}{n_{co}}$ that can be derived to be equal to $\frac{n_c}{n_s} = \frac{1}{2}\sqrt{2(\frac{n_c}{n_{co}})^2 + 2}$.

A boundary condition to the design is the composition of the layer system in which the coupling structures are going to be implemented. In our case, the complete sensor system has to be realised in the SiO_xN_y material system [15]. As a result, only layers with a refractive index in the range 1.46-2.01 can be realised. The wish to obtain the lowest $\frac{n_c}{n_{co}}$ can be fulfilled by choosing a core layer of Si_3N_4 (n=2.01) and no top cladding, ie. air (n=1.00). The optimum substrate material

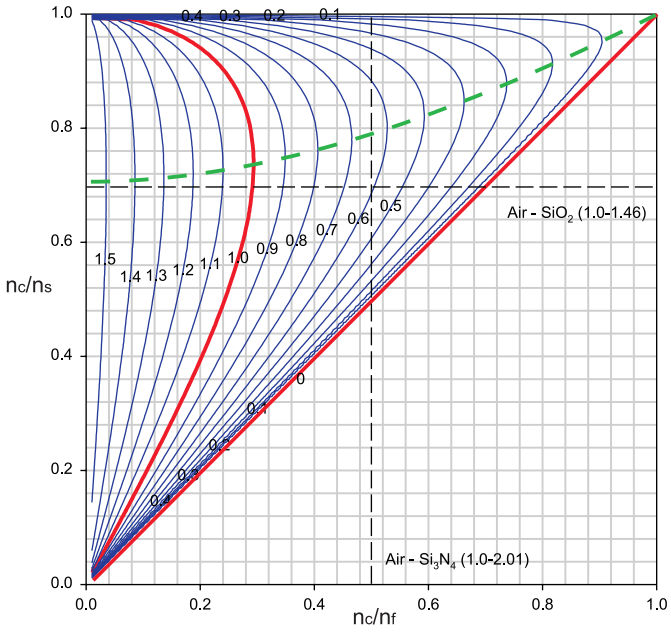

FIGURE 3. Iso-ΔV_{co} lines as a function of $\frac{n_c}{n_{co}}$ and $\frac{n_c}{n_s}$. The dotted line corresponds to $\frac{n_c}{n_{co}} = \frac{1}{2}\sqrt{2(\frac{n_c}{n_{co}})^2 + 2}$

.

then is SiO_2 (n=1.46). Note, that this type of layer structure also gives the highest sensitivity for evanescent field sensing [16] (ie. the application circuits). Now, $\frac{n_c}{n_{co}} = 0.49$ and $\frac{n_c}{n_s} = 0.68$ as can be seen from figure 3, and $V_{co,TM} - V_{co,TE} = 0.61$.

For the optimised material combination of the layer stack and an operating wavelength of 655 nm, the effective indices of the TE_{00} and TM_{00} are calculated as a function of the Si_3N_4 core layer thickness, see figure 4. The cut-off thicknesses for the TE_{00} and TM_{00} mode are 49 nm and 95 nm, respectively.

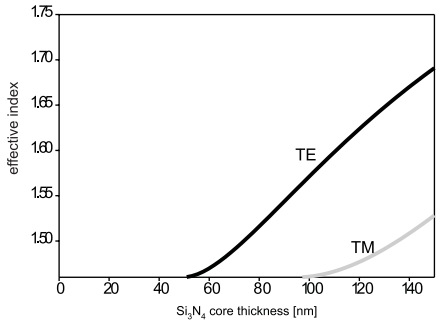

FIGURE 4. Effective indices of the lowest order TE and TM modes as a function of the core layer thickness, for the multilayer structure given in the text.

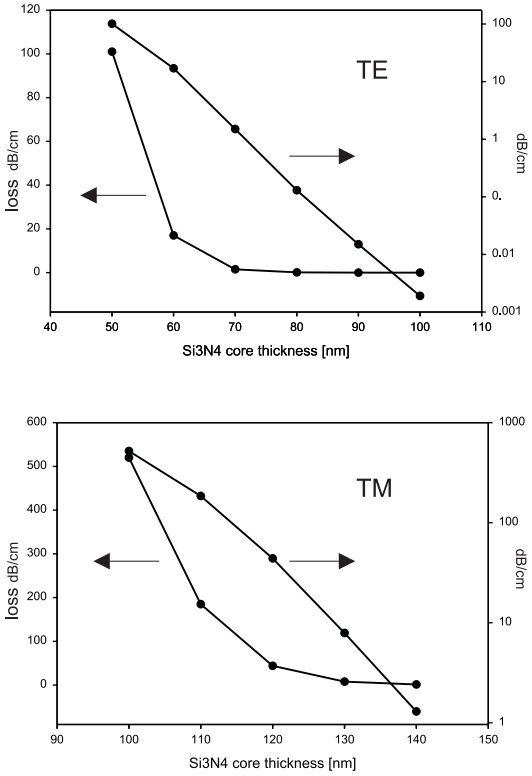

FIGURE 5. Losses, originating from leakage to the detector, as a function of the core layer thickness.

Simulations [17] have been performed in order to calculate the amount of optical power coupled from the waveguide to the Si detector (n=3.85+i0.019) for various layer structures. For the given material system, there are two parameters left for optimisation of the structure: the core layer thickness and the substrate layer thickness. The thinner the substrate layer, the higher the leakage of light into the Si. However, this is only desired at the position of the detectors, and therefore the substrate layer should be thick enough to have negligible leakage into the Si at other parts of the circuit. In the rest of the circuit, the core thickness is taken 137 nm, because this results in the highest sensitivity of the polarimeter [11]. Now, it can be calculated that for a leakage lower than 0.01 dB/cm in the rest of the circuit, the substrate layer thickness has to be larger than 1.5 μm. For this substrate layer thickness, the attenuation of the TE_{00} and TM_{00} mode are plotted as a function of the core layer thickness in figure 5.

For good operation of the sensing system, it is needed that over 0.99 (corresponding to 20 dB) of the power of a given mode is coupled into its appropriate detector, while the coupling of the other modes has to be less than 0.01 dB. For the TE coupling structure, a core thickness of 50 nm (attenuation 100 dB/cm) and a coupler length of 2500 μm (ie. 25 dB) will be used, while for the TM coupling structure the same parameters are 100 nm (attenuation 520 dB/cm) and 500 μm (ie. 26 dB), respectively. For the latter structure, the mode selectivity between both modes can be calculated to be -43 dB.

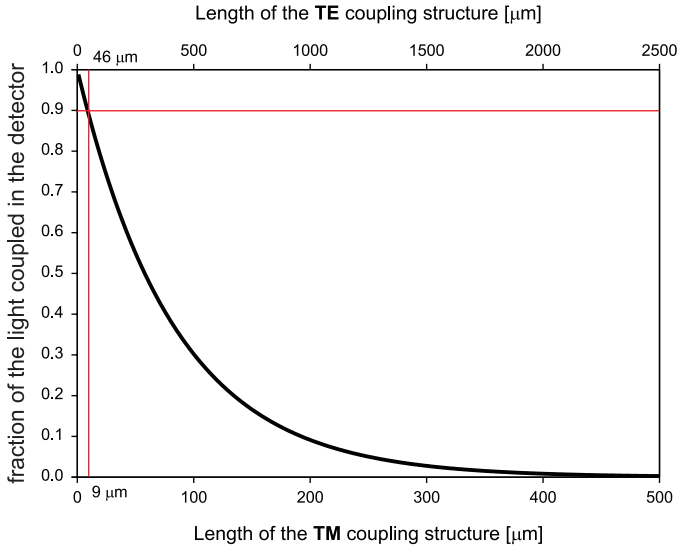

FIGURE 6. Fraction of the propagating optical power coupled into the detector as a function of the length of the coupling structure. The upper horizontal axis holds for TE polarised light, the lower axis for TM polarised light.

In order to minimise the number of process steps during the fabrication, the core layer thickness of the first and third TE coupling structure will be taken identical. From figure 6, it can be seen that for tapping the desired power fraction, 0.10, from the launched TE mode, a length of 46 μm is needed.

In figure 7, all three coupling structures and their relevant parameters are shown.

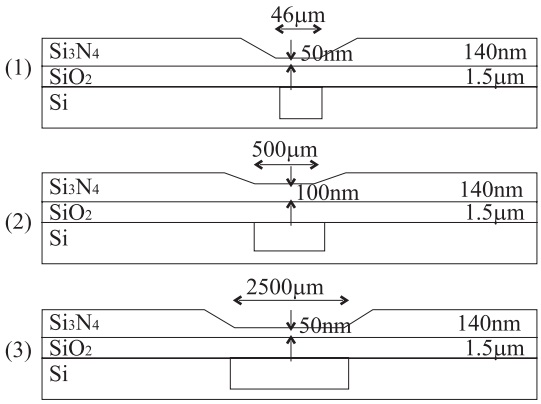

FIGURE 7. All three coupling structure required for the sensing circuit.

3. FABRICATION

The fabrication of the devices can be divided in three main steps. In the first step, the photodiodes are realised in the Silicon wafer. Second, the coupling structures and optical circuitry are fabricated and finally the electrical connections between the photodiodes and the outside world are made. We now will briefly describe these three steps.

The devices are fabricated using 3 inch <100> Silicon wafers with a resistivity of 2-5 Ωm (n-type, Phosphorus doped). A shallow p+ region is implanted through a 25 nm thick gate oxide layer (BF^{2+}, Dose $2e^{15}$ cm^{-2}, Acceleration voltage 70 keV).

After an anneal step needed to remove implantation damage, a 1.5 μm SiO_2 layer is deposited (plasma enhanced vapour deposition) [15] at 300^0C substrate temperature. In order to reduce the surface roughness of the SiO_2 layer, a chemical mechanical polishing step is performed [18]. After low pressure chemical vapour deposition of a Si_3N_4 layer [15] at 850^0C, the regions above the detectors are etched back to a thickness of 50 nm (TE diodes) and 100 nm (TM diodes) using BHF etching (etch rate 0.6 nm/min). The etching process allows for the realisation of nearly adiabatic tapers connecting the regions with different core thicknesses due to under etching of the photo resist. The depth of the etched holes have been measured using a surface profiler. The measured depths were 42 $\pm$ 3 nm (TM structure depth) and 100 $\pm$ 2 nm (TE structure depth). The optical circuit, an Y-junction

with on one branch the coupling structure while the other branch is used for intensity referencing during testing, is defined by ridge type monomodal channels (ridge height 1 nm, ridge width 4 μm) in the core layer, which are also realised by BHF etching. Next, a protective SiO_2 layer is deposited (PECVD) on top of the core layer. At the positions of the detectors, this layer is removed in order to obtain the asymmetrical layer stack as required for mode selective coupling.

Contact holes are etched through the optical layer stack to the p and n regions, after which an Aluminium layer is deposited and patterned in order to obtain bondpads connected to the photodiodes. After cleaving the wafers in order to obtain facets for end-fire coupling, the devices are ready for characterisation.

4. Experimental results

Experiments have been done in order to investigate the tapping performance and mode selectivity of the designed coupling structures.

First, TE and TM coupling structures with different lengths have been characterised in order to investigate the relation between the power fraction coupled into the detector and the device length. The detector current was referenced to the output of the reference branch of the Y-junction, and then normalised with respect to the referenced signal of the longest coupling structure (see figure 8). At the position of the TE coupling structures a lot of scatter points could be observed. Hence, there is a wider spread in the experimental points with respect to the fit in the TE case than in the TM case.

For the TE coupling structures, the fitted curve corresponds to an attenuation of 102 dB/cm (expected 100 dB/cm), which corresponds well to the designed core thickness of 50 nm. For the TM coupling structures, the fitted curve corresponds to an attenuation of 270 dB/cm (expected 520 dB/cm). From the profiler measurements, a difference in the core layer thickness of 58 nm between the TE and TM coupling structure was found. Assuming the core layer thickness at the position of the TM coupling structure should be 108 nm instead of the intended 100 nm, indeed an attenuation of about 270 dB/cm is calculated.

Next, the mode selectivity of the TM coupling structures has been investigated. In figure 9, two photographs of microscopic pictures of a TM coupling structure can be seen : in the right photograph TE polarised light was launched into the waveguide, in the left one TM light. Due to scattering, both branches of the Y-junction can be observed, one of them, the lower branch, with a the core layer thickness at the position of the detector that is thinned back to just above the cut-off thickness. It can clearly be seen that the TM polarised light is coupled out of the waveguide to the detector, while the propagation of the TE light does seem not to be affected by the coupling structure. However, quantitative measurements showed that the actual mode selectivity (-13 $\pm$ 1 dB) is not as low as theoretically expected (-43 dB): 5% of the propagating TE light is coupled into the detector. Because the crosstalk did not vary significantly ($\pm$ 1 dB) with the length of the coupling structure, its origin cannot be found in an enlarged scattering of TE light

at the high contrast Si_3N_4 interface as a result of the core layer etching. We attribute the crosstalk to non adiabaticity of the taper, as a result of

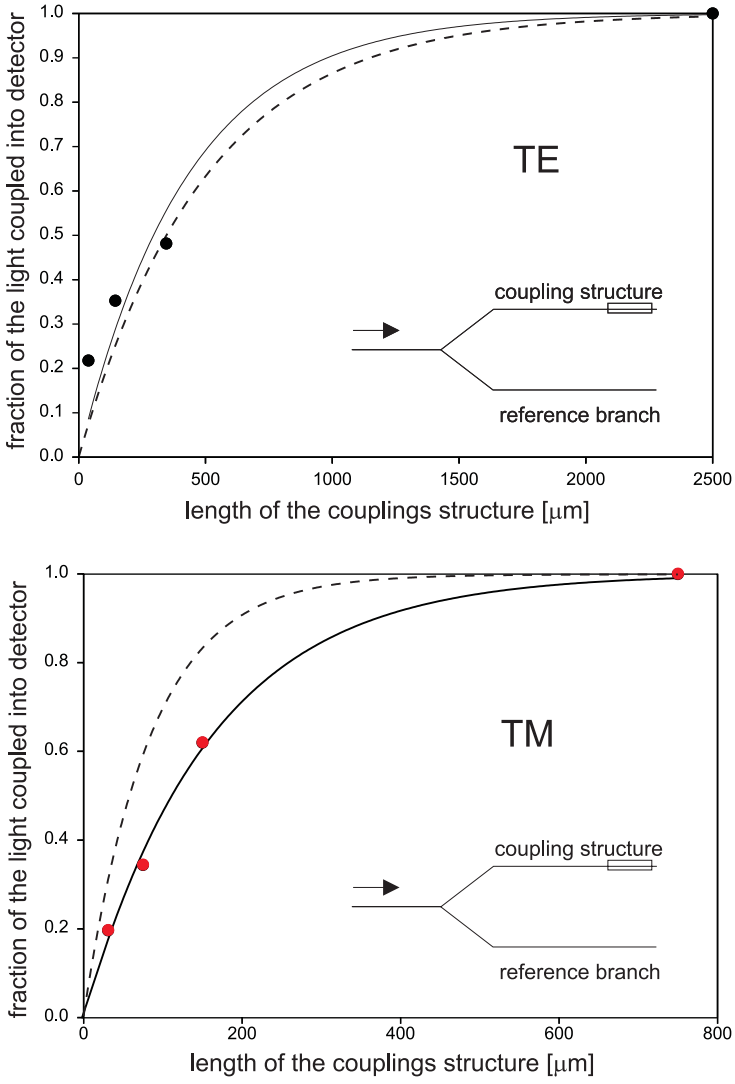

FIGURE 8. The fraction of the optical power coupled into the detector as a function of the length of the coupling structure (experimental=dots, fit=black line, theoretically expected=dashed line). In the insets, top views of the device structure are shown.

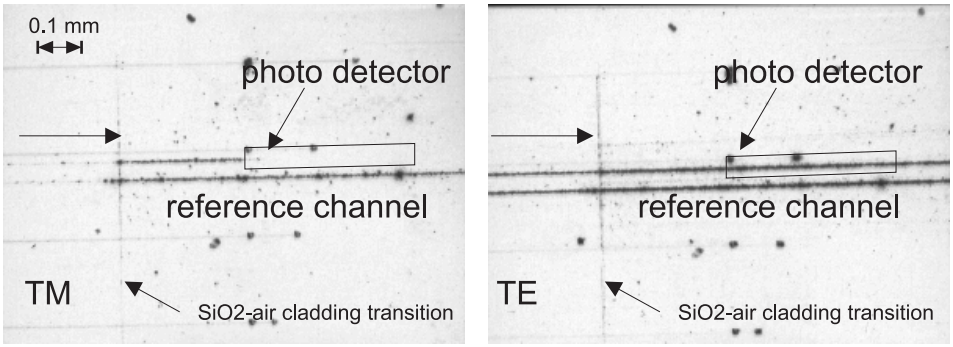

FIGURE 9. Two micrographs of the TM coupling structure. It can be seen that the TM polarised light is coupled into the detector (left), while the TE polarised light appears to propagates unperturbed through the structure.

5. SUMMARY

Coupling structures for complete, partial and mode selective optical power transfer from a waveguide to a detector by means of leaky wave coupling are presented. The structures are based on locally thinning down the core layer, causing the mode field to widen and to extend over the substrate layer to the inner of a detector that has been implemented into the Silicon substrate. In order to have the widening of the modal field especially towards the detector and to enhance mode specificity of the TM-coupling, an asymmetric high contrast three layer system is used. The designs of three coupling structures, required for implementation into an integrated optical sensing circuit, are presented. One coupling structure, used for referencing, having a length of $46\mu m$, couples a well defined part of the optical power carried by the lowest order TE mode into a detector, the other two, having lengths of 500 μm (TM) and 2500 μm, (TE), take care for a complete transfer of the optical power carried by the lowest order TM and TE mode, respectively. The first coupling structure is made mode selective, in the sense that the TM mode power only is coupled into the detector.

The coupling structures can be simply realised, as they require only one additional etch step. The experimentally obtained values for the power transfer are in an excellent agreement with theory. The mode selectivity of the TM coupling structure, -13 dB, however is worse than theoretically expected. This can be attributed to scattering from non perfectly adiabatic tapers at the beginning of the coupling structure. However, it is expected that by a re-optimisation of the photolithographic process, more adiabatic tapers and hence a solid reduction of the crosstalk can be achieved.

References

[1] R.J. Deri. Monolithic integration of optical waveguide circuitry with iii-v photodetectors for advanced lightwave receivers. *IEEE Journal of Lightwave Technology*, 11:1296–1323, 1993.

[2] S. Wunderlich, J.P. Schmidt, and J. Muller. Integration of SiON waveguides and photodiodes on silicon substrates. *Applied Optics*, 31:4186–4189, 1992.

[3] G.L. Bona, W.E. Denzel, B.J. Offrein, R. Germann, H.W.M. Salemink, and F. Horst. Wavelength division multiplexed add/drop ring technology in corporate backbone networks. *Optical Engineering*, 37:3218–3228, 1998.

[4] W. Lukosz. Integrated optical chemical and direct biochemical sensors. *Sensors and Actuators B*, 29:37–50, 1995.

[5] R.J. Deri. Monolithic integration of optical waveguide circuitry with iii-v photodetectors for advanced lightwave receivers. *IEEE Journal of Lightwave Technology*, 11:1296–1323, 1993.

[6] M. Moreno, C. Dominguez, J. Munoz, J. Calderer, and J.R. Morante. Photosensor and optical waveguide coupling in silicon technology. *Sensors and Actuators A*, 62:524–528, 1997.

[7] T.L. Koch and U. Koren. Semiconductor photonic integrated circuits. *IEEE Journal of Quantum Electronics*, 27:641–653, 1991.

[8] G. Mak, D.M. Bruce, and P.E. Jessop. Waveguide-detector couplers for integrated optics and monolithic optoelectronic switching arrays. *Applied Optics*, 28:4629–4636, 1989.

[9] T.M. Koster, V.E. Houtsma, P.V. Lambeck, D. Klunder, T.J.A. Popma, and J. Holleman. Mode selective coupling structures for monolithic integrated waveguide-detector systems. *SPIE*, 3630:9–18, 1999.

[10] F. Heismann. Integrated-optic polarisation transformer for reset-free endless polarisation control. *IEEE Journal of quantum electronics*, 25:1898–1906, 1989.

[11] T.M.Koster, N.E.Posthuma, and P.V.Lambeck. Fully integrated optical polarimeter. In *Proceedings Europt(r)ode V, 16-19 April 2000 Lyon, France*, 2000.

[12] U. Hilleringmann and K. Goser. Optoelectronic system integration on silicon: waveguides,photodetectors and vlsi cmos circuits on one chip. *IEEE Transactions on Electron Devices*, 42:841–845, 1995.

[13] D. Zurhelle, O. Blume, S. Popp, and J. Muller. Highly efficient waveguide-detector coupling structures for integrated opto-electronical circuits on silicon. *IEEE Journal of Lightwave Technology*, 14:410–416, 1996.

[14] H. Kogelnik and V. Ramaswamy. Scaling rules for thin-film optical waveguides. *Applied Optics*, 13:1857–1862, 1974.

[15] K.Worhoff, A.Driessen, P.V.Lambeck, L.T.H.Hilderink, P.W.C.Linders, and T.J.A.Popma. Plasma enhanced chemical vapour deposition silicon oxynitride optimised for application in integrated optics. *Sensors and Actuators A*, 74:9–12, 1999.

[16] O. Parriaux and G.J. Veldhuis. Normalised optimisation for the sensitivity optimisation of integrated optical evanescent-wave sensors. *Journal of Lightwave Technology*, 16:573–582, 1998.

[17] prometheus bpm and mask design, bbv software bv, Enschede, The Netherlands.

[18] C. Gui. *Direct wafer bonding with chemical mechanical polishing*. PhD thesis, University of Twente, Enschede, The Netherlands, 1998.

V. An integrated optical platform for absorptive sensing of chemical concentrations using chemo-optical monolayers

Abstract- In this paper, the design, fabrication and characterisation of a sensor is presented, optimised for sensing changes of the absorption coefficient of a monomolecular transduction layer, while at the same time being insensitive to environmental absorption changes. A functional analysis of the device is given, relating the effect of technological uncertainties to systematical errors in the determination of the measurand. A physical implementation of the functional design based on dual mode interrogation, using a polarisation converter and polarisation splitter, is presented and fabricated. From a tolerance analysis, using the values of the applied SiON technology, it was derived that over a range of 1 decade this implementation allows for an inaccuracy of an uncalibrated sensor less then 10 %.
The performance characteristics of the individual subfunctions are given. Propagation losses are 1.6 dB/cm, for both TE and TM polarised light. The relative wavelength shift of the resonance wavelength of the fabricated (grating assisted) polarisation converters to its intended value is 0.002 only. Experimentally, a 30 times decrease in the sensitivity to the output signal for changes in the absorption of the outer medium, compared to a mono modal sensor, has been observed.

1. Introduction

Many applications in such diverse fields as environmental control, the automotive industry, bio-engineering and health care [1]. require in situ measurements of chemical concentrations. For that, cheap, small, sensitive and reliable sensors are required. One of the ways to do so is to perform optical absorption measurements using integrated optical sensors.

If the measurand shows a relevant absorption at a practical wavelength, its concentration can be determined by measuring the absorption of the measurand itself, as in the case of NH_3 [2]. However, in most cases, for the desired concentration range, the absorption changes are very small and the concentrations cannot be determined in that way with the required resolution. Furthermore, as this type of measurement is completely non-selective, other chemicals which also show absorption at the operating wavelength must be absent, as their presence may cause an unacceptable error in the determination of the measurand. Also, often it is not well

possible to build a cheap and compact system including a lightsource and detector for a wavelength at which the measurand has an absorption band.

A solution to the problems regarding sensitivity , concentration range and selectivity is the use of indicators . They can be so designed that after association with the measurand, they show in the desired concentration range a large change in their absorption spectrum, which is at a practical wavelength region [3]. These indicators can be made selective, ie. they only associate with the measurand and not with other chemicals which might be present in the sample solution.

Indicators can be combined with small optical interrogation systems. For example, they can be added to the sample solution in a very controlled way, and changes in their absorption spectra can be detected using a transmission measurement scheme [4]. Indicators can also be immobilised by bonding them on waveguiding systems such as fibres or integrated optical waveguides. The resulting sensitive layers are generally called chemo-optical transduction layers or interfaces. Now the absorption changes induce changes in the power of guided modes propagating in these systems. For obtaining a high sensitivity and resolution,integrated optical waveguides offers some important advantages over the fibre based systems. First, in integrated optical systems, the indicators can be interrogated easily using evanescent field sensing [5]; due to the longer interaction length this results in a much higher sensitivity compared to fibre systems with indicators bonded on top of a fibre tip [6]. In the case of using fibres for evanescent field sensing, complicated side polishing procedures are needed. Second, waveguide systems offer the possibility of integrating the sensing part with other optical functionalities, resulting in small optical systems in which some basic optical signal processing can be performed for increasing the sensitivity and resolution.

A common way to bond indicators on top of a waveguide system is to incorporate them in a polymer membrane which is casted or spin coated on top of the optical layer system [7]. Then, using evanescent field sensing, the measurand induced change in the absorption spectrum of the indicator can be measured using as an interrogation signal a mode of the optical waveguide system, as shown in figure 1. In literature, integrated optical absorption sensors using membrane layers have been reported [7]. If the membrane is made thick enough, usually about 1 to 5 microns, all of the evanescent field is confined in the membrane resulting in a high sensitivity of the sensor for absorption changes in the membrane and insensitivity for changes in the optical properties of the outer medium. However, a disadvantage of such a membrane is its long response time . This response time depends on the diffusion rate of the measurand molecules from the outer medium to the interface of the membrane and on the time needed to penetrate into the membrane and to establish an equilibrium state in the membrane itself. The first contribution is intrinsic to all types of sensors based on interface sensing . The latter contribution is due the membrane itself, and depends on the speed of the mass transport of the measurand (figure 1, black dots) and other molecules which might play a role in establishing an equilibrium in the membrane (figure 1, white dots). The time needed to reach an equilibrium can be of the order of magnitude of minutes to

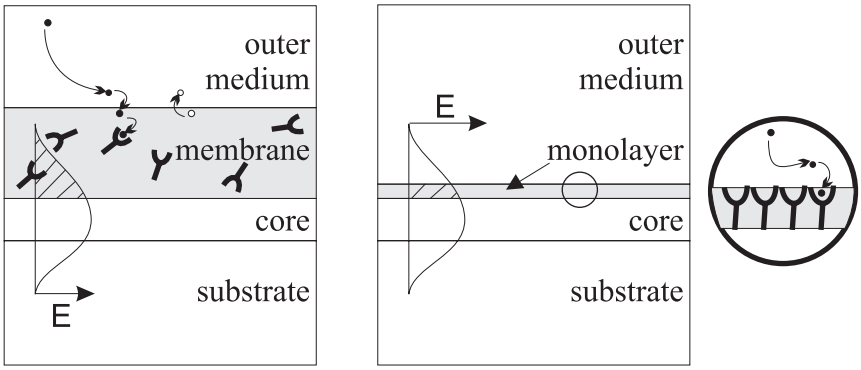

FIGURE 1. Membrane and monolayer evanescent field sensing. The modal E-field distribution has been indicated.

hours, which is too long for alarming purposes or for monitoring in a feedback control loop.

To decrease the response time, research focusses on monomolecular transduction layers [8] , see figure 1, where the receptor molecules are covalently bonded to the waveguide surface.

However, in monolayer sensor systems the evanescent field is not confined to the active layer, but also penetrates in the outer medium , which has two harmful consequences. First, the interrogation mode is less sensitive to the change in the absorption coefficient of the active layer. Second, absorption in the outer medium is also experienced by the interrogating mode, thereby introducing an error in the determination of the measurand. As the sensitivity to absorption changes in the outer medium can be 50 times higher than the sensitivity to absorption changes in the monolayer, this might cause a serious degradation of the sensor performance.

In order to be able to eliminate or to compensate for absorption in the outer medium, additional information is needed. This information can be obtained by launching a second interrogation mode which also experiences the absorption in the monolayer and in outer medium. Then, by having two orthogonal signals being different functions of the two unknown absorption coefficients, an accurate value for the absorption in the monolayer can be obtained regardless of the absorption coefficient in the outer medium. In addition, the two mode approach may reduce the disturbing effects of lightsource noise.

Several couples of interrogation modes can be chosen. The difference in the modes can be in the mode order, the mode polarisation, the mode wavelength or in the waveguide through which the modes are propagating. The choice of interrogation modes is based on several considerations,

- Regarding the wavelength, there are several reasons to prefer a single lightsource over several of them. First of all, this results in a cheaper and less complex system, especially when intensity fluctuations of the lightsource which

lower the resolution of the system have to be compensated for. Second, the absorption coefficients generally are wavelength dependent, thereby increasing the number of unknowns from two to at least three.

- The use of a signal and reference mode propagating through two different waveguides can cause errors due to a possible positional dependence of the absorption coefficients or unintended differences between both waveguides.

Therefore, a good alternative might be a sensor using two modes of the same wavelength and propagating through the same waveguide channel, and here the evaluation of this solution will be reported. Which modes are most advantageous to use will be discussed more quantitatively in the design section.

However, the extension from one to two interrogation modes requires additional optical functionalities. Two interrogation modes can be obtained whether by launching both modes in the waveguide from an external source, or by launching only one and next adding an integrated optical mode converter . The latter option might have the advantage of a better control of the power ratio of both modes before arriving at the sensing function than choosing the difficult way of controlled launching of two modes with a fixed power ratio from the outside. After passing the sensing function, the powers of both modes have to be detected separately, ie. mode splitting is required, after which the modal powers have to be coupled into photo detectors.

In our devices the mode generating, sensing and mode splitting functions are implemented in the integrated optical circuit. The light is transferred into and out of the circuit by end-fire coupling. Further integration, involving the implementation of fibre chip couplers [9] and monolithically integrated photodiodes [10] is currently under investigation.

In this paper, the analysis, the design, the fabrication and the characterisation of a differential absorption sensing platform are presented. In section two, a brief introduction to evanescent field absorption sensing is given. Next, in section three the functional design of the sensing platform is discussed. An analysis relating technological uncertainties to systematical measurement errors is given, enabling to determine the accuracy of uncalibrated sensors. In section four, the physical design of the sensor in a $SiON$ technology based waveguide system is presented. After a short description of the fabrication of the device in section five, experimental results are presented in section six. We conclude this paper with a summary.

2. Absorptive sensing

Here, first the case of bulk absorption sensing will be discussed. The optical power $P_j(z)$ carried by mode j propagating through a waveguide can be expressed as

$$P_j(z) = P_j(0)e^{-\frac{4\pi}{\lambda}N_j^{"}(\lambda,C)z} \tag{1}$$

λ the operating wavelength, $N_j^{"}(\lambda, C)$ the imaginary part of the effective index of mode j and z the coordinate along the propagation direction. In all waveguides, $N_j^{"}(\lambda, C)$ contains a part $N_{j,const}^{"}(\lambda)$ due to absorption and scatter losses in the absence of the measurand. Over the interaction length $0 < z < L_{int}$ it also contains a measurand induced part $\Delta N_j^{"}(\lambda, C)$, where C is the concentration of the measurand. At a given wavelength, this part can be written as

$$\Delta N_j^{"}(C) = \frac{\partial N_j^{"}}{\partial n^{"}} \Delta n^{"}(C) + \frac{\partial N_j^{"}}{\partial n^{'}} \Delta n^{'}(C) \approx S_j \Delta n^{"}(C), \tag{2}$$

where S_j can be seen as the sensitivity of the imaginary part of the effective index to changes in the imaginary part of the refractive index $\Delta n^{"}(C)$ in the sensing layer . This sensitivity includes the relatively small effect of the change in the real part of the refractive index $\Delta n^{'}(C)$, a change that always accompanies $\Delta n^{"}(C)$ as described by the Kramers-Kronig relations [11]. It should be noted that due to $\Delta n^{'}(C)$ the field profile of the mode changes a little bit and hence S_j is altered somewhat. Here, it is assumed that the $\Delta n^{"}$ change in the sensing layer is homogeneous, implying that the relation holds for a chemical equilibrium state only.

Combining (1) and (2), the power at the end of the interaction region $P(L_{int})$ can be expressed as

$$P_j(L_{int}) = P_j^0(L_{int}) e^{-\frac{4\pi}{\lambda} S_j \Delta n_i^{"}(C) L_{int}}, \tag{3}$$

with

$$P_j^0(L_{int}) = P_j(0) e^{-\frac{4\pi}{\lambda} N_{j,const}^{"} L} \tag{4}$$

the optical output power in the absence of the measurand. From a measurement of $P_j(L_{int})$, $\Delta n^{"}(C)$ can be calculated if the other parameters in the equation are known,

$$\Delta n^{"}(C) = -\frac{\lambda}{4\pi L_{int} S_j} \ln \frac{P_j(L_{int})}{P_j^0(L_{int})} \tag{5}$$

For a specific chemo optical transduction layer, C can be derived from $\Delta n^{"}(C)$, but for generality $\Delta n^{"}$ will be regarded as the quantity to be determined.

Contrary to the homogenous sensing systems considered above, in the case of the thin monomolecular transduction layers, the evanescent field penetrates through the transduction layer into the outer medium. Changes in the absorption coefficient of this outer medium can be taken into account by adding an extra factor to (3),

$$P_j(L_{int}) = P_j^0(L_{int}) e^{-\frac{4\pi}{\lambda} S_{j,ml} \Delta n_{ml}^{"}(C) L_{int}} e^{-\frac{4\pi}{\lambda} S_{j,om} \Delta n_{om}^{"} L_{int}}, \tag{6}$$

where 'ml' and 'om' refer to the monolayer and the outer medium, respectively. If this absorption in the outer medium $\Delta n''_{om}$ were ignored, the error $\delta\Delta n''_{ml}$ in the determination of Δn_{ml} can be calculated to be

$$\delta\Delta n''_{ml} = \frac{S_{j,om}}{S_{j,ml}}\Delta n''_{om} \tag{7}$$

Due to the small thickness of the monolayer, the sensitivity $S_{j,ml}$ is generally orders of magnitude lower than $S_{j,om}$. Therefore, this error can be detrimental to the accuracy of the sensor. As an example, in figure 2, for a representative SiON based layer system provided with a 1 nm thick monolayer, S_{ml} and the ratio of the sensitivities, $\frac{S_{om}}{S_{ml}}$, are shown as a function of the core layer thickness. The highest sensitivity for monolayer absorption is obtained for a core thickness of 73nm. Here, S_{om} is approximately 50 times higher than S_{ml}.

This error can be eliminated by interrogating the sensing region by two modes,1 and 2, each probing the changes in both layers in a different way. The ratio of the powers of these two modes can be written as

$$R \equiv \frac{P_1^0(L_{int})}{P_2^0(L_{int})} e^{-\frac{4\pi}{\lambda}[(S_{1,ml}-S_{2,ml})\Delta n_{ml}(C)+(S_{1,om}-S_{2,om})\Delta n_{om}]L_{int}}, \tag{8}$$

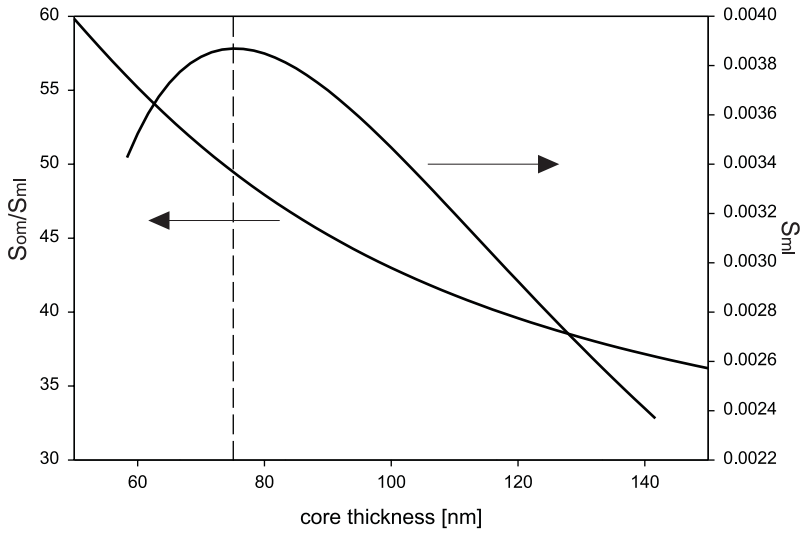

FIGURE 2. The sensitivity of a mode for changes in the absorption coefficient in the monolayer and the ratio of the sensitivities for changes in the absorption coefficient in the monolayer and the outer medium as a function of the core layer thickness.

Now, it can readily be seen that for

$$S_{1,om} - S_{2,om} = \Delta S_{om} = 0, \tag{9}$$
$$S_{1,ml} - S_{2,ml} = \Delta S_{ml} \neq 0,$$

the influence of absorption changes in the outer medium on R should be completely eliminated, while from R $\Delta n_{ml}(C)$ can be determined. We will investigate the feasibility of this $\Delta S_{om} = 0$ concept. Hence, the main design objectives are a waveguide structure in which $\Delta S_{om} = 0$, ΔS_{ml} is as large as possible and $\frac{P_1^0(L_{int})}{P_2^0(L_{int})}$ being given with an appropriate accuracy.

3. Functional design of the circuit

The functional design of the sensor is shown in figure 3. Light is coupled into one single mode of a channel type waveguide using a coupling function. With a mode converter, a fraction ($\sin^2\gamma$) of the power carried by the launched mode is transferred to the second interrogation mode. So, after the converter two modes propagate through the waveguide which after having past the sensing region, are separated into different output waveguides by a mode splitter. The output powers from both output waveguides are coupled into detectors, and finally it will be the ratio of both detector signals that contains the information on the measurand induced absorption change.

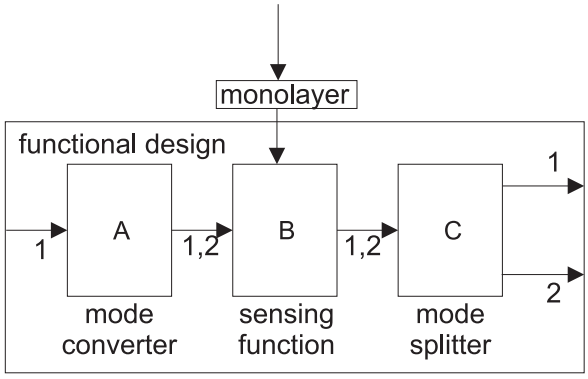

Figure 3. Functional design of the sensing platform. '1' and '2' denote the two interrogation signals.

For the functional design shown in figure 3, the optical powers in the output waveguides, in the case mode 1 was launched into the circuit, are

$$
\begin{aligned}
(10) \qquad P_{1,out} &= \{(1-CT_1)\cos^2\gamma A_1^* e^{-\frac{4\pi}{\lambda}\left(S_{1,ml}\Delta n''_{ml}(C)+S_{1,om}\Delta n''_{om}\right)L_{int}} + \\
&\quad CT_2\sin^2\gamma A_2^* e^{-\frac{4\pi}{\lambda}\left(S_{2,ml}\Delta n''_{ml}(C)+S_{2,om}\Delta n''_{om}\right)L_{int}}\}P_{in}, \\
P_{2,out} &= \{(1-CT_2)\sin^2\gamma A_{2,}^* e^{-\frac{4\pi}{\lambda}\left(S_{2,ml}\Delta n''_{ml}(C)+S_{2,om}\Delta n''_{om}\right)L_{int}} + \\
&\quad CT_1\cos^2\gamma A_1^* e^{-\frac{4\pi}{\lambda}\left(S_{1,ml}\Delta n''_{ml}(C)+S_{1,om}\Delta n''_{om}\right)L_{int}}\}P_{in}.
\end{aligned}
$$

Here, CT_j is the amount of optical power of mode j coupled into the wrong output waveguide of the mode splitter. P_{in} is the optical power at the beginning of the mode converter. In A_j^*, the background absorption is taken into account. Notice that the converter and splitter have been assumed to be lossless.

First, we will discuss a sensor, that has been realised with perfect technology, ie. the realised sensor is identical to the designed sensor. We assume that the design allows for complete elimination of the influence of the outer medium, see (9), and that the mode splitter should be crosstalk free. Then, R, the ration signal, equals

$$
(11) \qquad R = \frac{P_{1,out}}{P_{2,out}} = \frac{A_1^*}{A_2^*}\frac{1}{\tan^2(\gamma)}e^{-\frac{4\pi}{\lambda}\Delta S_{ml}\Delta n''_{ml}(C)L_{int}},
$$

and in reverse

$$
(12) \qquad \Delta n''_{ml}(C) = -\frac{\lambda}{4\pi L_{int}}\frac{1}{\Delta S_{ml}}\ln\left(\frac{\tan^2(\gamma)}{\frac{A_1^*}{A_2^*}}R\right)
$$

However, no technology is perfect.We will now analyse the influence of several technological uncertainties on the determination of $\Delta n''_{ml}(C)$, with the objective to apply their quantitative relationships for designing a sensor with minimised effects of these uncertainties on its performance. This minimisation offers the prospect of a larger number of applications for which no calibration of individual sensors should be required. For that, also a good estimation of the values of the systematical errors are necessary. In the analysis we first focus on the individual functions. First on the sensing function, next on the mode converter and finally on the mode splitter.

Main effects of the technological uncertainties in the sensing region are deviations in the modal sensitivities to absorption changes in both the monolayer and the outer medium. Similar effects arise from variations of the ambient temperature during the measurements, but in the used SiON based waveguide systems these temperature effects are relatively small, and they shall be disregarded. With $\delta\Delta S_{ml}$ and $\delta\Delta S_{om}$ the technologically induced deviations in the differential sensitivities, the relative error in $\Delta n''_{ml}$ can be calculated to be

$$\frac{\delta\Delta n^{"}_{ml}}{\Delta n^{"}_{ml}} = \frac{\delta\Delta S_{ml}}{\Delta S_{ml}} + \frac{\delta\Delta S_{om}}{\Delta S_{ml}}\frac{\Delta n^{"}_{om}}{\Delta n^{"}_{ml}} \tag{13}$$

The first term on the right hand side is a systematic error, independent of the absorption. The second term is no systematic error, but reflects the effect of the in principle unknown absorption in the outer medium as a consequence of $\Delta S_{om} \neq 0$.

For the mode converter, imperfectness of technology implies that the amount of mode conversion of the realised converter might differ from its designed value, causing an error

$$\delta\Delta n^{"}_{ml} = -\frac{\lambda}{4\pi L_{int}}\frac{1}{\Delta S_{ml}}\ln\frac{\tan^2\gamma_d}{\tan^2\gamma_r}, \tag{14}$$

where γ_d and γ_r are the designed and realised γ values of the converter, respectively. For a small deviation of γ, $\delta\gamma$, the introduced error is the smallest for $\gamma_d = \pi/4$, and is in good approximation given by

$$\delta\Delta n^{"}_{ml} \approx \frac{\lambda}{\pi L_{int}}\frac{\delta\gamma}{\Delta S_{ml}} \tag{15}$$

For a realistic example (a wavelength of 600nm, $L_{int} = 5mm$, $\Delta S_{ml} = 0.002$ and $\delta\gamma = \pi/20$), (16) implies a $\delta\Delta n^{"}_{ml} = 3 * 10^{-3}$, which corresponds with a difference of 3 dB between the expected R and the actual R. The error is an absolute error, independent on the actual $\Delta n^{"}_{ml}$. Hence, the higher $\Delta n^{"}_{ml}$, the lower the relative error in $\Delta n^{"}_{ml}$.

For the mode splitter, technological uncertainties result in crosstalks CT_1 and $CT_2 \neq 0$. Under the assumptions that the crosstalk terms are small (ie. $CT_{1,2} << 1$) and that $S_{1,ml} > S_{2,ml}$, $\delta\Delta n^{"}_{ml}(C)$ can be derived to be approximately

$$\begin{aligned}(16)\Delta n^{"}_{ml}(C) &\approx -\frac{\lambda}{4\pi L_{int}}\frac{1}{\Delta S_{ml}}\ln x \\ x &= \left(1 + (CT_2 - CT_1) + CT_2\frac{A^*_2}{A^*_1}\tan^2(\gamma)e^{+\frac{4\pi}{\lambda}\Delta S_{ml}\Delta n^{"}_{ml}(C)L_{int}}\right)\end{aligned}$$

Apart from decreasing the crosstalks themselves or their difference, the error can be made smaller by designing the mode converter such, that after the converter most of the optical power is in the mode which will be attenuated most. Here, where mode 1 is most attenuated ($S_{1,ml} > S_{2,ml}$), this means decreasing the γ of the mode converter.

Because lightsource noise is nearly completely eliminated by considering the ratio between both output powers, the main noise sources are detector noise, fluctuations in the temperature and in the composition of the outer medium and vibrations, the

latter influencing the amount of scattered light incident on the detector. The first one is a system property and co defines to the detection limit, that therefore is a function of the propagational and functional losses and of the interaction length, but also data not known a priori such as the input power. The other noise sources depend on the experimental conditions and on the packaging, and their influence cannot be quantified beforehand.

From the analysis, the following design objectives can be given: First, in order to make the output signal R independent on Δn", a $\Delta S_{om} = 0$ is required (9). From all mode combinations, that with the highest ΔS_{ml} for $\Delta S_{om} = 0$ should be chosen. By taking a 50:50 converter, effects of inaccuracy of the converter are the lowest (14). In order to minimise the effects of crosstalk, the crosstalks and their difference have to be as low as possible (15).

4. Physical design of the sensor

As a boundary condition to the design, the structures have to be realised using the Silicon-oxynitride technology as is available in our laboratory [12]. Using this technology, multi layer structures can be realised using materials ranging from n=1.457 (SiO_2) to n=2.01 (Si_3N_4) (@650nm). The basic sensor structure contains a ridge type channel waveguide as shown in figure 4. It consists of a high index Si_3N_4 core layer on top of a SiO_2 substrate layer, a layer combination chosen as it gives the highest sensitivity for changes in the absorption coefficient of the monomolecular transduction layer [5]. On top of the core layer a protective SiO_2 layer (n=1.47) is deposited. In the sensing region, this protective is replaced by the sensitive monolayer. Outside this monolayer is the outer medium (here assumed to be an aqueous solution with n=1.33) in which the measurand is dissolved. The thickness of the sensitive monolayer we intend to use is approximately 2.4 nm, and its refractive index about 1.55. The structure will be designed for an operation wavelength of 655 nm. However, the design presented here can easily be recalculated for any given wavelength.

Now, first the mode combination which should be used for the differential sensor has to be chosen. This choice can be based on several criteria, such as obtaining the highest differential sensitivity for absorption changes in the monolayer, achieving large technological tolerances of the structure for $\Delta S_{om} = 0$, a simple fabrication

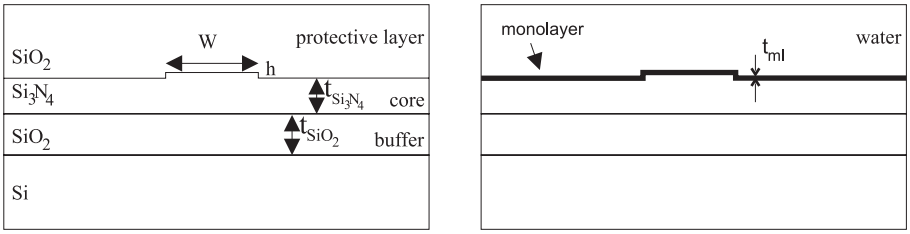

Figure 4. The starting-point waveguide cross sections of the design.

of the subfunctions etc. Which criterion should prevail depends on the specific application requirements. Here, we have given priority to the first criterion, ie. the highest ΔS_{ml}. From a practical point of view, we will only consider the zeroth and first order TE and TM modes, resulting in the following six possible combinations of modes : TE_0/TE_1, TE_0/TM_0, TE_0/TM_1, TE_1/TM_0, TE_1/TM_1 and TM_0/TM_1. We have calculated for each of these mode combinations the ΔS_{ml} value for the core layer thickness where the corresponding $\Delta S_{om} = 0$ For this, we have assumed the SiO_2 buffer layer thickness to be semi-infinite. As can be seen in figure 5, the highest ΔS_{ml} for a $\Delta S_{om} = 0$ is achieved for the $TE_0 - TM_0$ mode combination, which together with the ease of launching a TE_{00} mode from a fibre and the prospects of $TE_{00} - TM_{00}$ conversion leads us to the decision of investigating this combination. Also the $TM_0 - TM_1$ couple is a good candidate, and is currently under investigation.

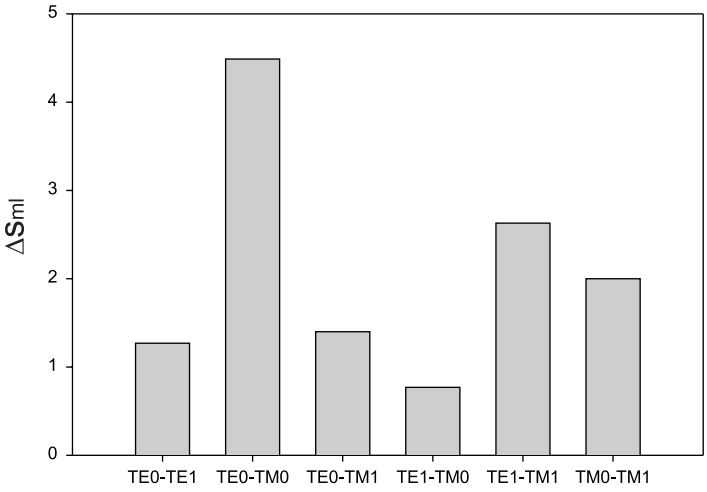

FIGURE 5. The mode combination versus ΔS_{ml}.

For the $TE_{00} - TM_{00}$ couple, ΔS_{ml} and ΔS_{om} have been calculated as a function of the core layer thickness, see figure 6. For this type of calculations, the channel structure can be well approximated by a slabguide structure of similar thickness of the core layer. For a layer thickness of 82 nm, $\Delta S_{om} = 0$. It can be seen that the condition $\Delta S_{om} = 0$ is very sensitive to variations in the core layer thickness. However, in the range of a few nanometers around the optimum core thickness, this differential sensitivity is still orders of magnitude lower than the sensitivity in the case of monomodal sensing. Because of the crucial character of $\Delta S_{om} = 0$ the influence of all technological uncertainties on ΔS_{om} have been calculated. In the table, worst case deviations are given.

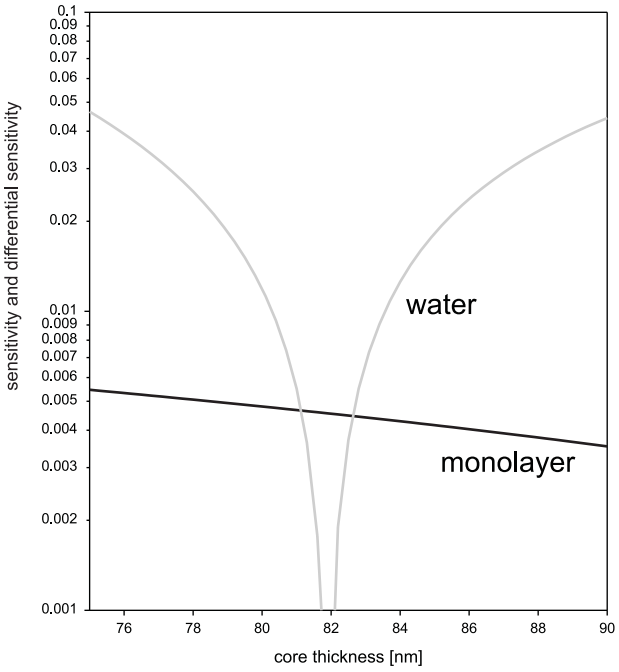

FIGURE 6. The differential sensitivities for changes in the absorption coefficients of the outer medium (water) and the monolayer.

parameter	**deviation**	$\delta\Delta\mathbf{S_{om,wc}}$	$\delta\Delta\mathbf{S_{ml,wc}}$
$n_{Si_3N_4}$	$5 * 10^{-4}$	$3 * 10^{-4}$	$5 * 10^{-6}$
n_{SiO_2}	$2 * 10^{-3}$	$2.8 * 10^{-3}$	$2.2 * 10^{-6}$
n_{ml}	10^{-3}	$1.8 * 10^{-5}$	$8.4 * 10^{-6}$
n_{om}	10^{-3}	$1.2 * 10^{-3}$	$1.8 * 10^{-6}$
d_{ml}	0.5 nm	$1.8 * 10^{-3}$	$2 * 10^{-5}$
$d_{Si_3N_4}$	2 nm	$12.2 * 10^{-3}$	$2.4 * 10^{-4}$

The total worst case $\delta\Delta S_{om,wc}$ and $\delta\Delta S_{ml,wc}$ are approximately $1.8 * 10^{-2}$ and $2.4 * 10^{-4}$, respectively. The latter corresponds to a relative error of 0.05. In both, the largest contribution arises from deviations in the core layer thickness.

As explained in the introduction, the mode converter is used to obtain the two interrogation modes. Launching the lowest order TE_{00} mode, a polarisation converter is required for the partial mode conversion into a TM_{00} mode. Within our material system, a polarisation converter based on an asymmetrical ridge grating structure has been developed [13]. The layout of the structure is shown in figure 7. Due to the asymmetry in the alternating cross sections, at each transition a part of the power in the TE_{00} mode can be coupled into the TM_{00} mode and vice versa. As the converter is a grating structure, only for a small range of wavelengths

the power transfer builds up constructively, the centre (resonance) wavelength, λ_c, obeying the relation

$$\lambda_c = (N_{eff,TE_{00}} - N_{eff,TM_{00}})\Lambda, \tag{17}$$

where Λ is the grating period [14]. A disadvantage of this grating structure is the wavelength dependence of the amount of optical power coupled from the TE mode to the TM mode. The converter has been designed for a core thickness of 137 nm, as for this core thickness the largest fabrication tolerance with respect to its resonance wavelength is achieved [15]. Remaining deviations of the resonance wavelength can be compensated by thermo-optical tuning [16].

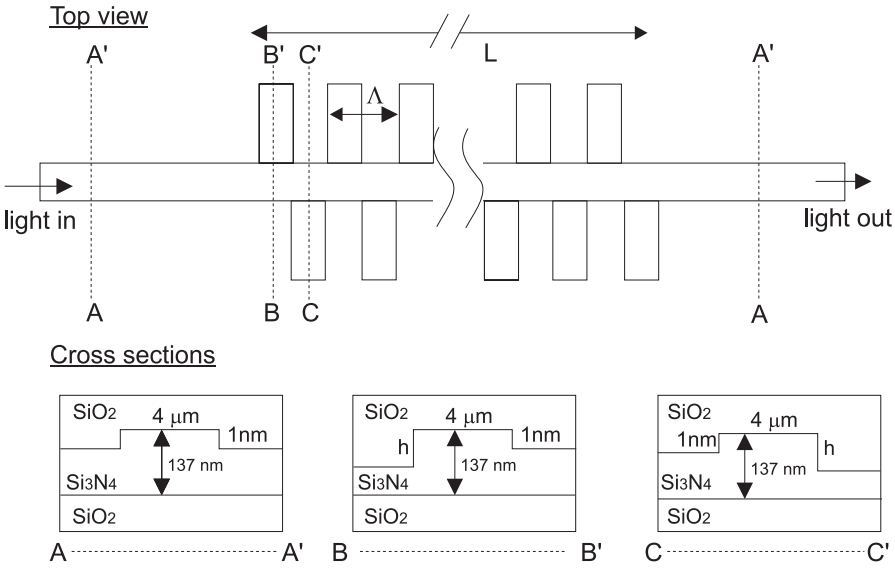

FIGURE 7. Topview and crosssections of the polarisation converter.

As a polarisation splitter a two mode interferometer (TMI) was used, similar to the one developed by [17]. For limiting the number of process steps, the TMI was designed for the core layer thickness already taken for the sensing region, i.e. 82 nm. For the TE_{00} mode being in the bar state (phase difference 6π) a crosstalk of -30dB and a functional loss of -0.13dB have been calculated. Then, the TM_{00} mode has to be in the cross state (phase difference 5π), and here the crosstalk is -27.5dB and the functional loss -0.27dB. The designed TMI is shown in figure 9.

As $S_{TE,ml} - S_{TM,ml} > 0$ is chosen, the TE_{00} mode will be more attenuated than the TM_{00} mode. From the analysis of the mode splitter, it was concluded that in this case CT_{TM} is the largest disturbing factor, and hence it was decided to implement a TM polariser in the TE output branch. The structure of the polariser

is shown in figure 8. At the window again the core thickness is 82 nm, which for an air-'cladding' is well underneath the TM_{00} cutoff thickness (95 nm) and well above the TE_{00} cutoff thickness (49 nm). Therefore, the TM light is no longer guided and coupled out of the waveguide. The TM_{00}/TE_{00} extinction ratio can calculated to be -125 dB. However, in practice, due to stray light and scattered light some crosstalk will remain.

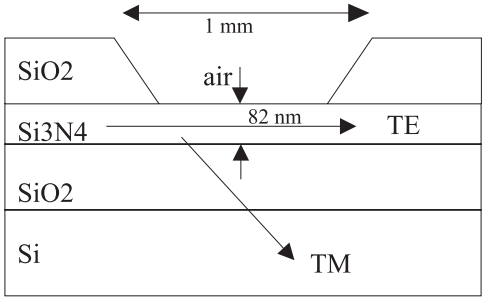

FIGURE 8. Structure of the integrated optical polariser.

In figure 9, the complete design is shown with all design parameters and also the main data on the expected performance of the individual components. For this specific design, in figure 10 the influence of technological uncertainties on the relative accuracy with which $\Delta n^{"}(C)$ can be determined without calibration is shown.

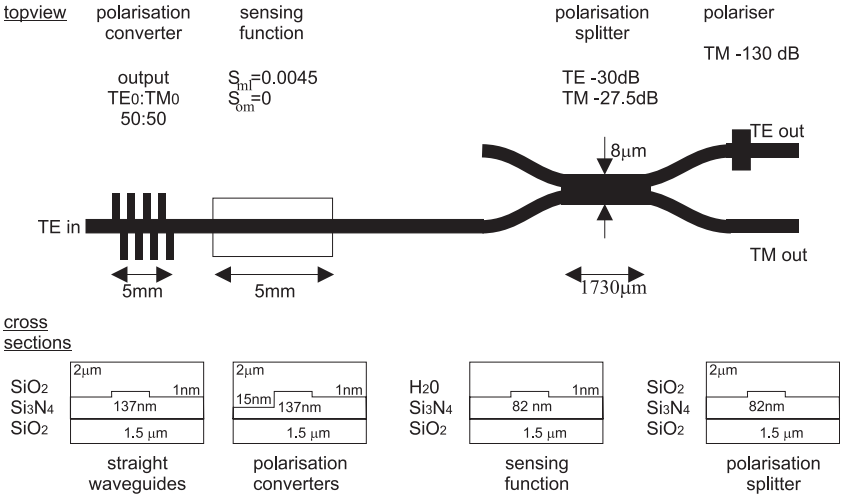

FIGURE 9. Topview, crosssections of the complete sensing platform and the calculated performances of the individual subfunctions.

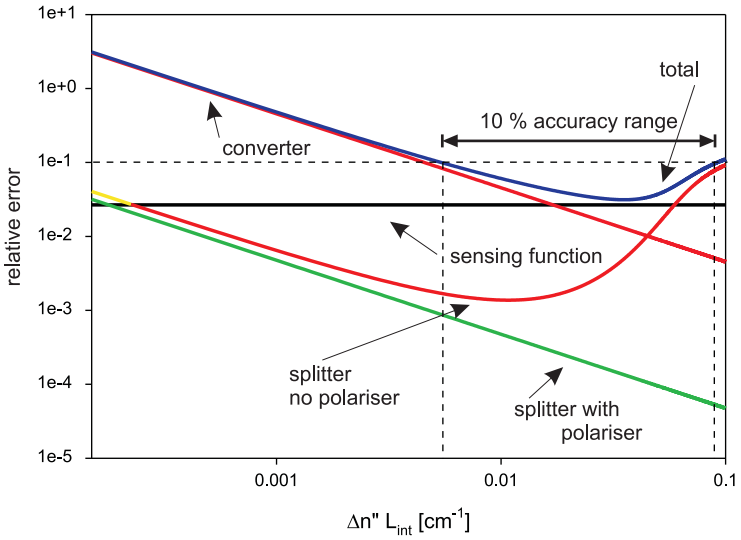

FIGURE 10. The relative error $\frac{\delta\Delta n^{"}(C)}{\Delta n^{"}(C)}$ as a function of $\Delta n^{"}(C)L_{int}$, showing the effect of technological uncertainties in the sensing window, mode converter and the mode splitter.

$\frac{A_2^*}{A_1^*}\tan^2(\gamma) = 1$ and $\delta\gamma$ was taken 5 degrees. The main contribution to the relative error for low $\Delta n^{"}(C)L_{int}$ originates from the converter, for moderate $\Delta n^{"}(C)L_{int}$ from the sensing function and for high $\Delta n^{"}(C)L_{int}$ from the splitter. If an accuracy of 10 % is required, sensors which operate in the $\Delta n^{"}(C)L_{int}$=0.007 to 0.09 range can be used without calibration. Note the influence of the interaction length L_{int}: small changes of $\Delta n^{"}(C)$ can be read out well by using long interaction lengths. The latter can be realised e.g. by applying spiral shaped channels in the sensing region. Using the splitter/polariser combination, this range widens significantly at the higher $\Delta n^{"}(C)L_{int}$ side. Effects of the lightsource noise is eliminated nearly completely, because the final information is presented as the ratio of two output signals, just as when applying a reference branch. The main noise contributions arises from the detector system, while there is some unpredictable influence of scattered light. Detector system noise effects can be reduced by choosing a higher input power and lowering the background propagation losses in the sensor system.

5. Device fabrication

The devices are realised on 3 inch prime quality $< 100 >$ Si wafers . First, using a thermal wet oxidation step , a 3 μm SiO_2 buffer layer is grown. Then, a 137 nm thick Si_3N_4 core layer is deposited using Low Pressure Chemical Vapour Deposition (LPCVD) . At the positions of the sensing function, polarisation splitter and polariser, the core layer thickness is thinned down to 82 nm. The etching process

allows for producing nearly adiabatic tapers between the regions of different core thicknesses. Because the $\Delta S_{ml} = 0$ condition requires 82nm exactly, the thinning down was done in two steps. First, after measuring its original thickness, the layer was thinned back to approximately 90-95 nm. Then, the real etch rate and etching depth were calculated using a dummy wafer which had been etched simultaneously with the device wafer. Now, with the etch rate precisely known, the wafer was thinned back to 82nm. This way, an accuracy of 1 to 2 nm in the layer thickness can be obtained. Next, 1 nm deep ridge waveguides are etched using Buffered Hydro Fluoric Acid (BHF). Using a double exposure step [18], the polarisation converter is etched using Reactive Ion Etching (RIE). By Plasma Enhanced Chemical Vapour Deposition (PECVD) , the protective SiO_2 layer is deposited, and this layer is subsequently etched off at the positions of the sensing function and the polariser. After cleaving the wafers in order to obtain end facets for end-fire coupling, the devices are ready for characterisation. For testing purposes, besides the complete device also individual straight waveguides, polarisation converters and splitters have been realised on the same wafer.

6. Experimental results and discussion

First, the channel propagation losses of the TE_{00} and TM_{00} mode of straight waveguides (for a Si_3N_4 core thickness of 137 nm sandwiched in between two SiO_2 layers) have been calculated from the position dependence of the scattered light intensity, both losses being 1.6+/-0.1dB/cm.

Using an Argon pumped dye laser (Spectra Physics, DCM dye 620-680nm, step size 0.03nm), the polarisation converter has been characterised. A conversion efficiency of 0.50 was achieved for a wavelength of 656.46nm. With respect to the intended wavelength (655nm), this is a deviation of 1.46nm. This is within the specifications as given by the tolerance analysis [15], but is a too large deviation for practical applications. Adjustment of the converter is required in order obtain the desired amount of conversion for the intended operating wavelength. In order to achieve this adjustment, thermal tuning of the resonance wavelength of the converter is currently investigated [19].

The polarisation splitter has been characterised by launching TE and TM polarised light into the structure and measuring the output signals of both polarisations at both output waveguides. The crosstalks were determined to be -11.7 dB for TE and -13.7 dB for TM. These crosstalks are worse than the calculated (-30 dB (TE) and -27.5 dB (TM)). As the TMI is most intolerant for deviations in the lateral effective index contrast, these worse crosstalks are most likely due to a deviation in the etch depth used to define the channel waveguide structure. In order to compensate for these worse crosstalks, for the characterisation of the complete device on the TM output channel a bulk polariser was used in order to get rid of the TE polarised light in this channel.

As a test of the complete sensing circuit, the differential sensitivity ΔS_{om} to the outer medium was determined. As no monolayer was available at the time,

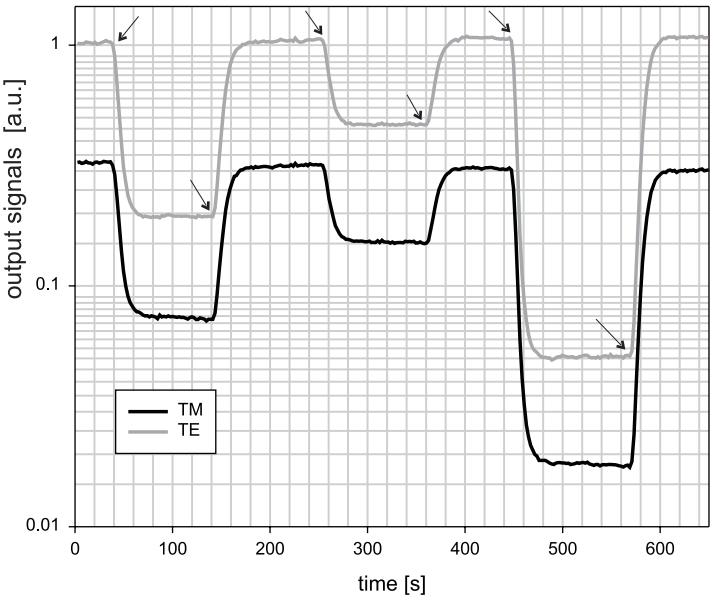

FIGURE 11. In time, the sensing function was exposed to different concentration of dye solution, ie. a different absorption coefficient of the outer medium. In this figure the output powers of the TE and TM mode are shown versus time. The arrows indicate the injections of different concentrations of BCG.

these experiments were performed without a monolayer, which has to be taken into account in the interpretation of the results.
The experiment was as follows: A pH indicator (BCG) was dissolved in a $H_3PO_4 : NaOH = 2 : 3$ buffer solution (4.91 mmol/l) in order to have a constant pH=7.2. From this solution, three dilutions were made, with concentration ratio's 0.05, 0.1 and 0.2. Now, using a flow injection system, the buffer solution and the dye solutions (with different concentrations) were injected in a flow cell clamped on top of the sensing window, while detecting both the TE and TM output signals. The result is shown in figure 11. In figure 12, the TE and TM attenuation together with the attenuation of the ratio of TE and TM are shown as a function of the normalised concentration. As can be seen, there is a slight difference between the TE and TM attenuation. From an exponential fit, it can be found that $\Delta S_{om}/S_{TE,om}$=0.08, which, if assumed to be mostly due to a deviation in the core layer thickness can be calculated to correspond to a core layer which is approximately 1.4 nm too thin. In case the intended monolayer of 2.4nm should have been applied on top of the waveguide layer, this would mean a differential sensitivity $\Delta S_{om} = 8 * 10^{-3}$.

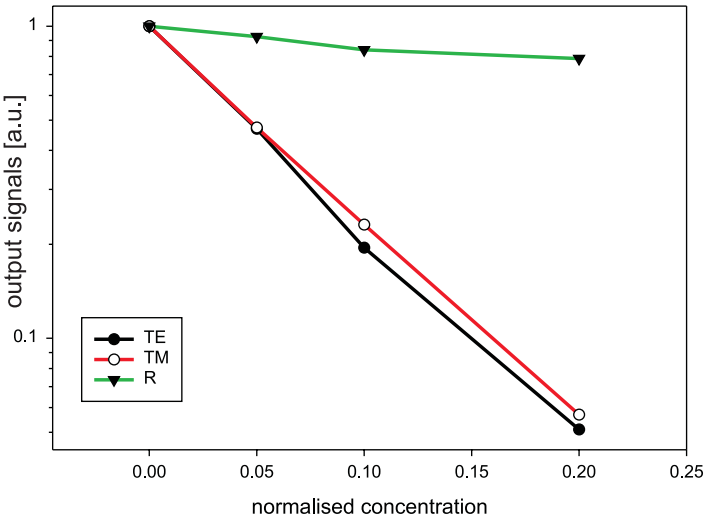

FIGURE 12. The normalised output versus the normalised concentration for the TE and TM output powers and the differential signal R.

Although ΔS_{om} is not zero, with respect to solely the TE signal as an output signal the ratio signal R is 30 times less sensitive to changes in the absorption coefficient of the outer medium then using monomodal sensing.

From the experimental results, the following can be concluded: at the sensing region, instead of the designed core layer thickness a slightly lower thickness was obtained. This resulted in a small deviation of ΔS_{om} from its intended value, 0, and although the influence of environmental absorption on the ratio signal R is not eliminated completely, it is strongly reduced. Whether this reduction is acceptable will depend on the specific application. The fabrication tolerances make the sensor performance somewhat uncertain, and for most applications calibration of individual sensors will be required. These uncertainties mainly arise from the polarisation converter and polarisation splitter, and therefore they are related to the mode couple used. Using the principle as has been developed here, alternative implementations of the functionalities and even other mode couples [20] have to be considered too.

7. SUMMARY

The analysis, the design, the fabrication and some experimental results of a differential integrated optical platform for absorptive sensing of monolayer chemo-optical transduction layers have been presented. A system has been proposed, in which the sensitive layer is interrogated by two modes, the TE_{00} and TM_{00} mode, simultaneously. This approach appears to offer the advantage of a remarkable reduction of influences of both spurious absorptions by the medium outside the monolayer

and the influence of lightsource noise on the output signal. The latter affords for higher detection limits and a larger resolution. All required optical functionalities, a mode converter, a sensing function and mode splitter, have been implemented in a single integrated optical circuit. The influence of technological tolerances on the determination of the chemically induced absorption, given as the imaginary part of the refractive index, $\Delta n"(C)$, has been investigated, and it has been concluded that with the current state of technology within our laboratory, for most applications these sensors have to be individually calibrated. However, using calibrated sensors, there is a wide range over which $\Delta n"(C)$ can be accurately determined, being mainly defined by the optical input power, detector noise and background absorption of the optical system. In a fabricated demonstrator device, compared to the monomodal case a 30 times reduction of the influence of environmental absorption changes on the output signal has been achieved.

References

[1] P.V. Lambeck. Integrated chemo-optical sensors. *Sensors and Actuators B*, 8:103–116, 1992.

[2] K. Chan, H. Ito, and H. Inaba. An optical fibre based gas sensor for remote absorption measurements of low-level methane gas in the near-infrared region. *Journal of Lightwave Technology*, 2:234–237, 1984.

[3] K. Seiler and W. Simon. Theoretical aspects of bulk optode memranes. *Analytica Chimica Acta*, 226:73–87, 1992.

[4] T.T. Veenstra, R.M. Tiggelaar, R. Mateman, R.G.P. Sanders, J.M. Wissink, A. Prak, J.G.E. Gardeniers, M.C. Elwenspoek, and A. van den Berg. Maffias in modules. In *Proceedings of the 3th Symposium on Microsystems in Practice, 20-21 January , Urecht, the Netherlands*, 2000.

[5] O. Parriaux and G.J. Veldhuis. Normalised optimisation for the sensitivity optimisation of integrated optical evanescent-wave sensors. *Journal of Lightwave Technology*, 16:573–582, 1998.

[6] edt. O.S. Wolfbeis. *Fibre optic chemical sensors and biosensors.* CRC press.

[7] R. Klein and E. Voges. Integrated-optic ammonia sensor. *Fresen J. Anal Chem*, 160:513–517, 1994.

[8] N.J. van der Veen, S. Flink, M.A. Deij, R.J.M. Egberink, F.C.J.M. van Veggel, and D.N. Reinhoudt. Monolayer of a na+-selective fluoroionophore on glass: connecting the fields of monolayers and optical detection of metal ions. *Journal of the American Chemical Society*, 122:6112–6113, 2000.

[9] R.G. Heideman and P.V. Lambeck. Simple and reusable fibre-to-chip interconnect with adjustable coupling efficiency. *SPIE*, 3099:238–247, 1997.

[10] T.M. Koster, V.E. Houtsma, P.V. Lambeck, D. Klunder, T.J.A. Popma, and J. Holleman. Mode selective coupling structures for monolithic integrated waveguide-detector systems. *SPIE*, 3630:9–18, 1999.

[11] J.R. Reitz, F.J. Milford, and R.W. Christy. *Foundations of electromagnetic theory.* Addison-Wesley.

[12] K.Worhoff, A.Driessen, P.V.Lambeck, L.T.H.Hilderink, P.W.C.Linders, and T.J.A.Popma. Plasma enhanced chemical vapour deposition silicon oxynitride optimised for application in integrated optics. *Sensors and Actuators A*, 74:9–12, 1999.

[13] T.M.Koster and P.V.Lambeck. Fabrication tolerant passive polarisation converter realised in SiON technology. In *Proc. LEOS Benelux Chapter, 26 november, Gent, Belgium, 1998*, pages 117–120, 1998.

[14] Amon Yariv. *Optical waves in crystals.* John Wiley and Sons, New York.

[15] T.M.Koster and P.V.Lambeck. Passive polarisation converter in SiON technology. *Submitted to Journal of Lightwave Technology.*

[16] Z. Tang, O.Eknoyan, H.F. Taylor, and V.P. Swenson. Tunable guided-wave optical polarisation converter in lithium tantalate. *Applied Physics Letters*, pages 1059–1061, 1993.

[17] F.Wehrmann, C.Harizi, H.Herrmann, U.Rust, W.Sohler, and S.Westenhofer. Integrated optical, wavelength selective acoustically tunable 2 x 2 switches (add-drop multiplexers) in $linbo_3$. *IEEE Journal of Selected Topics in Quantum Electronics*, 2:263–296, 1996.

[18] E.C.M. Pennings. *Bends in optical ridge waveguides : modelling and experiments.* PhD thesis, University of Delft, Delft, The Netherlands, 1990.

[19] T.M.Koster and P.V.Lambeck. Thermally tunable polarisation converter. *Submitted to Pure and Applied Optics.*

[20] M. Lohmeyer, T.M.Koster, and P.V.Lambeck. Integrated optical polariser based on the cross strip interferometer configuration. In *Proc. LEOS Benelux Chapter, 30 oktober, Delft, The Netherlands, 2000*, 2000.

VI. Fully integrated optical polarimeter

Abstract- A fully integrated optical polarimeter is presented, in which all purely optical functionalities are implemented in an integrated optical (IO) circuit. This way, using IO polarisation converters, splitters, polarisers and sensing functions, a small and robust sensor is obtained. An analysis is presented of the effect of varying input signals, technological uncertainties and noise on the resolution of the sensor. The design of the complete polarimeter is given, together with a description of the device fabrication. Experimental results show an excellent agreement with the theoretical design. A fringe visibility of 0.80, phase sensitivity of $1096 * 2\pi$ and refractive index resolution of $1 * 10^{-6}$ have been obtained.

1. Introduction

Over the years, integrated optical circuits have proven to be reliable, high resolution sensing platforms for the measurement of the concentration of chemical species [1]. This can be done either by directly measuring an optical property of the desired species [2], or by using a chemo optical interface layer which transduces the chemical concentration into an optically detectable parameter [3].

In integrated optical sensors, nearly always evanescent field sensing is applied. Here, due to the interaction within the evanescent field region, a guided mode propagating along a waveguiding channel experiences the presence of the measurand, be it directly or by means of a transduction mechanism. Two types of evanescent field sensing can be distinguished, see figure 1. The first is homogeneous evanescent field sensing, where the measurand is homogeneously distributed within a medium and the evanescent field extends only in this medium. The second is surface sensing, where the interaction aimed at between the measurand and the evanescent field

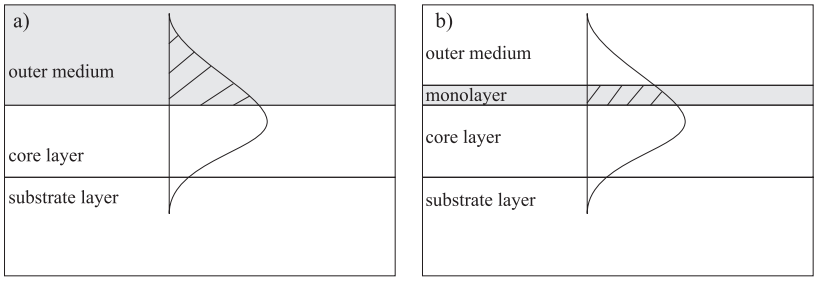

Figure 1. a) Homogeneous and b) surface evanescent field sensing.

takes place within a thin layer on top of the core layer. In the latter, only part of the evanescent field in confined within the thin layer.

A well known class of sensing platforms is based on interference. Here, changes of the concentration of the chemical species are translated into changes in the real part of the effective index of a guided mode in a waveguide. The function of the sensing circuit is to convert this change of the effective index into an intensity change which then can be measured electrically. Many platforms with this functionality are known, for example the Fabry-Perot type [4], the Mach-Zehnder type [5], the Young Interferometer type [6] and the differential interferometer [7]. In this paper the focus is on the differential interferometer.

In figure 2, the principle of a difference interferometer is shown. Over a given interaction length L_{int}, two modes propagating in the same waveguide both experience a measurand induced change in the effective index. Due to the mode dependence of this change, the phase shift between both modi at $z = L_{int}$ is a function of the concentration of the measurand. After having past the sensing function, both modes are brought to interference, and as a result generally two output signals can be obtained with intensities behaving as sinusoidal function of that phase shift. Often, and also in our case, the two modi used are the lowest order TE and TM mode, and the difference interferometer is called a polarimeter. However, other combinations of modes are possible [8].

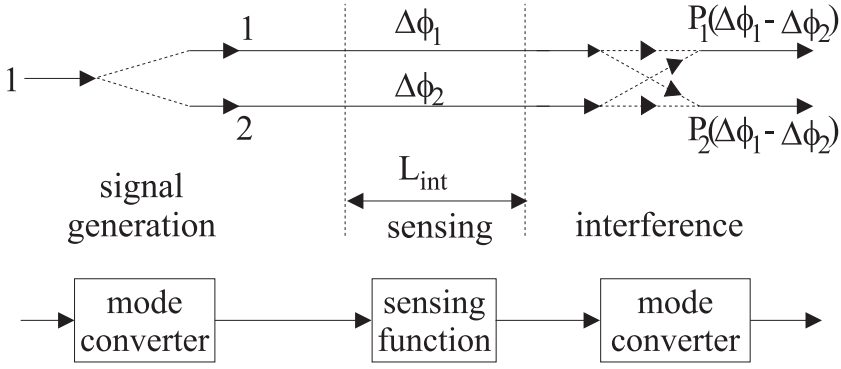

FIGURE 2. Principle of the difference interferometer.

The output signals of the polarimeter are a TE and TM mode of which the powers are sinusoidal functions of the measurand induced phase shift $\Delta\phi$, just as in the case of the a Mach- Zehnder interferometer. Comparing the polarimeter to the more familiar Mach Zehnder Interferometer (MZI), it can be seen that the principle of both sensing platforms is identical, and in fact the same type of functionalities are used. While in the case of an MZI, the measurand induced phase shift between a mode in the sensing waveguide and a mode in the reference waveguide is measured, in the polarimeter the 'sensing' and 'reference' mode propagate through the same waveguide and both experience a mode dependent measurand induced phase shift. As in

the polarimeter both modi have a positive nonzero sensitivity to the measurand, this results in a maximum sensitivity of the polarimeter that is intrinsically lower than that of a MZI. However, when optimised, the sensitivity is of a polarimeter can be of the same order of magnitude as that of a MZI. For example, consider the slab guide system $SiO_2 - Si_3N_4 - H_2O$ and the detection of index changes in the aqueous environment. The relevant sensitivity is $\partial N/\partial n_{H2O}$. For an operation wavelength of 650 nm, an optimised MZI has a sensitivity of 0.20 (optimised for TE polarisation) or 0.27 (optimised for TM polarisation). The optimised differential sensitivity of the polarimeter, $\partial \Delta N/\partial n_{H2O}$ can be shown to be around 0.15.

When slab waveguide systems are used where only the sensing function is implemented using integrated optics, and all other functionalities as bulk optical components, a polarimeter offers a clear advantage over an MZI . With the polarimeter, both polarisations propagate through the same slab guide, and therefore it is easier to have them interfere than in the case of an MZI which needs an external reference beam. Another advantage of a polarimeter over an MZI arises in the case of surface sensing, for example when using monomolecular chemo optical layers, as is the case of enzyme or dna sensing [9]. Here, one is only interested in the influence of changes in the monolayer on the optical signals. Now, as the evanescent field also penetrates in the cladding layer on top of the monolayer, time dependent changes in the refractive index of this layer (usually the sample solution) on the optical signals result in a degradation of the performance of the sensor. Due to the small thickness of the monolayer, and hence the small sensitivity for changes of the monolayer compared to changes in the cladding layer, this is an eminent problem. For example, for the $SiO_2 - Si_3N_4 - monolayer - H_2O$ slab guide system as described before, the maximal surface sensitivity $\partial N_{eff}/\partial d$ (small layer growth which occurs for example in immuno sensing) is $3.6 * 10^{-3}/nm$. For this optimised layer system, the sensitivity for index changes in the H_2O, $\partial N_{eff}/\partial n_{h2O}$ is 0.20, which is 56 times larger. With an MZI this problem can be eliminated by, in addition to the sensitive layer in the signal branch, implementing a nearly identical but insensitive chemo optical layer in the reference branch. This implies that two layers, one sensitive and one insensitive, have to be available and that one has to be able to structure both layers at their respective position on a waveguide, which is from the point of technology a daunting task.

However, in section 2, it will be shown that a polarimeter, using the same sensitive layer for both modes, can be designed in such a way that there is a zero differential sensitivity for effects in the cladding layer and a nonzero differential sensitivity for effects in the monolayer [10].

In literature, various polarimeters have been described [11],[12],[13],[14]. In all cases, only the sensing function was integrated optical, while all other optical functionalities were implemented in bulk optics, e.g. Wollastone prisms, bulk polarisation rotators and splitters etc. As a result, relatively large and expensive setups have been obtained in which the need of a precise alignment of the components limits the use to the controlled environment of a laboratory.

In this paper, we present a fully integrated optical polarimeter, where all purely optical functionalities are build within an integrated optical circuit [15]. Using ridge waveguides, integrated optical polarisation converters, splitters, polarisers and sensing windows, a small, cheap and robust sensing platform is obtained which is mechanically stable and promises a high level of performance. Realisation of these functions however, is expected to require more technological steps then making an MZI.

The device as analysed, realised and characterised in this paper has been optimised for homogeneous sensing. However, in the analysis section, also a design for surface sensing of thickness variations in monomolecular layers is given, in which the effects of cladding index changes on the output signal are eliminated.

In section 2, the functional design and in section 3 the physical design of the fully integrated optical polarimeter are presented, followed by a short description of the fabrication in section 4. Experimental results on the individual optical functionalities and the complete polarimeter and the discussion thereof are given in section 5, followed by a summary of the results in section 6.

2. Functional analysis of the polarimeter

In figure 3, the functional structures of two types of polarimeters are given, showing all subfunctions. Keeping future implementation of signal processing techniques

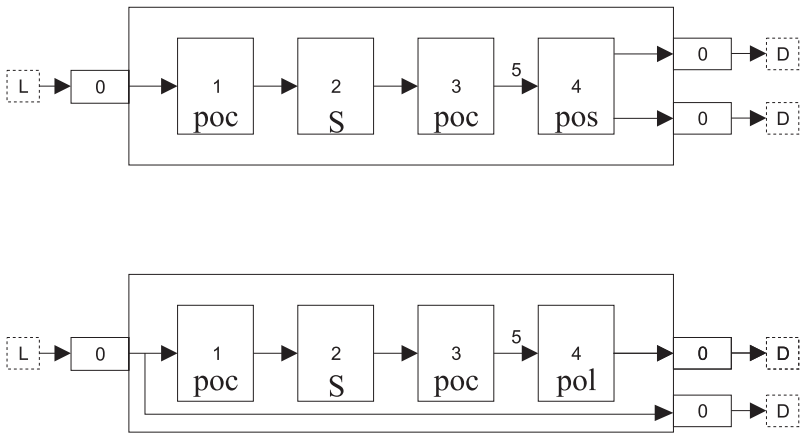

Figure 3. Functional structure of both fully integrated optical polarimeters. The components ((1,3,poc)=polarisation converter, (2,S)=sensing function, (4,pol)=polarisation splitter, (5)=monomodal channel waveguide and (6,pol)=polariser are integrated on the chip. The lightsource (L) and detectors (D) are outside the chip, hence the need for the coupling structures (0). For a further discussion of the sub functions, it is referred to the text.

in mind, in the upper structure, two output signals of different polarisation are detected. In the lower structure, by introducing a polariser only one output signal is detected. As the main results of the analysis are similar for both structures, we will focus on the upper structure and if required comment on the differences with the lower structure.
Light from a lightsource (L) is launched into a monomodal channel waveguide. The main subfunctions of the device are a polarisation converter (poc) in order to obtain a desired distribution of the incident optical power over both modes, a sensing function (S) where both modes experience a different measurand induced phase shift, a second polarisation converter (poc), where both modes interfere and which has as output signals a TE and TM mode of which the amplitudes depend on the phase shift and finally a polarisation splitter (pos) to couple light of different polarisation in different channel waveguides. All functions are connected by identical monomodal channel waveguides, capable to support the lowest order TE and TM mode only. The light in both output channel waveguides is coupled out of the integrated optical circuit (I) into photodiodes (D). In the second polarimeter, the polarisation splitter is replaced by a polariser (P) which is meant to transmit one of the polarisations only. Also, a reference branch is included.

A theoretical description of the first device has been made using the matrix transfer method [16]. In this model, the optical field in the waveguide (amplitude and phase) is represented by a 1*2 array, where the elements symbolise the optical field of the TE and TM mode, respectively. Each subfunction is represented by an 2*2 matrix. The transfer function of the complete polarimeter can then be written as

$$\overline{E}_{out} = \overline{M}_4\overline{M}_{5,3}\overline{M}_3\overline{M}_2\overline{M}_{5,2}\overline{M}_1\overline{M}_{5,1}\overline{E}_{in} \tag{1}$$

Here, $\overline{E}_{out}, \overline{E}_{in}$ correspond to the output and input fields, respectively. The matrix $\overline{M}_i$ corresponds to the i^{th} integrated optical functionality and $M_{5,j}$ to the j^{th} straight waveguide section.
The amplitudes of the input fields are given by

$$\overline{E_{in}} = \begin{bmatrix} \sqrt{A} \\ \sqrt{1-A}e^{i\theta} \end{bmatrix} \sqrt{P_{in}}\overline{E}_{norm}. \tag{2}$$

Here, A and $(1-A)$ are the fractions of the input power in the TE and TM mode, respectively, θ their phase difference at the input of the sensing platform and P_{in} is the total input power. $\overline{E}_{norm}$ is the array, defined by the maxima of the modal field distributions, corresponding with modal powers equal to 1 W.
The complex output fields are represented by

$$\overline{E}_{out} = \begin{bmatrix} A_{TE,out} \\ A_{TM,out} \end{bmatrix}, \tag{3}$$

where the corresponding output powers are given by $|A_{TE,out}|^2$ and $|A_{TM,out}|^2$. Note that the phase factor is irrelevant for the detection.
The transfer matrix of the j^{th} straight channel waveguide sections is

$$\overline{M}_{5,j} = \begin{bmatrix} e^{-i\beta_{TE}L_j} e^{-\frac{1}{20}\ln(10)\alpha_{TE}} & 0 \\ 0 & e^{-i\beta_{TM}L_j} e^{-\frac{1}{20}\ln(10)\alpha_{TM}} \end{bmatrix}, \tag{4}$$

where L_j is the length of section j, β_{TE} and β_{TM} represent the real parts of the propagation constants and α_{TE} and α_{TM} the losses (in dB) in channel section j for the TE and TM mode, respectively.
The (lossless) transfer matrices for the first and second polarisation converter are

$$\overline{M}_j = \begin{bmatrix} \cos(C_j L_j) & i\sin(C_j L_j) \\ i\sin(C_j L_j) & \cos(C_j L_j) \end{bmatrix}, \tag{5}$$

with i the complex number and C_j and L_j the coupling strength and the length of the j^{th} converter [17].
The transfer matrix for a (lossless) polarisation splitter is

$$\overline{M}_4 = \begin{bmatrix} \sqrt{1-\kappa_{TE}} & \sqrt{\kappa_{TE}} \\ \sqrt{\kappa_{TM}} & \sqrt{1-\kappa_{TM}} \end{bmatrix} \tag{6}$$

where κ_{TE} and κ_{TM} represents the power fractions coupled into the 'wrong' output waveguide. So, the crosstalk of the splitter (in dB) equals $-10log_{10}(\kappa_j/(1-\kappa_j))$.
The matrix for a (lossless) polariser in the second structure in figure 3 is

$$\overline{M}_4 = \begin{bmatrix} 1-\gamma & x\sqrt{\eta_{TM}} \\ y\sqrt{\eta_{TE}} & \gamma \end{bmatrix} \tag{7}$$

In the case of a TE polariser (γ = 0,x=1,y=0) it is η_{TM} and for a TM polariser (γ = 1,x=0,y=1) η_{TE} that represent the transmittance of light with the undesired polarisation.

Now, first a hypothetical polarimeter will be discussed, for which it has been assumed that the intended device can be realised exactly using a perfect fabrication technology. Furthermore, it will be assumed that the structure is lossless, the polarisation splitter has no crosstalk, for both polarisation converters $CL = \pi/4$ and that the input light is TE polarised. Then the transfer function of the device can be written as

$$\begin{aligned} \frac{P_{TE}}{P_{in}} &= \frac{1}{2}\{1+\cos(\Delta\phi+\Phi_0)\} \\ \frac{P_{TM}}{P_{in}} &= \frac{1}{2}\{1-\cos(\Delta\phi+\Phi_0)\} \end{aligned} \tag{8}$$

Here, $\Delta\phi$ is the measurand induced phase shift and Φ_0 is a phase offset due to the difference in the propagation constants of the TE and TM modes. In figure 4, for $\Phi_0 = 0$ both output signals are shown as a function of the measurand induced phase shift. Because of their similarity in the type of output signals, the polarimeter shows the same intrinsic problems for the determination of the phase shift as the MZI, namely directional ambiguity, fringe order ambiguity and sensitivity fading [5].

In literature, several solutions to these problems have been given, many of them described in [18]. Active modulation of the sensor can be applied, e.g. a feedback loop is used as to obtain instead of a sinusoidal a linear output signal [19]. A triangular $\phi = 2\pi$ modulation affords a quadrature point detection, offering extremely large sensitivities [5]. Methods avoiding active modulation have also been presented. For example, a couple of sensors with different phase sensitivity can be used, and from all output signals the real $\Delta\phi$ can be derived. [20]. In [11], four output signals are obtained, which after some basic post-signal processing also result in a linearised signal. In the device presented in this paper, as our intention is to demonstrate the feasibility of a fully integrated optical polarimeter only, none of the solutions presented in the references above have been implemented. Whether or not these intrinsic problems are relevant in a practical situation of course depends on the specific application of the sensing platform. However, if required, all of the before mentioned methods can be implemented into our device, without any doubt leading to a strongly improved resolution.

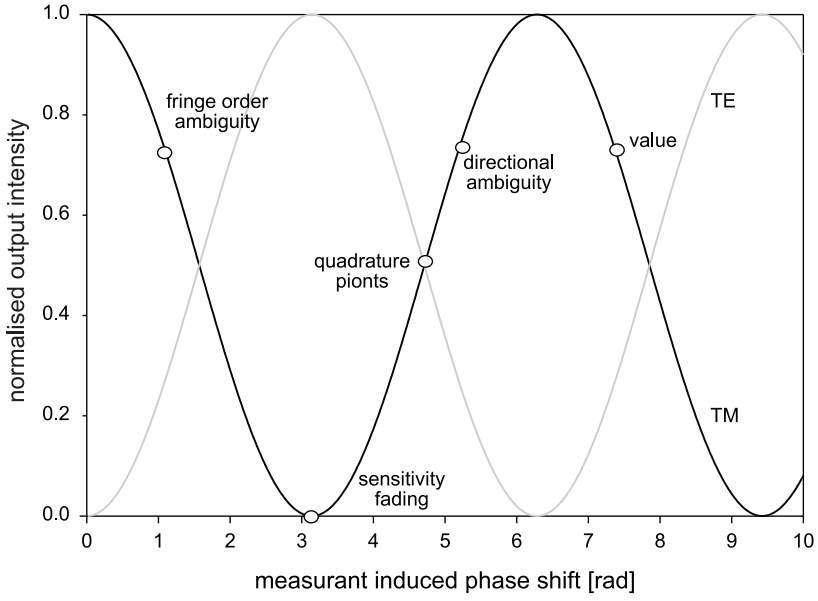

FIGURE 4. Output signals of the ideal polarimeter, showing all intrinsic measurement problems.

Equations (8) were derived for TE polarised input light. For an arbitrary state of polarisation of the input light, the output powers are a complicated function of both the amplitude ratio $\sqrt{A}/\sqrt{1-A}$ of and the phase difference θ between the TE and TM input fields. In a laboratory setup, this feature can be used to adjust the polarisation state of the input signal to obtain an optimum working point where highly sensitive measurements can be performed. If $A \neq 0, 1$, a factor V, the fringe visibility, has to be added as a multiplication factor to the cosine functions, where V is defined as

$$V = 2\frac{P_{ma}}{P_{ma} + P_{mi}} - 1, \tag{9}$$

with P_{ma} and P_{mi} the maximum and minimum output signals. This fringe visibility V is an important parameter because the resolution increases, the higher V, as will be shown later on. In figure 5, the fringe visibility is shown as a function of A and ϕ. From that figure it can be seen that for circular polarised input light, the fringe visibility is zero. In order to have the highest fringe visibility and to avoid undesired phase shifts in the output signals caused by an unintended change of

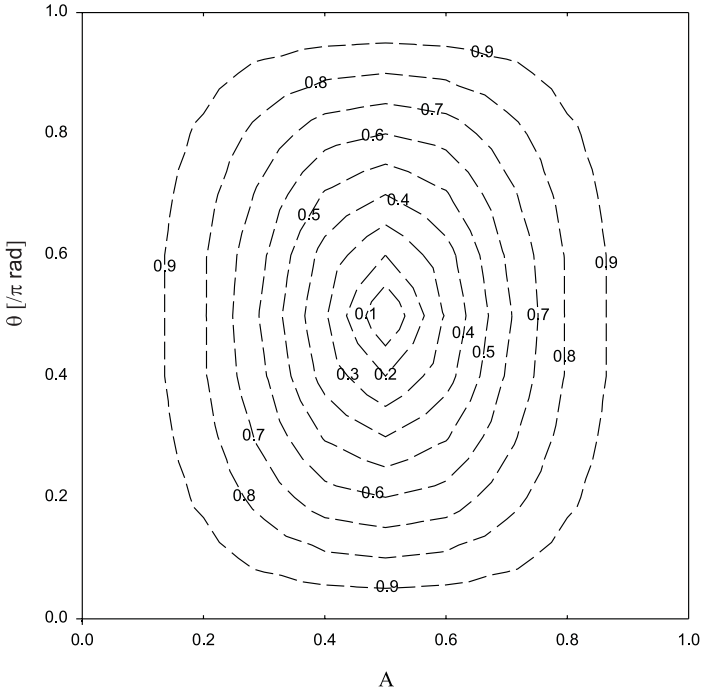

FIGURE 5. Fringe visibility as a function of the composition of the light launched into the integrated optical polarimeter, for explanation see the text.

the polarisation state of the input light, this polarisation state should be fixed. In practical situations this comes down to launching light of one polarisation only in the polarimeter.

If the light is launched from an ordinary fiber into the circuit, and there is no control over its polarisation, a polariser has to be incorporated in the circuit. However, now the problem arises that for example, no light is launched in the polarimeter circuit when the input light happens to be completely TM polarised while a TM polariser was incorporated. Although this problem can be overcome, e.g. by introducing an extra tunable polarisation converter and a feedback loop [21], it is simpler to apply polarisation maintaining fibers for the light transport.

For a monomodal input signal, the fringe visibilities for both output signals can be written as a function of the propagation losses α_b and α_c in the straight waveguide sections connecting the converters and the CL products (assuming lossless converters):

(10)
$$V_b = 2\frac{4\cos(C_1L_1)\cos(C_2L_2)\sin(C_1L_1)\sin(C_2L_2)e^{-\frac{1}{10}\ln(10)(\alpha_b+\alpha_c)}}{[\sin(C_1L_1)\sin(C_2L_2)e^{-\frac{1}{10}\ln(10)\alpha_c}+\cos(C_1L_1)\cos(C_2L_2)e^{-\frac{1}{10}\ln(10)\alpha_b}]^2}-1$$

(11)
$$V_c = 2\frac{4\cos(C_1L_1)\cos(C_2L_2)\sin(C_1L_1)\sin(C_2L_2)e^{-\frac{1}{10}\ln(10)(\alpha_b+\alpha_c)}}{[\sin(C_1L_1)\cos(C_2L_2)e^{-\frac{1}{10}\ln(10)\alpha_c}+\cos(C_1L_1)\sin(C_2L_2)e^{-\frac{1}{10}\ln(10)\alpha_b}]^2}-1$$

If the input light is TE polarised, the 'b'=TE and 'c'=TM, for TM polarisation the reverse holds.

It can be derived that the fringe visibilities equal to one can be obtained only for the bar ('b') and the cross ('c') output signal if the following relations are obeyed:

(12) $$C_1L_1 = \arctan(\frac{e^{-\frac{1}{20}\ln(10)(\alpha_b-\alpha_c)}}{\tan(C_2L_2)}) \text{ for the bar output signal}$$

and

(13) $$C_1L_1 = \arctan(e^{-\frac{1}{20}\ln(10)(\alpha_b-\alpha_c)}\tan(C_2L_2)) \text{ for the cross output signal}$$

These relations can only be fulfilled simultaneously if C_2L_2 is $\pi/4$. If the loss difference $\alpha_b - \alpha_c$ is known, C_1L_1 can then be calculated using equation (12) or (13). For small loss differences ($< 3\ dB$),

(14) $$C_1L_1 \approx \frac{\pi}{4} - \frac{\ln(10)}{40}(\alpha_b - \alpha_c)$$

Losses in the converters themselves can be incorporated into an effective CL product [22]:

$$(CL)_{eff} = CL\sqrt{1 - \frac{(a_{TE} - a_{TM})^2}{16C^2}} \tag{15}$$

Here, a_{TE} and a_{TM} are the functional losses in the converter for the TE and TM mode, respectively. From this equation, it can be seen that only a difference between the functional losses for both modes results in an effectively lower CL product. Then, for compensating the effects of these losses on the amount of conversion, the length of the converter has to be increased.

Besides obtaining the desired coupling strength, the strong wavelength dependence of the converters to be used also has to be taken into account. The maximum amount of conversion occurs for the resonance wavelength λ_r. Now, for the intended coupling strength, the desired amount of conversion can only be obtained if the resonance wavelength of a realised converter coincides with its intended value. This aspect of the converter will be addressed to in the experimental section.

In absence of noise, the phase resolution of the sensor should be infinite except when the phase is $n\pi/2$ (sensitivity fading, see figure 3). However, in practice noise is inevitable. As the resolution of the sensor is determined by the signal to noise ratio, and the signal level strongly depends on the fringe visibility, a relation between the resolution and the noise and V will be derived. It will be shown that, if no reference signals or signal processing is used, the quadrature points are in general not the preferred working points for performing the most sensitive measurements. In figure 6, the sinusoidal output signal is shown as a function of $\Delta\phi - \Phi_0$. This signal can be written as

$$\frac{P_{out}}{P_{in}} = \frac{1}{2}\left\{1 + V\cos(\phi - \Phi_0)\right\}, \tag{16}$$

where V is given by (9). Assuming that the noise of the CW laser input signal is a constant fraction δ of the laser signal itself, the noise in the detector signal can be written as

$$P_{noise} = \delta P_{out} + P_{min}. \tag{17}$$

Here P_{min} is the minimum detectable optical power, which is given by the NEP of the detector system.

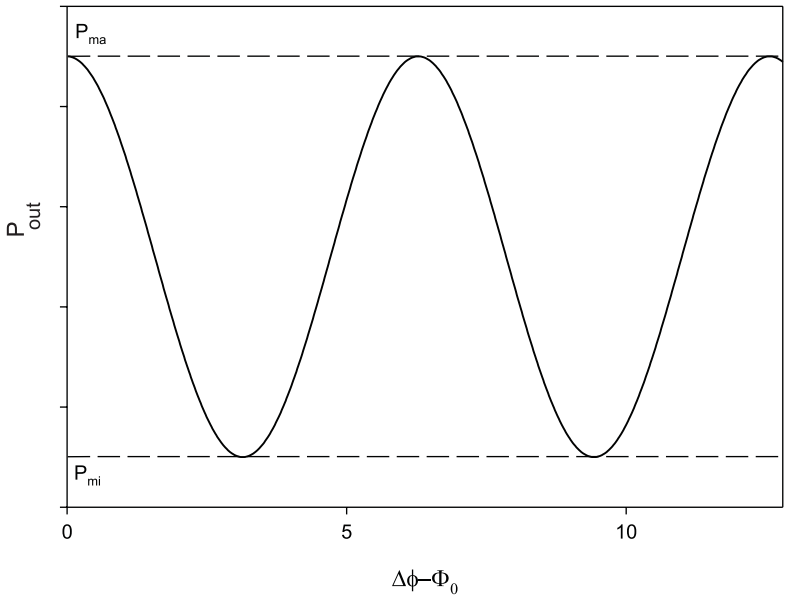

FIGURE 6. The sinusoidal output signal of the polarimeter.

The phase resolution $\Delta\phi_{res}$ can be written as

(18)
$$\Delta\phi_{res} = \frac{\partial(\phi - \Phi_0)}{\partial P}\Delta P = \frac{-2\,(\delta P_{out} + P_{min})}{V P_{in}\sin(\phi - \Phi_0)} = -\frac{\delta(1 + V\cos(\phi - \Phi_0)) + 2\frac{P_{min}}{P_{in}}}{V\sin(\phi - \Phi_0)}.$$

Hence it is relevant to investigate under which conditions $\Delta\phi$ should be at a minimum. At first we will look at the ϕ-dependence . A minimum can be obtained at the zero points of the derivative

(19)
$$\frac{\partial\Delta\phi_{res}}{\partial(\phi - \Phi_0)} = \frac{(\delta + 2\frac{P_{min}}{P_{in}})\cos(\phi - \Phi_0)}{V\sin^2(\phi - \Phi_0)} + \frac{\delta(1 + \tan^2(\phi - \Phi_0))}{\tan^2(\phi - \Phi_0)} = 0,$$

giving the optimum working point

(20)
$$\Phi_0 = -\arccos\left(-\frac{\delta V}{\delta + 2\frac{P_{min}}{P_{in}}}\right).$$

Then, the minimum resolution can be found to be

$$\Delta\phi_{res,min} = \frac{1}{V}\sqrt{(\delta + 2\frac{P_{min}}{P_{in}})^2 - \delta^2 V^2} \tag{21}$$

For $\delta = 0$, the minimum resolution is obtained at the quadrature points, $\phi - \Phi_0 = \pi/2$ as is always mentioned in literature. An increasing δ however results in a shift of the optimum phase angle towards π, which extreme value can be reached when $V = 1$ and $P_{min}/P_{in} \to 0$. Note from (20), that $\Delta\phi_{res,min}$ is minimal for $V = 1$, for which the resolution

$$\Delta\phi_{res,min} = \sqrt{(\delta + 2\frac{P_{min}}{P_{in}})^2 - \delta^2} \tag{22}$$

is obtained for

$$\Phi_0 = -\arccos\left(-\frac{1}{1 + 2\frac{1}{\delta}\frac{P_{min}}{P_{in}}}\right), \tag{23}$$

and,

$$\frac{P_{out}}{P_{in}} = \frac{1}{\delta\frac{P_{in}}{P_{min}} + 2}. \tag{24}$$

In figure 2, for V=0.5, 0.8 and 1 the minimum resolution is given as a function P_{min}/P_{in} and δ (for realistic parameter ranges of these variables) . For V=1, $\Delta\phi_{res,min}$ has a strong dependence on δ and P_{min}/P_{in}. As can be expected, for $V < 1$, the influence of P_{min}/P_{in} becomes smaller and for the higher δ-values $\Delta\phi_{res,min}$ depends mainly on δ.
By adjusting the Φ_0 to the optimal $\phi - \Phi_0$, the resolution is enhanced with respect to $\Delta\phi_{\pi/2}$ with a factor

$$\frac{\Delta\phi_{\pi/2}}{\Delta\phi_{res,min}} = \frac{1}{\sqrt{1 - V^2\frac{\delta^2}{\left(\delta + 2\frac{P_{min}}{P_{in}}\right)^2}}} \tag{25}$$

The resolution enhancement is the larger, the larger V. In figure 2, for V=0.5, 0.8 and V=1, the resolution enhancement is given as a function of P_{min}/P_{in} and δ. For V=1, the resolution enhancement is even being spectacular, for example, for 12.5 for $\delta = 0.005$ and $P_{min}/P_{in} = 10^{-5}$.

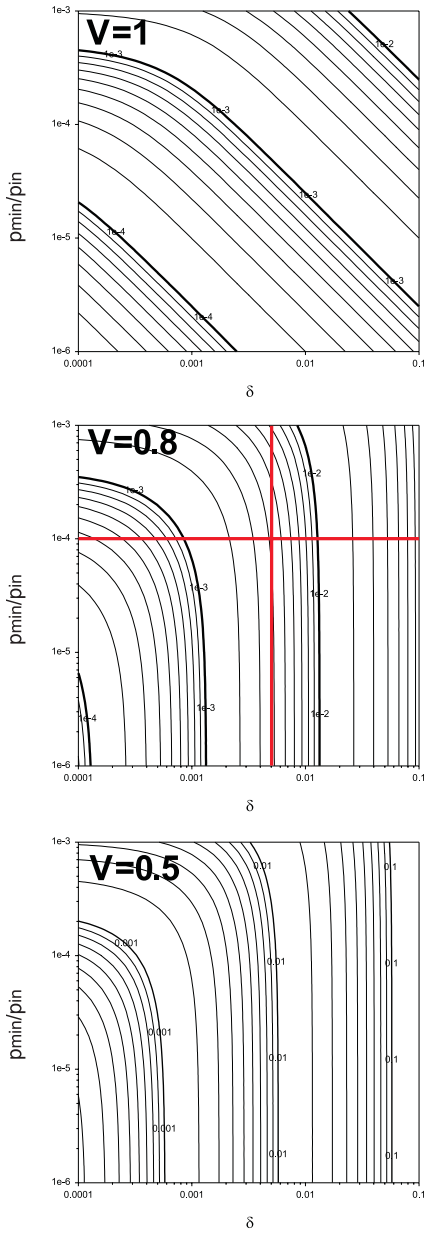

FIGURE 7. Phase resolution of the polarimeter versus δ and P_{min}/P_{in} for several values of V.

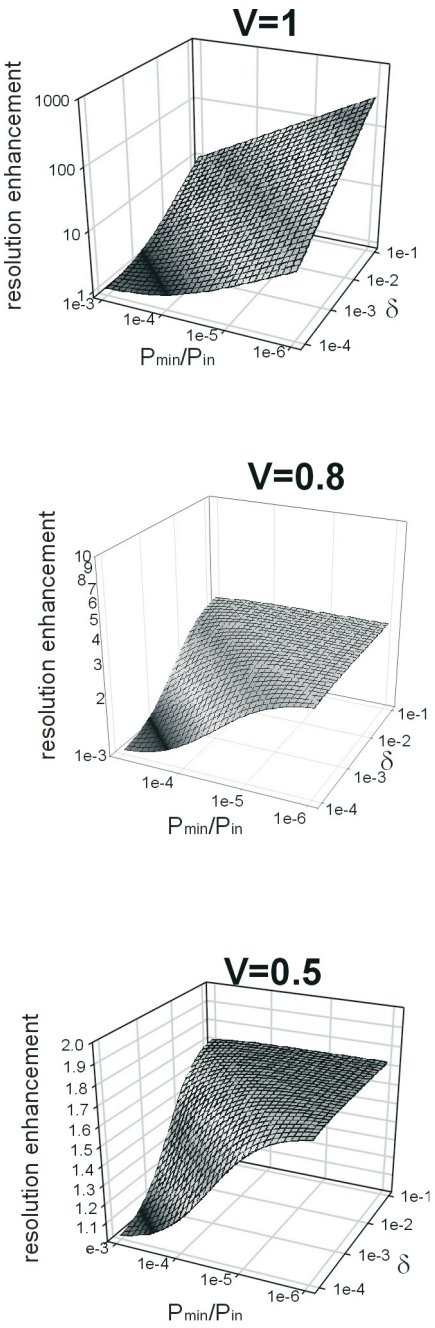

FIGURE 8. The resolution enhancement of the polarimeter versus δ and P_{min}/P_{in} for several values of V.

The phase resolution is correlated to the resolution in the effective index difference by

$$\Delta N_{eff} = \frac{\Delta\phi_{res}\lambda}{2\pi L_{int}} \tag{26}$$

For an operation wavelength of 655nm, an interaction length $L_{int} = 5mm$ and a phase resolution of 0.0014 ($\delta = 0.005, P_{min}/P_{in} = 10^{-4}, V = 1$), the lowest resolution in the effective index is $2.9*10^{-8}$ at $\phi_{min} = 0.91\pi$. For the realistic value $\frac{\partial\Delta N_{eff}}{\partial n_c} = 0.2$ this implies a resolution in the refractive index of about $1.5*10^{-7}$.

The analysis emphasises the importance of having a high fringe visibility and low noise terms, especially the laser noise δ which can be decreased by choosing a low noise lightsource. P_{min}/P_{in} can be reduced by using low-noise detectors and taking a high input power. Also emphasised is the need for obtaining the information by dividing two output signals, both proportional to P_{in}, as this will drastically decrease the influence of the lightsource noise.

Up to now, it had been assumed that the splitting ratio of the polarisation splitter was infinite. A finite splitting ratio decreases the accuracy of the sensor, especially at the minima of the sinusoidal output signals. The accuracy decreases for two reasons. First, not all the power of a mode is coupled into its intended output waveguide, but a fraction is 'lost' in the wrong output guide. Second, a fraction of the power of the 'wrong' mode is coupled in each output waveguide. In order to minimise these effects, the splitting ratio should be as large as possible.

Apart from the effects of imperfectness of the individual components, also environmental effects can influence the accuracy of the sensor. Temperature fluctuations may give rise to variations in the amount of light coupled in and out of the chip, they can give rise to undesired phase shifts due to the temperature dependence of the refractive indices of the layer system, they may influence the chemistry of a transduction layer, thereby altering the chemo-optical response of this layer etc. This manifold of temperature effects in practice excludes effective modelling. Therefore, temperature effects have to be studied experimentally, and in case of unacceptable performance degradation, temperature stabilisation has to be introduced.

Summarising the main conclusions : for obtaining a good performance it is necessary to launch light of one polarisation only in the polarimeter. The best performance is obtained in the case the complete device should be lossless, of both converters the CL-product should be $\pi/4$ and the polarisation splitter should be crosstalk free. Effects on the resolution caused by a difference in the propagation losses of both modes in the converters and in the waveguide sections inbetween both converters can be compensated for by choosing specific values for the CL-product of both converters. It was shown that in case one output signal can be obtained only the quadrature points as working points (Φ_0) result in the best resolution for noise free lightsources only. Otherwise, the optimum working point depends on the lightsource noise, the detector noise, the fringe visibility and the input power.

Quantitative relations have been given, from which it can be concluded that the fringe visibility and the input power should be maximised and δ and P_{min} should be minimised. By division of the output signal by a reference signal or a second output signal also being proportional to P_{in}, the influence of the lightsource noise can be completely suppressed.

3. Physical design of the polarimeter

In this section, the implementation of the subfunctions will be discussed. First, the material system in which the structure will be realised will be introduced. Then, the design of the sensing function (optimisation in the case of homogeneous and surface sensing), the converters, polarisation splitter and polariser will be discussed.

The device will be realised in SiO_xN_y technology [23] on a Silicon substrate. In figure 9, a cross section of the ridge channel waveguide is shown. The layer stack consists of a SiO_2 buffer layer (n=1.456) in order to prevent undesired losses due to absorption of the light into the Silicon substrate, a Si_3N_4 core layer (n=2.01) in which a small ridge is realised and on top a SiO_2 protective layer (n=1.47), which protects the propagating light from environmental influences (i.e. dust etc.).

The protective layer is locally removed for obtaining the sensing function where a mode in the waveguide is exposed to the measurand, which here is assumed to be a diluted solution of some chemical compound in water (n=1.33). The high index Si_3N_4 is taken as to obtain a high sensitivity [24].

The layer structure shown in figure 9 will be the starting point of the design for all subfunctions. Optimisation of the different subfunctions is achieved by defining the optimal core layer thickness and heights of the ridges of the waveguiding channel. As will be shown in the section describing the fabrication of the device, sections with different core thicknesses can be connected together using adiabatic tapering.

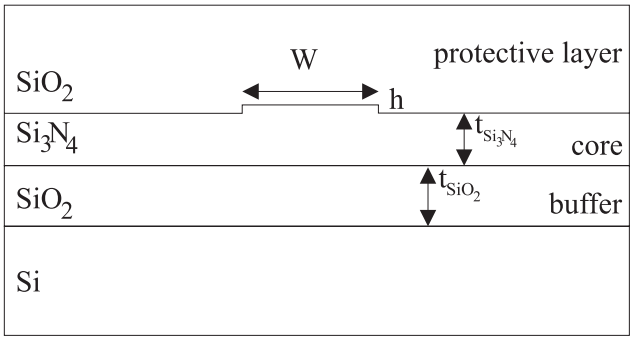

Figure 9. The basic optical layer structure.

The sensing function has to be optimised for obtaining the largest phase sensitivity, $\frac{\partial \phi}{\partial n_{sens}}$, where n_{sens} is the refractive index of the sensing layer. For the polarimeter, this phase sensitivity equals

$$\frac{\partial \phi}{\partial n_{sens}} = \frac{2\pi}{\lambda} L_{int} \left(\frac{\partial N_{TM}}{\partial n_{sens}} - \frac{\partial N_{TE}}{\partial n_{sens}} \right) \tag{27}$$

Here, λ is the operation wavelength and L_{int} the interaction length along which the light experiences the refractive index changes. The two derivatives between the brackets correspond to the sensitivities of the effective indices of the individual modes to changes in the sensing layer index. These later terms are functions of the wavelength and the optical layer structure. Figure 10 shows these modal sensitivities of the effective indices and their difference as a function of the Si_3N_4 core thickness for an operating wavelength of 655nm and an aqueous environment. It can be seen that for a core thickness of 136 nm, a maximum of 0.152 in the differential sensitivity is obtained. The maximum is fairly broad, i.e. the differential sensitivity is rather insensitive to variations in the Si_3N_4 core thickness. The maximum differential sensitivity is about 60% of the maximum sensitivity of the individual TM-mode.
For an interaction length of 5mm, the sensitivity $\frac{\partial \phi}{\partial n_{sens}}$ can be calculated to be $1169 * 2\pi$ rad, which means that a phase shift of 2π corresponds to an index change Δn_{sens} of $8.55 * 10^{-4}$.

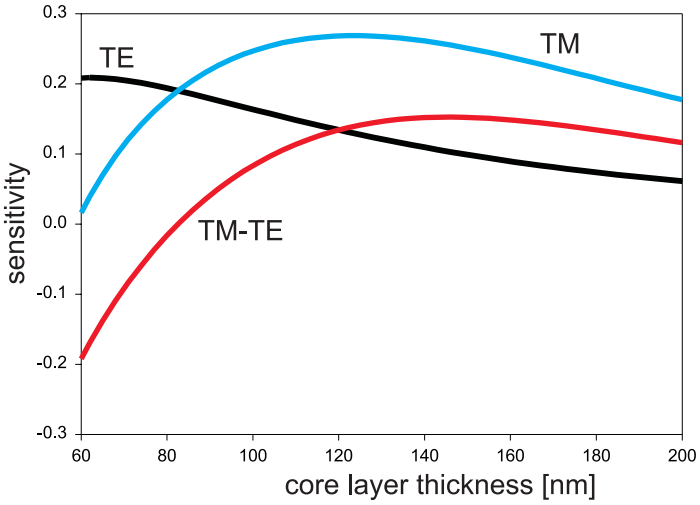

FIGURE 10. Various sensitivities as a function of the core layer thickness.

For bulk sensing, this analysis suffices. For surface sensing, there is an additional problem. The refractive index of the environment just outside the thin (sometimes monomolecular) transduction layer may also vary within the evanescent field region, and the sensor has to be made insensitive to these variations. This implies a zero differential sensitivity for environmental refractive index changes, while having a nonzero differential sensitivity for changes in the thickness (due to for example

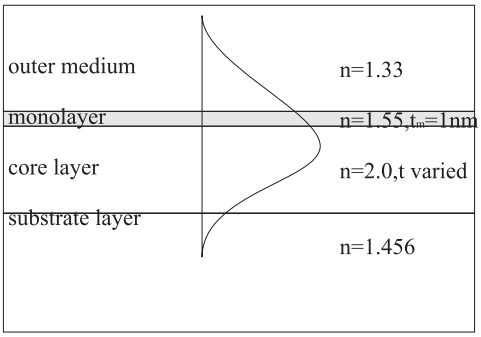

FIGURE 11. Layer structure in the case of monolayer transduction layers.

an antibody-antigen reaction) or refractive index of the transduction layer, see figure 11. For a wavelength of 655nm, in figure 12 the differential sensitivities of the effective indices for monomolecular thickness changes and environmental refractive index changes are shown as a function of the core thickness for a 1nm thick monolayer with n=1.55. It can be seen that the differential sensitivity for cladding index changes is zero for a core thickness of 82.5 nm, while the monolayer differential sensitivity $\partial \Delta N / \partial d$ is 0.0019. Also, it can be seen that this elimination

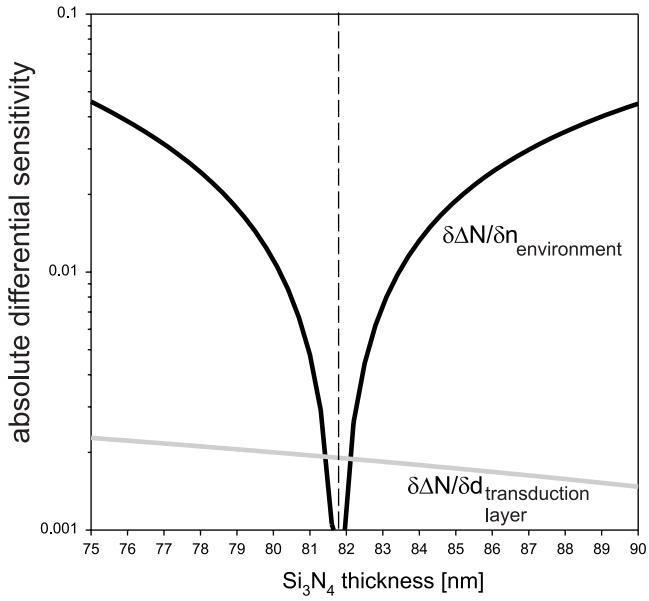

FIGURE 12. Differential sensitivities versus the core layer thickness for the case of monolayer transduction layers.

method is rather critical regarding the required core thickness, so when fabricating the device this thickness has to be controlled very accurately. The significance of the phase error induced by a nonzero differential sensitivity to environmental index changes of course depends on the thickness and refractive index change of the monolayer. For example, a bio-reaction giving a thickness increase of 0.01nm [25] of the transduction layer will result into a ΔN change of $1.9 * 10^{-5}$. A temperature change of 5 degrees results in an index change of the water of $5 * 10^{-4}$. Then, taking a differential sensitivity of 10^{-3}, the relative phase error due to the temperature fluctuations is only 0.026. So, even with temperature fluctuations of 5 degrees, this bio-reaction can be observed.

We will focus on polarimeters for bulk sensing in aqueous solutions for a wavelength of 655 nm.

The polarisation converters, used to obtain the two modes with different polarisations before the sensing function and to obtain interference of these modes after the sensing function are co-directional grating assisted couplers, as described in [ref]. The structure of these couplers consists of alternating segments with asymmetrical cross sections, as shown in figure 13. Due to this asymmetry, resonant coupling between the otherwise orthogonal TE and TM modes is achieved.

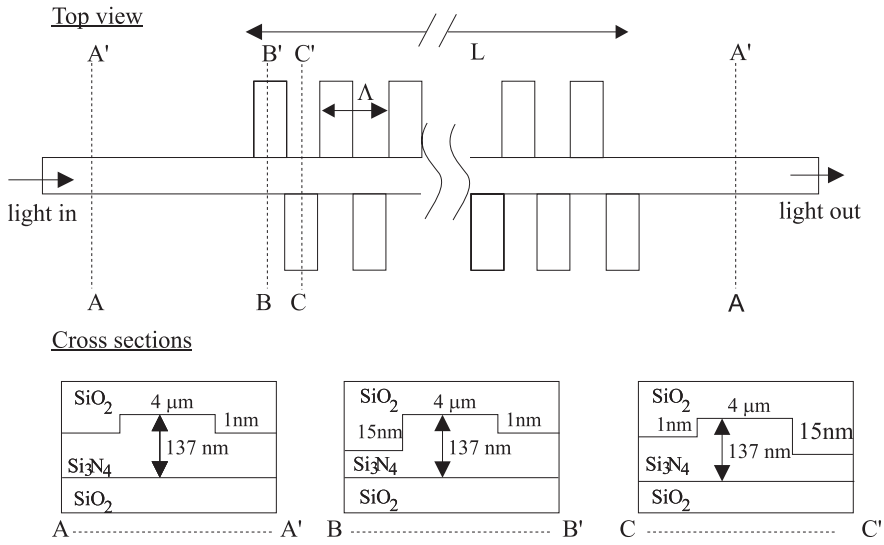

FIGURE 13. Topview and cross sections of the polarisation converter.

In order to minimise the number of technological steps, the converters will be realised in the same 137 nm thick Si_3N_4 core layer as is used for the sensing function. This thickness has the additional advantage of a $\partial(N_{TE} - N_{TM})/\partial d_{Si_3N_4} = 0$, resulting into a large insensitivity to small variations of this core thickness [26].

Applying a shallow and deep etch step of 1 nm and 15 nm respectively, the effective indices of the TE_{00} and the TM_{00} modes are 1.7080 and 1.6005, respectively, calculated using the EIM of [27]. The grating period Λ required for grating induced coupling (phase matching) is 6.09 μm. A tolerance analysis, as given in [26], shows that for the realised device the resonance wavelength can be expected to be 655 $\pm$ 3.7 nm.
We assume that the propagation losses for the TE and TM modes in the waveguide sections inbetween the converters are identical (as will appeare to be true for the realised device), so both converters will be designed to have $CL = \pi/4$. Experimentally, it has been found that, for shallow and deep etch steps of 1 and 15 nm, complete mode conversion occurs for grating lengths of 10 mm [26]. So, in order to have $CL = \pi/4$, the converters will be designed to have a length of 5 mm. Also, it has been found [28] that the functional losses of the converters are identical for both polarisations, namely 1.5 $\pm$ 0.15 dB / converter.

The polarisation splitter has to show a crosstalk as low as possible, as has been shown in the analysis section. Two different types of polarisation splitters have been investigated. The first were polarisation selective coupling structures [29] combined with monolithically integrated photodiodes, as shown in figure 14. These coupling structures are based on the mode dependent mode field widening when thinning down the core layer thickness. This affords that the TM mode is coupled into the first detector while the TE mode passes without any perturbation and can be subsequently coupled into the second detector. However, it was found that, although theoretically very low crosstalks (<-40dB) can be achieved, experimentally the TE crosstalk appeared to be limited (-13 to -15 dB) due to scattering of TE light into the TM photodiode [30]. As this crosstalk is rather high, we also investigated a polarisation splitter which splits TE and TM modes into different output channels. For this, we used a two mode interferometer [31] which we optimised (using [32]) for our layer system. The theoretically designed TMI should show a crosstalk of -30dB and an insertion loss -0.13dB for the TE mode and a crosstalk of -27.5dB and an insertion loss -0.27dB for the TM mode.

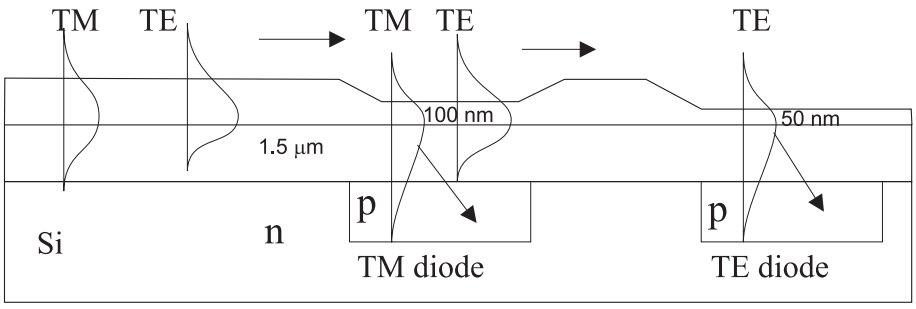

FIGURE 14. The mode selective waveguide-detector coupling structures.

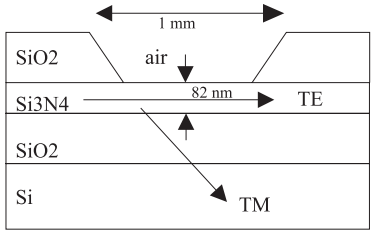

FIGURE 15. Structure of the polariser.

In an alternative structure, we would like to measure the TE output of the second converter only. For blocking all TM light in the TE output channel,a TM polariser can be used. The structure of the polariser is shown in figure 15, an is identical to that of the mode selective coupling structures of figure 14. By thinning the core layer down to 82 nm, which is well between the cutoff thicknesses of the TE mode (49 nm) and the TM mode (95 nm), a TM polariser is obtained. Calculations using beam propagation methods [32] show a TM attenuation of 125dB/mm. Therefore, with a polariser length of 1 mm, a TM attenuation of 125 dB is obtained, while the TE losses are calculated to be only 0.01dB.

In figure 16, for the first polarimeter, their functional structure already being given in figure 3, the physical design and the expected performance features are given. In the first device, the light is launched into and coupled out of the polarimeter using end fire coupling. For practical devices, we can switch to polarimeters

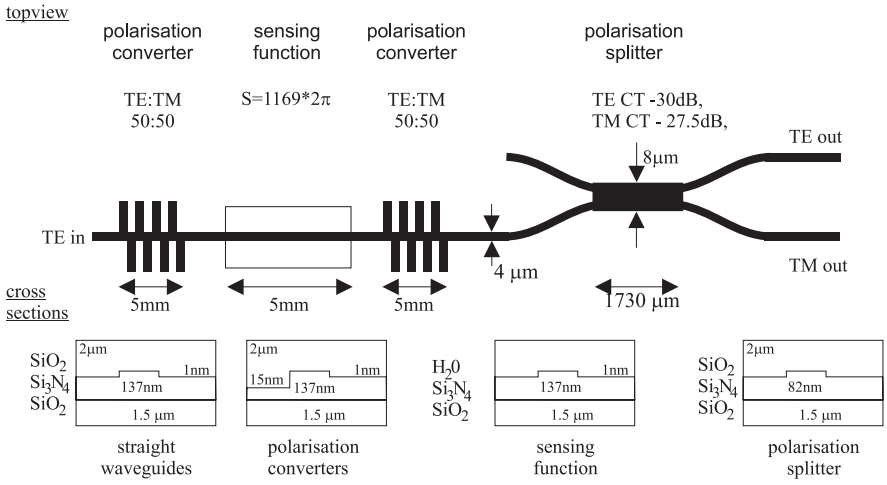

FIGURE 16. The complete physical design of the polarimeter, and the expected performance characteristics of the subfunctions.

with integrated fiber to chip couplers [33] as are currently being realised in our laboratory.

4. Device fabrication

The devices are fabricated on 3 inch $< 100 >$ Silicon wafers. On these wafers, the device is realised by growth, deposition and etching of thin layers. We will now in short describe the fabrication sequence for the realisation of the device.

The first step is the growth of a 3 μm thick SiO_2 layer by wet oxidation of a Silicon wafer at 1150^o Celcius. Next, using Low Pressure Chemical Vapour Deposition (LPCVD) [23], a 136 nm thick Si_3N_4 core layer is deposited. The core layer is then tapered down to 82 nm at the position of the polarisation splitter using Buffered Hydro-Fluoric (BHF) acid and exploiting the under etching of the photoresist mask material for obtaining adiabatic tapers with low tapering angles [34]. Now, the ridge waveguides are defined by a 1 nm etch step in the Si_3N_4 layer again using BHF etching. Next, using a double exposure step, the polarisation converters (15 nm deep etch step) are realised by Reactive Ion Etching (RIE). Finally, the protective SiO_2 layer is deposited using Plasma Enhanced Chemical Vapour Deposition (PECVD), and sensing windows are etched using photolithography BHF etching. After cleaving the devices, for making appropriate end faces, they are ready for characterisation.

5. Experimental results

For characterising the polarimeter, the experimental setup shown in figure 17 was used. The light source was a Spectra Physics Argon pumped (515 nm) Dye laser (DCM dye, 620-680 nm, step size 0.03 nm).

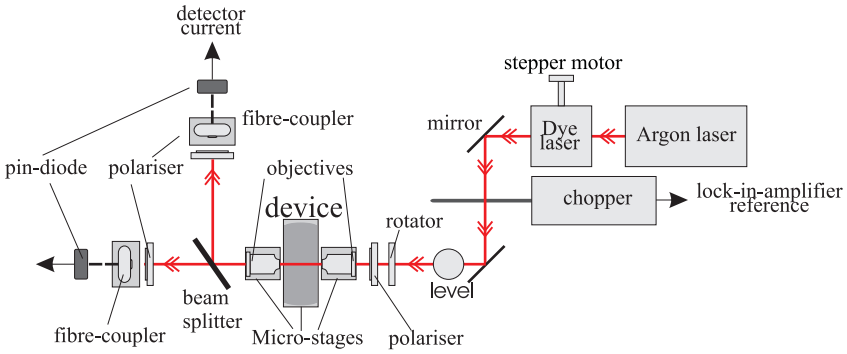

Figure 17. The experimental set up.

First, the theoretically calculated sensitivity of $1169 * 2\pi$ has been experimentally verified. Using a flow injection system, the phase change when substituting

methanol (n=1.329) for ethanol (n=1.360) as cladding material in the sensing window was measured. This phase change was found to be 68π rad, which corresponds to a phase sensitivity of $1096 * 2\pi$. The measured phase sensitivity deviates only 6% from its theoretically calculated value. This deviation is assumed to be mainly due to the limited accuracy with which the refractive indices of ethanol and methanol have been determined (using a conventional Abbe refractometer).

After tuning of the operating wavelength to the resonance wavelength of the converters, the fringe visibility of the polarimeter was measured to be 0.8 for both polarisations. Over several fabrication batches, the same value ($\pm$ 0.05) was found. From this it can be concluded that the tolerance in the design is sufficient to give a high fringe visibility and that the fabrication of the polarisation converters is well reproducable.

From measurements on devices upon several wafers, a resonance wavelength of 655.3 ± 4.3nm was found. The devices show an average deviation from the design resonance wavelength of $\Delta\lambda/\lambda$ of 0.007. The experimentally resonance wavelength is in good accordance with the theoretical value of 655 ± 3.7nm. However, as the resonance peak is only a few tenths of a nanometer wide, a tunable lightsource or tuning, for example thermo-optically, of the polarisation converters is necessary. As shown in [35], polarisation converters being a slight modification of the one presented here can be made that show a tuning range of 10 nm arising from a maximum temperature change of 70 K.

The measured crosstalks of the polarisation splitter were -27dB (TE) and -23dB (TM) for a TMI length of $1690\mu m$. The deviation in the crosstalk is most likely due to a small deviation in the ridge height. As a result, the effective index difference between the zeroth and first order mode in the TMI is slightly altered compared to the intended value.

The resolution of the sensor having one output only can be calculated using the experimental data presented above. The intensity dependant noise term, δ in equation 17, was found to be 0.005 and P_{min}/P_{in} was approximately 10^{-4}. With the measured fringe visibility of 0.8 and phase sensitivity of $1096 * 2\pi$, the refractive index resolution of the sensor at the optimum set point is $1 * 10^{-6}$.

A practical application of the second type of polarimeter (which does not even need any referencing) can be the discrimination between tap water and mineral water for controlling the nature of some restaurant output. In order to show the feasibility of such a sensor, the following experiment was performed. A bottle of tap water and mineral water were placed in a thermostate in order for both to have to same temperature. Next, using a flow injection system, both types of water were successively injected into a flow cell on top of the sensing window of the polarimeter. In figure 18, the result of the measurement is shown. A clear distinction of the output signal for tap water and mineral water can be seen, corresponding to a $\Delta n = 6.8 * 10^{-5}$.

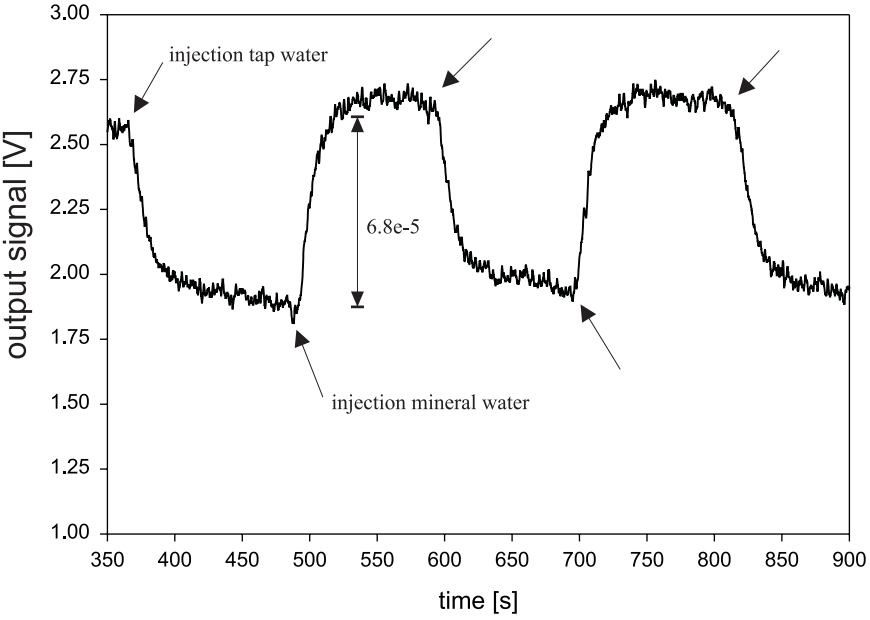

FIGURE 18. The output signal as a function of the type of water (tap or mineral). The arrows indicate the switching between a flow of mineral to a flow of tap water or vice versa. The difference in both output signals corresponds to $\Delta n = 6.8 * 10^{-5}$.

6. SUMMARY

The analysis, design, fabrication and performance of a fully integrated optical polarimeter have been presented. The small and compact polarimeter consists of two grating type polarisation converters, a sensing region, and whether a polarisation splitter or polariser. The complete system as well as the individual subfunctions have been analysed, optimised and characterised.

It is concluded that in case of one output signal only in general the best resolution will not be obtained in the quadrature points, but at ϕ values depending on the fringe visibility of the signals, the laser and detector noise. Also, in the case of surface sensing, it appears feasible to eliminate influences of refractive index changes in the environment.

A sensor, for homogeneous sensing of aqueous solutions has been optimised and realised in SiON technology. The experimentally obtained characteristics of all subfunctions agree well with the theoretical expectations. The sensitivity of the realised system differs only 6% from its theoretical value, which is most likely due to the experimental error in the determination of the refractive indices of the used calibration solutions. The realised structure shows a high fringe visibility of 0.8, showing accurate control of the coupling strength of the polarisation converters. Within the technological tolerances, $\pm$ 3.7 nm, the obtained resonance wavelength

of the polarisation converters agrees well with the designed wavelength. This means that in the absence of a tunable lightsource, a tuning mechanism may be required for tuning the polarisation converters to the operating wavelength of the lightsource, i.e. to maximise the fringe visibility and hence the resolution of the polarimeter. Recently, the possibilities of thermally tuned converters have been investigated, and it appears that the required tuning range is well feasible. The experimental data points to a resolution of $1 * 10^{-6}$ in the refractive index.

For characterisation purposes, for the devices described in this paper light was launched in and out of the waveguide using end-fire coupling. As the next step towards a completely packaged integrated optical sensor, currently devices are fabricated in which fiber chip couplers are integrated within the polarimeter. Also, the detectors can be incorporated within the IO-chip by adding the described mode selective coupling structures to the TMI based polarisation splitter. It can be expected, that by implementing an additional modulation function just as for the MZI [5], the resolution can be improved remarkably yet.

References

[1] R.E. Kunz. Miniature integrated optical modules for chemical and biochemical sensing. *Sensors and Actuators B*, 38-39:13–28, 1997.

[2] K. Chan, H. Ito, and H. Inaba. An optical fibre based gas sensor for remote absorption measurements of low-level methane gas in the near-infrared region. *Journal of Lightwave Technology*, 2:234–237, 1984.

[3] K. Seiler and W. Simon. Theoretical aspects of bulk optode memranes. *Analytica Chimica Acta*, 226:73–87, 1992.

[4] E.R. Cox and B.E. Jones. Fibre optic colour sensors based on fabry-perrot interferometry. *Proc. First international conference on optical fibre sensors, London*, 1993.

[5] R.G. Heideman and P.V. Lambeck. Remote opto-chemical sensing with extreme sensitivity: design, fabrication and performance of a pigtailed integrated optical phase modulated mach-zehnder interferometer system. *Sensors and Actuators B*, 61:100–127, 1999.

[6] A. Brandenburger. Differential refractometry by an integrated-optical young interferometer. *Sensors and Actuators B*, 39:266–71, 1997.

[7] C. Stamm and W. Lukosz. Integrated optical difference interferometer as immunosensor. *Sensors and Actuators B*, 31:203–207, 1996.

[8] S.S. Sarkisov, M.J. Curley, D. Diggs, H. Guo, R.D. Clark, and G. Adamovsky. Optical sensor based on single arm dual mode polymeric waveguide interferometer. *SPIE*, 3281:289–299, 1998.

[9] W. Lukosz. Integrated optical chemical and direct biochemical sensors. *Sensors and Actuators B*, 29:37–50, 1995.

[10] T.M. Koster and P.V. Lambeck. Bimodal evanescent field integrated optical sensors for the measurement of chemical concentrations. *Workshop Sensor Technology, Zeist, The Netherlands*, page 23, 2000.

[11] W. Lukosz, C. stamm, H.R. Moser, R. Ryf, and J. Dubendorfer. Difference interferometer with new phase-measurement method as integrated-optical refractometer, humidity sensor and biosensor. *Sensors and Actuators B*, 38-39:316–323, 1997.

[12] C. Fattinger, H. Koller, D. Schlatter, and P. Wehrli. The difference interferometer: a highly sensitive optical probe for quantification of molecule surface concentration. *Biosensors and Bioelectronics*, 8:99–107, 1993.

[13] A. Klotz, A. Brecht, and G. Gauglitz. Channel waveguide mode beat interferometer. *Sensors and Actuators B*, 38-39:310–315, 1997.

[14] C. Stamm and W. Lukosz. Integrated optical difference interferometer as biochemical sensor. *Sensors and Actuators B*, 18-19:183–187, 1994.
[15] T.M.Koster, N.E.Posthuma, and P.V.Lambeck. Fully integrated optical polarimeter. In *Proceedings Europt(r)ode V, 16-19 April 2000 Lyon, France*, 2000.
[16] C.K. Madsen and J.H. Zhao. *Optical filter design and analysis: a signal processing approach*. John Wiley and Sons, 1999.
[17] B.E. Little, C. Wu, and W.P. Huang. Synthesis of codirectional couplers with ultralow sidelobes and minimum bandwidth. *Optics Letters*, 20:1259–1261, 1995.
[18] T.J.Ikkink. *Interferometric interrogation concepts for integrated electro-optical sensor systems*. PhD thesis, University of Twente, Enschede, The Netherlands, 1998.
[19] edt. Eric Udd. *Fibre optic sensors*. John Wiley and Sons, New York.
[20] D. Cambell. Integrated multianalyte sensors. In *Proceedings Europt(r)ode V, 16-19 April 2000 Lyon, France*, 2000.
[21] F. Heismann. Integrated-optic polarisation transformer for reset-free endless polarisation control. *IEEE Journal of quantum electronics*, 25:1898–1906, 1989.
[22] H.Berends. Integrated optical filters, 1992.
[23] K.Worhoff, A.Driessen, P.V.Lambeck, L.T.H.Hilderink, P.W.C.Linders, and T.J.A.Popma. Plasma enhanced chemical vapour deposition silicon oxynitride optimised for application in integrated optics. *Sensors and Actuators A*, 74:9–12, 1999.
[24] O. Parriaux and G.J. Veldhuis. Normalised optimisation for the sensitivity optimisation of integrated optical evanescent-wave sensors. *Journal of Lightwave Technology*, 16:573–582, 1998.
[25] K. Tiefenthaler and W. Lukosz. Sensitivity of grating assisted couplers as integrated optical chemical sensors. *Journal of the Optical Society of Amerika B*, 6:209–220, 1989.
[26] T.M.Koster and P.V.Lambeck. Passive polarisation converter in SiON technology. *Submitted to Journal of Lightwave Technology*.
[27] 2d mode solver selene, bbv software bv, Enschede, The Netherlands.
[28] T.M.Koster and P.V.Lambeck. Fabrication tolerant passive polarisation converter realised in SiON technology. In *Proc. LEOS Benelux Chapter, 26 november, Gent, Belgium, 1998*, pages 117–120, 1998.
[29] T.M. Koster, V.E. Houtsma, P.V. Lambeck, D. Klunder, T.J.A. Popma, and J. Holleman. Mode selective coupling structures for monolithic integrated waveguide-detector systems. *SPIE*, 3630:9–18, 1999.
[30] T.M.Koster and P.V.Lambeck. Mode selective waveguide-detector couplers. *Submitted to Applied Optics*.
[31] F.Wehrmann, C.Harizi, H.Herrmann, U.Rust, W.Sohler, and S.Westenhofer. Integrated optical, wavelength selective acoustically tunable 2 x 2 switches (add-drop multiplexers) in $linbo_3$. *IEEE Journal of Selected Topics in Quantum Electronics*, 2:263–296, 1996.
[32] prometheus bpm and mask design, bbv software bv, Enschede, The Netherlands.
[33] R.G. Heideman and P.V. Lambeck. Simple and reusable fibre-to-chip interconnect with adjustable coupling efficiency. *SPIE*, 3099:238–247, 1997.
[34] J.T. Boyd, C.M. Chuang, and C.L. Chen. Fabrication of optical waveguide taper couplers utilising sio_2. *Applied Optics*, 18:506–509, 1979.
[35] T.M.Koster and P.V.Lambeck. Thermally tunable polarisation converter. *Submitted to Pure and Applied Optics*.

VII. Epilogue

In this final chapter, the main results will be summarised and a general evaluation of the research will be given.

1. Summary of the individual chapters

- **Chapter 1:** The research topics which have been investigated within this project have been stated, together with a brief introduction to chemo-optical sensors and (transduction layer based) absorptive evanescent field sensing. The relations between the different chapters in this thesis have been described.

- **Chapter 2:** A passive polarisation converter based on grating induced coupling between a TE_{00} and TM_{00} mode has been designed, fabricated and characterised. Principally, the converter structure can be realised in any type of transparent material system for each operational wavelength, as it is only a geometrical disturbance of the waveguide which does not depend on specific material properties. The coupling strength can be controlled by varying an etch step, without significantly altering the resonance wavelength. The structure has been optimised with respect to minimisation of its sensitivity to technological fluctuations. This optimisation resulted into a converter with a spread in the resonance wavelength of 3.7 nm (calculated), being in excellent agreement with the experimentally obtained spread of 4.3 nm. The fabrication process has been optimised, amongst others by using a double exposure technique, to obtain a large tolerance in the alignment of the different masks. The converter appears to be highly efficient; for a device length of 12 mm a conversion efficiency of 98% has been obtained with moderate functional losses of 3 dB/cm. An experimentally observed beat pattern could be explained to be due to a leaky mode which is captured by the grating. Due to the narrow FWHM of the conversion response, the converter offers the prospect of being applied as a wavelength selective element in WDM networks.
- **Chapter 3:** Due to technological uncertainties it could not be guaranteed that the resonance wavelength and thus the amount of conversion of a fabricated converter coincides with its intended value. A design has been presented with which this resonance wavelength can be thermo optically tuned to its intended value,requiring an actuation power of 214 mW and driving voltage of 1.25 V maximally. Experimental results on a demonstrator type device showed a 12 nm wavelength shift of the resonance wavelength for a 100 K temperature increase, being sufficient for appropriately tuning the converter.
- **Chapter 4:** Novel coupling structures both for mode selective and partial power transfer from a mode in a waveguide into a detector have been designed, fabricated and characterised. The structures are simple to fabricate, as they require only one additional core layer etching step. For avoiding the need of calibration, the final core layer thickness has to be accurately defined. The

experimentally determined partial power transfer is in excellent agreement with theory. The measured mode selectivity of the TM-coupling structure (-13 dB) was lower than calculated (-43 dB), which could be ascribed to scattering of TE light into the TM detectors as a result of one of the tapers being not perfectly adiabatic.

- **Chapter 5:** The analysis, the design, the fabrication and experimental results of a differential integrated optical absorptive sensing platform have been presented. Using two interrogation modes a system can be designed of which the output signal is nearly insensitive to environmental absorption changes, i.e. $\Delta S_{om} = 0$. All purely optical functionalities, a mode converter, sensing function and mode splitter have been implemented in one integrated optical circuit. An analysis, taking technological tolerances into account, showed that with the current state of technology, individual calibration of the sensors is required. Characterisation showed that the dual mode interrogation allows for a reduction of the sensitivity of the sensing structure to absorption changes in the environment with a factor 30. This reduction can be improved by a more careful control of the core layer thickness. The TMI-type mode splitter however appeared to be too sensitive to the tolerances of the present technology, and has to be replaced by the mode selective coupling functions described in chapter four. Unfortunately, due to the non availability of a monomolecular transduction layer, operational at 655 nm, the theoretical predicted sensor performance could not be verified experimentally.
- **Chapter 6:** The analysis, the design, the fabrication and experimental results of a fully integrated optical polarimeter have been presented. An outcome of the analysis is that in absence of referencing the best resolution will in general not be obtained in the quadrature points, but at ϕ values depending on the fringe visibility of the signals and the laser- and detector-noise. The theoretical and experimentally determined phase sensitivity of the sensor are in excellent agreement being $1169 * 2\pi$ and $1096 * 2\pi$, respectively. The complete sensor shows a high fringe visibility of 0.8. A practical application has been demonstrated, showing an experimental resolution of $5 * 10^{-6}$, which is of the same order as the calculated one at the optimum set point, $1 * 10^{-6}$.
- **Appendix:** As changes in the real part of the refractive index are related to changes in the imaginary part of the refractive index, here it has been shown that the polarimeter can also be used to interrogate transduction layers primarily designed for absorptive sensing.

2. Matching of the sensing platform - transduction layer

Within the Supra Molecular Engineering group, transduction layers have been developed which respond to several heavy metal ions. Two types of transduction layers have been synthesised; membranes, where the receptor molecules are embedded in a polymer matrix and a monomolecular transduction layer, where the receptors are directly bonded onto a surface, e.g. the core layer. Upon association,

both layers showed relevant changes in their absorption spectrum in the wavelength region around 530 nm, while in the 655 nm region no absorption changes occurred. In the final stage of the project, some preliminary experiments regarding the transduction layer-waveguide system have been performed. As the operating wavelength of the sensing platform (655 nm) did not coincide with the region in which the transduction layer shows relevant absorption changes, the latter were bonded on simpler waveguiding systems to at least show the feasibility of these kind of systems. The reproducible bonding of the transduction layers proved to be more difficult than expected. With the membranes, one prototype has been realised which showed a >20 dB attenuation for changes in the Pb^{2+} concentrations in the range $10^{-8} - 10^{-4}$. With the monomolecular transduction layers, no results were obtained.
The here presented absorptive sensing platform was designed for a wavelength of 655 nm, but can easily be redesigned for an operating wavelength of 530 nm to match the absorptive transduction layers. In figure 1, the physical design for this wavelength is given.

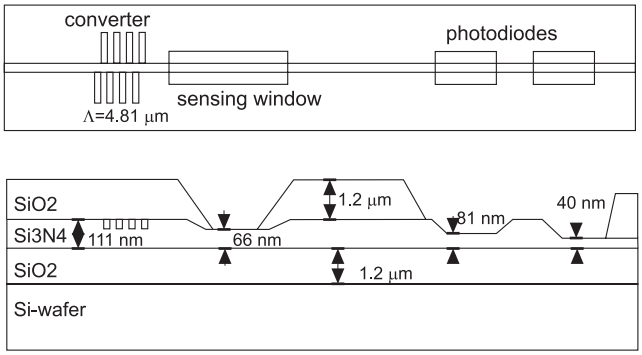

FIGURE 1. Physical design of the differential absorptive sensing platform for an operating wavelength of 530 nm.

3. General evaluation

Reviewing the research project, it is clear that the concept of dual mode interrogation introduced here offers several clear advantages over the single mode interrogation method. First, when using monomolecular transduction layers, the influence of disturbing changes of the optical properties of the environment can be reduced remarkably (a factor 30 has been experimentally shown, but higher factors are expected to be feasible). Second, by dividing the output signals of the individual modes, the influence of laser noise on the output signal can be drastically reduced.

Using a polarisation converter, a well controlled power ratio of the TE_{00} and TM_{00} interrogation modes is obtained. However, due to the strong wavelength dependence of this converter a special tuning facility has to be implemented. Alternatives to this

mode converter, and therefore other possible mode couples have to be investigated. An alternative might be the $TM_{00} - TM_{10}$ couple, generated by a thickness step in the core layer from a launched TM_{00} mode [1].

During the project two novel functionalities have been developed, an asymmetrical grating based tunable polarisation converter and structures for coupling mode selectively optical power from the waveguide to a monolithically integrated Si-detector.

One of the aims of the project has been to implement all the required functionalities in the integrated optical system. This should result into a sensor chip, receiving its optical input power from a fibre and delivering the desired information within the electrical domain. All functionalities for such a system, both an absorptive an a refractive sensor, have been made available, and most of them have been integrated together. So, full integration, although not obtained due to the limited time available, is made feasible.

In the design process tolerance analysis has been given a prominent position. This was made possible by having available a well developed technology, for which most uncertainties have been well established. In addition, that analysis shows which technological uncertainties dominates the functional performance, and thus which one has to be diminished preferentially. Also, the analysis enables to predict the reproducibility, and so proves to be an important guide for determining whether for a given application calibration of individual sensors should be needed or not.

From a qualitative comparison between the polarimeter and the Mach Zehnder interferometer the following remarks can be made. When implemented in the SiON material system, the sensitivity of both types of sensors are of the same order, 0.15 (polarimeter) and 0.20 (Mach Zehnder, TE polarised interrogation signal). The sensitivity of the polarimeter can be enlarged by having one mode to be insensitive to the measurand [2], thereby effectively creating a vertical Mach Zehnder structure. A strong advantage of the polarimeter is in case of surface sensing, for which it can be designed such that the output signal is insensitive to changes in the environment without requiring difficult multiple patterning of active and passivated transduction layers. Also, temperature differences between the signal and reference branch, although strongly reduced in a well designed Mach Zehnder [3], are though to be one of the sources of error limiting its resolution. In a polarimeter the signal and reference signal propagate through the same waveguide, and this temperature difference is not existing here. A disadvantage of the polarimeter developed here is its limitation to one wavelength only, a limitation absent in a Mach Zehnder provided with Y-junctions. Possibly, the generality of the polarimeter platform can be enlarged by introducing another mode combination [1]. Also, the fabrication of the polarisation converters requires an additional technological step.

When comparing the here presented polarimeter to polarimetric devices previously reported in literature, it can be concluded that due to the integration of all optical functionalities a more robust, more stable and more compact sensor is obtained

which allows for operation under non laboratory conditions and the implementation in fibre sensing networks.

Comparing the here presented integrated optical absorptive sensing platform to fibre based absorptive sensors, where absorptive transduction layers have been positioned at the fibre tips [4], the advantages are obvious. The integrated optical approach allows for higher sensitivities and higher resolutions by using evanescent field sensing, while the integration with optical functions also results in more robust and more compact systems. Compared to the other integrated optical absorptive sensors reported upon in literature [5], where only a single straight waveguide in which the sensing region has been implemented is discusses, likewise the higher level of integration of functionalities results in a more robust and compact sensor which allows for operation under non laboratory conditions and the implementation in fibre sensing networks. Also, the dual mode interrogation results in a stronger reduction of the lightsource noise and , in the case of surface sensing, the possibility of elimination of the effect of changes in the environment on the output signal.

From the analysis and the experimental results some key challenges to technology can be defined:

- Increasing the reproducibility of the PECVD process for depositing SiON layers, primarily for decreasing of the uncertainty in the refractive index.
- Increasing the reproducibility of the wet-etching steps.

References

[1] M. Lohmeyer, T.M.Koster, and P.V.Lambeck. Integrated optical polariser based on the cross strip interferometer configuration. In *Proc. LEOS Benelux Chapter, 30 oktober, Delft, The Netherlands, 2000*, 2000.

[2] Z.M. Qi, K. Itoh, M. Murabayashi, and H. Yanagi. A composite optical waveguide-based polarimetric interferometer for chemical and biological sensing applications. *IEEE Journal of Lightwave Technology*, 18:1106–1110, 2000.

[3] R.G. Heideman and P.V. Lambeck. Remote opto-chemical sensing with extreme sensitivity: design, fabrication and performance of a pigtailed integrated optical phase modulated mach-zehnder interferometer system. *Sensors and Actuators B*, 61:100–127, 1999.

[4] edt. O.S. Wolfbeis. *Fibre optic chemical sensors and biosensors*. CRC press.

[5] R. Klein and E. Voges. Integrated-optic ammonia sensor. *Fresen J. Anal Chem*, 160:513–517, 1994.

Appendix: Absorption induced real refractive index changes

Changes in the imaginary ($\Delta n"(C,\lambda)$)and real part ($\Delta n'(C,\lambda)$)of the refractive index are related to each other as described by the Kramers-Kronig equation [1]. As a result, transduction layers with receptors developed for absorptive sensors can also be interrogated using refractometers. In this appendix, we will study the real refractive index changes resulting from shifts in the absorbance spectrum of a transduction layer.

1. K-K relations and Lorentzian solution

For Lorentzian absorption bands, a solution of the Kramers Kronig relation [1] for $\Delta n"(C,\lambda)$ and $\Delta n'(C,\lambda)$ in terms of the wavelength λ is

$$\Delta n"(C,\lambda) = \frac{A(C)B}{\left(\frac{\lambda-\lambda_0}{\lambda\lambda_0}\right)^2 + B^2}, \tag{1}$$

and

$$\Delta n'(C,\lambda) = \frac{A(C)\frac{\lambda-\lambda_0}{\lambda\lambda_0}}{\left(\frac{\lambda-\lambda_0}{\lambda\lambda_0}\right)^2 + B^2}, \tag{2}$$

with B a constant and $A(C)$ an amplitude term depending on the measurand C. In figure 1 $\Delta n"(C,\lambda)$ and $\Delta n'(C,\lambda)$ are shown.

2. Estimation of the refractive index changes

Generally, the transition from the empty to the filled receptor gives rise to a change in the optical absorption. Using a Lorentzian approximation of the absorption spectra of a receptor described in [2], we will give an estimation of the maximum refractive index change which is achieved when all empty receptors are filled (or vise versa). Here we shall assume that the effects of generally unknown absorption changes in the UV region can be neglected.
In figure 2, the Lorentzian approximations of the absorbance spectra of the empty and filled receptor are shown. The spectra have been normalised to an absorbance equal to 1 at the resonance wavelength of the empty receptor, 480 nm. For this receptor, in figure 3, the absolute value of $\Delta n'(C,\lambda)$ is plotted. Due to the small bandshift and small changes in the extinction coefficients and FWHM of both absorption bands, the resulting $\Delta n'(C,\lambda)$ is small; for a wavelength of 850 nm, $\Delta n'(C,850nm) = 6 * 10^{-7}$. As for a given wavelength $\Delta n'(C)$ is linear with the absorption, a higher absorbance will result in a higher $\Delta n'(C,\lambda)$. For example, for

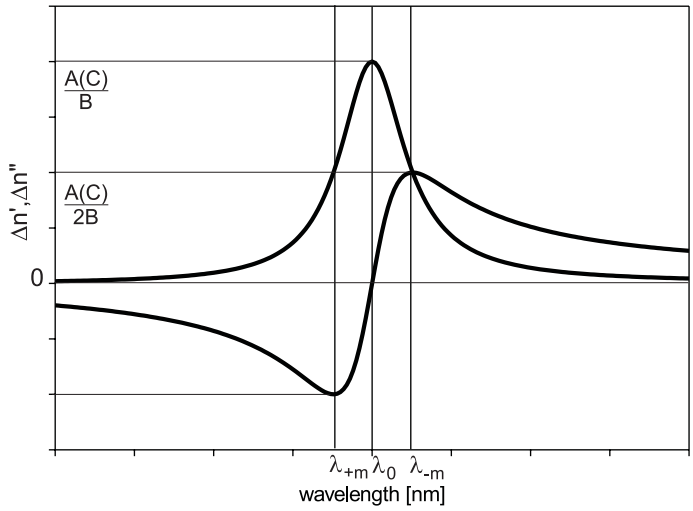

FIGURE 1. Graph of $\Delta n^{"}(C,\lambda)$ and $\Delta n^{'}(C,\lambda)$ versus the wavelength showing some characteristics of these solutions.

an empty receptor absorbance of 100 at a wavelength of 480 nm when all receptors are in their empty state, the maximum refractive index change is $6*10^{-5}$. However,

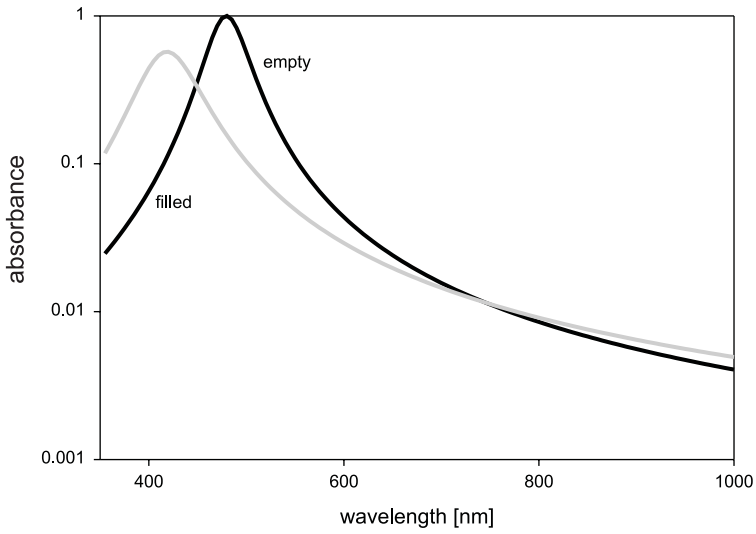

FIGURE 2. Lorentzian approximations of the absorbance spectra of the empty and filled receptor as described in [2].

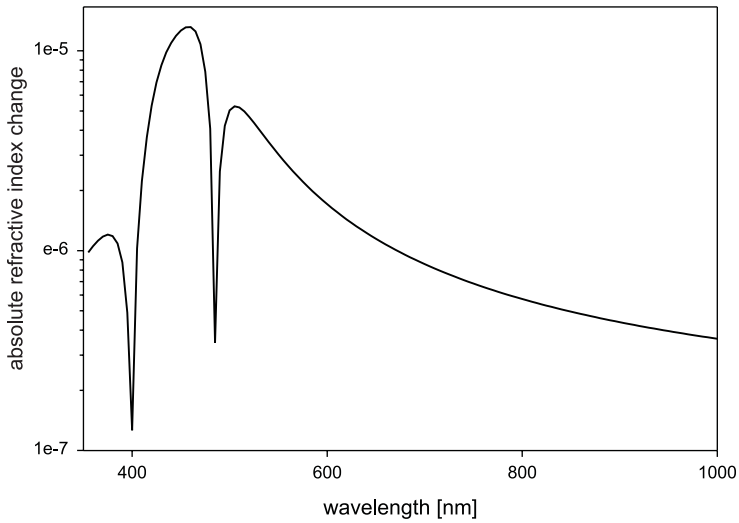

FIGURE 3. Absolute value of the refractive index change when all receptors go from the empty state to the filled state (or vise versa).

the absorbance at this wavelength will now vary between 0.68 and 0.76, which has to be taken into account when performing refractometric measurements.

3. SUMMARY

Refractometric sensing of absorptive transduction layers is possible as changes in the real part of the refractive index are related to changes in the imaginary part. Preferable, there should be a large difference between the absorbance spectrum of the empty and filled receptor; and preferentially, only one of the states should show an (narrow band) optical absorbance in the relevant wavelength region. However, generally, both the empty and filled state show an optical absorbance which results in, when going from one state to another, a lower $\Delta n^{'}(C,\lambda)$. Using a Lorentzian approximation of the absorption spectrum of a receptor described in [2], the corresponding maximum $\Delta n^{'}(C,\lambda)$ has been calculated. This spectrum scales linearly with the amount of receptors and hence, by increasing the receptor concentration, $\Delta n^{'}(C,\lambda)$ can be increased. The changes in the real part of the refractive index of that given receptor are of the order $10^{-7} - 10^{-5}$, depending on the concentration of the receptor molecules. Therefore, a highly sensitive refractometer is required for an accurate determination of C. However, as a tradeoff, for large receptor concentrations, the measurand induced absorbance change at the refractometric operating wavelength has also be taken into account, making an interpretation of the experimental data less straightforward.

References

1. J.R. Reitz, F.J. Milford, and R.W. Christy, *Foundations of electromagnetic theory*, Addison-Wesley.
2. N. van der Veen, *Optical sensing of metal ions with calix[4]arene chromoionophores*, Ph.D. thesis, University of Twente, Enschede, The Netherlands, 2000.

Samenvatting

Deze samenvatting is een bewerking van de samenvatting in hoofdstuk 7 ('Epilogue').

Het werk beschreven in dit proefschrift kan als volgt worden samengevat:

- **Hoofstuk 1 : 'Introduction'** De doelstellingen van het onderzoek worden gegeven, en chemo-optische sensoren worden geintroduceerd. Uit een analyse van evanescente-veld-absorptie-metingen met behulp van transductielagen worden vanuit het optisch meetsysteem eisen aan de transductielaag afgeleid. Afsluitend wordt de samenhang tussen de verschillende hoofdstukken gegeven.
- **Hoofdstuk 2 : 'Passive polarisation converter in SiON technology'** Bij de sensoren beschreven in de hoofdstukken 5 en 6 wordt, vanwege het meet principe en om verstoringen op het uitgangssignaal te onderdrukken, gemeten met twee modi. Deze modi worden verkregen met behulp van een passieve polarisatie converter, die 50% van het vermogen van een inkomende TE mode naar de TM mode koppeld. In dit hoofdstuk wordt het ontwerp, de fabricage en de karakerisatie van de converter beschreven, waarbij een asymmetrische traliestructuur voor de energie overdracht tussen de TE en TM mode zorgt. Deze overdracht berust alleen op een geometrische verstoring van de golfgeleider dwarsdoorsnede. Daarom kan de converter voor iedere golflengte ontworpen en in ieder transparant materiaalsysteem gerealiseerd worden. Bij de optimalisatie van het ontwerp is de gevoelligheid voor technologische onzekerheden geminimaliseerd. Anderzijds zijn onzekerheden in kritische stappen omlaag gebracht. Zo vertoond het fabricageprocess een hoge tolerantie voor het onderling uitrichten van de diverse maskers, wat onder andere bereikt wordt door het gebruik van een dubbele belichtingsstap. De koppelsterkte kan technologisch ingesteld worden door de tijdsduur van een etsstap. De invloed van deze etsstap op de resonantie golflengte is verwaarloosbaar. Uiteindelijk zijn de volgende karakteristieken verkregen: een experimenteel gemeten spreiding in de resonantie golflengte (4.3 nm) die goed overeenkomt met de berekende spreiding (3.7 nm), een hoge efficientie: voor een device met een lengte van 12 mm is een conversie van 98% gemeten. De functionele verliezen zijn 3 dB/cm.

  Een experimenteel waargenomen interferentiepatroon kon toegeschreven worden aan interferentie van de geleide mode met een stralende mode die gevangen is in de traliestructuur. Door het smalbandig conversie versus golflengte gedrag biedt de converter eveneens de mogelijkheid om als golflengte selectief element in een WDM netwerk toegepast te worden.
- **Hoofdstuk 3 : 'Thermally tunable polarisation converter'** Door technologische onzekerheden kan het behalen van de beoogde waarde van de resonantiegolflengte en daarmee verbonden de hoeveelheid modeconversie niet gegarandeerd worden. In dit hoofdstuk wordt een ontwerp gepresenteerd

waarin de resonantie golflengte met behulp van thermo-optisch verstemmen op z'n ontworpen waarde ingesteld kan worden. Hiervoor is maximaal een vermogen van 214 mW nodig bij een spanning van 1.25 V. Experimentele resultaten verkregen aan een demonstrator laten zien dat als gevolg van een temperatuursverhoging van 100 graden de resonantie golflengte 12 nm verschoven is. Gezien de experimentele spreiding van 4.3 nm is dit ruimschoots voldoende.

- **Hoofdstuk 4 : 'Mode selectieve waveguide-detector couplers'** Voor sommige toepassingen is het nodig om het vermogen in de TE en TM modi onafhankelijk van elkaar te meten. Dit kan gedaan worden met koppelfuncties die het licht vanuit een golfgeleider in fotodiodes koppelen die monolithisch met het golfgeleider circuit geintegreerd zijn. Een nieuw type van dergelijke koppelfuncties, voor mode selectief en/of gedeeltelijke vermogenskoppeling, is ontworpen, gefabriceerd en gekarakteriseerd. De structuren zijn eenvoudig te fabriceren; er is maar een extra proces stap nodig. Bij voldoende bekende dikte van de core laag vervalt de noodzaak tot calibratie van het systeem. De experimenteel gevonden waardes voor het gedeeltelijk overgekoppelde vermogen komen zeer goed overeen met de theoretisch berekende. De gemeten mode selectiviteit van de voor TM gepolariseerd licht ontworpen koppelstructuur (-13 dB) is lager dan berekend (-43 dB), wat toegeschreven kan worden aan verstrooiing van TE gepolariseerd licht in de TM detectoren als gevolg van het niet goed adiabatisch zijn van een van de tapers.

- **Hoofdstuk 5 : 'An integrated optical platform for absorptive sensing of chemical concentrations using chemo-optical monolayers'** Bij evanescente veld metingen in combinatie met zeer dunne (monomoleculaire) transductielagen verlaagt de penetratie van het evanescente veld in de sample vloeistof de nauwkeurigheid van de sensor. In dit hoofdstuk wordt de analyse, het ontwerp, de fabricage en het experimenteel bepaalde gedrag van een differentieel geintegreerde optische absorptie sensor gepresenteerd. Door een transductielaag af te tasten met twee modi kan een sensor ontworpen worden waarvan het uitgangssignaal ongevoellig is voor een eventuele absorptieverandering van de sample vloeistof. Alle puur optische functies, zijnde een mode converter, sensor functie en een mode splitter, zijn geintegreerd in een enkel optisch circuit. Een analyse, waarbij de technologische toleranties in ogenschouw zijn genomen, laat zien dat met de huidige staat van de technologie individuele calibratie van de sensoren noodzakelijk is. Metingen laten zien dat door deze aftasting met twee modi de gevoelligheid van het uitgangssignaal voor absorptie in de omgeving met een factor 30 gereduceerd kan worden. Deze reductie kan nog verbeterd worden door een betere controle van de core laagdikte. De toegepaste TMI mode splitter bleek te gevoellig voor de onzekerheden van de huidige technologie, en zal vervangen moeten worden door de mode selectieve koppelstructuren zoals beschreven in hoofstuk 4. Helaas kon, doordat er geen transductie laag beschikbaar was die absorptieveranderingen vertoonde bij de golflengte waarvoor het device ontworpen was (655 nm),

de theoretisch voorspelde sensor performance niet experimenteel geverifieerd worden.

- **Hoofdstuk 6 : 'Fully integrated optical polarimeter'** Een polarimeter is een refractometrische sensor, waarbij de uitgangssignalen een functie zijn van het door de measurand veroorzaakte faseverschil tussen een TE en een TM mode. De analyse, het ontwerp, de fabricage en experimentele resultaten van een volledig geintegreerde polarimeter worden gepresenteerd. Uit de analyse bleek dat, voor een systeem zonder intensiteits referentie signaal, de beste resolutie in het algemeen niet in het quadratuur punt bereikt wordt, maar voor een instelpunt dat een functie is van de fringe visibility en de laser -en detector ruis. Met een gemeten afwijking van maar 6% zijn de theoretisch en experimenteel bepaalde fase gevoelligheid voor brekingsindex veranderingen in water in goede overeenstemming. De fringe visibility van de complete sensor is hoog: 0.8. Een practische toepassing van het gehele systeem is gedemonstreerd, met een experimentele bepaalde resolutie van $5 * 10^{-6}$. Deze is van dezelfde grootteorde als de resolutie in het optimale instelpunt ($1 * 10^{-6}$).
- **Hoofdstuk 7 : 'Epilogue'** Een samenvatting van het onderzoek gepresenteerd in dit proefschrift, alsmede een algemene evaluatie zijn gegeven.
- **Appendix : 'Absorption induced real refraction index changes'** Veranderingen in het reele gedeelte van de brekingsindex zijn gerelateerd aan veranderingen in het imaginaire gedeelte van de brekingsindex. Hierdoor kunnen transductielagen die primair ontwikkeld zijn voor absorptie sensoren ook uitgelezen worden door refractieve sensoren zoals de polarimeter. Voor een bepaalde transductielaag is een afschatting van de grootte orde van de veranderingen van het reele gedeelte van de brekingsindex gegeven.

Thanx

Morgen het boekje naar de drukker, en dat kan natuurlijk niet zonder dat er een dankwoord in staat (de eerste en meest gelezen bladzijde van ieder proefschrift). Kom't ie:

Theo Popma, de promotor. Paul Lambeck, gever van veel vrijheid de eerste drie en een half jaar en veel (nuttig) commentaar het laatste half jaar. STW/NWO voor de centjes. Niels van der Veen, de chemical-wizzard verantwoordelijk voor de transductie laagjes. De mensen met gouden handjes die 1e klas devices uit het cleanroom toverden, meetopstellingen automatiseerden en allerlei vage chemische oplossingen aanmengden: Peter Linders, Toon Andringa, Iwan Heskamp en Meindert Dijkstra. De studenten die het aandurfden om onder mijn 'dagelijkse' begeleiding hun afstudeerwerk te doen: Dion Klunder en Niels Posthuma. Vincent Houtsma en Ronald Dekker voor het diode-gebeuren. Anton Hollink en Henk van Wolferen, voor het oplossen van technische problemen, AEX problemen, harde schijf problemen etc. De smurfen Johnny, Gerard, Stan, Jan, Samantha en Peter voor het draaiende houden van alle apperatuur in het cleanroom. Huib en Arie voor het flitsen van heeeeeeeeeeeeeeeeeeel veel maskers. Simone, Ingrid, Jose en Dirk voor alle regel, papier en financiele werk. Lucie voor de mooie nitride en oxide laagjes. Alle mensen met wie ik de afgelopen jaren de verschillende kamers gedeeld heb: Han (tralie goeroe en oud afstudeer begeleider), Folkert (vul maar in), Erik Radius (de Amsterdam-Enschede vergelijkingen), Peter Bollerman (het optellen en delen en zingen en zo), Harm (de (virtuele) pool sessies en andere sessies), Marcel (de vagere gesprekken), Sulur (de vriendelijke groet iedere morgen), Iwan (tja,... maar wel positief) en de laatste paar weken natuurlijk Geert (your personal latex companion) en Wico (inmiddels Atr goeroe). In de buurt van de kamer zaten Rene de Ridder (fietsbikkel, goed voor motiverende opmerkingen en geen 'Rage against the Machine' liefhebber) en Hugo 'blauw' Hoekstra (zie verder Rene). Voor de live smartlappen, het oprichten van het Zombie gebeuren en het 'voorbereidend' werk op sensorgebied: Rene Heideman. De fietsrondjes in Nederland, Belgie en Frankrijk en oprichter van de vrijdagmiddagborrel (nu staat dat tenminste zwart op wit): Erwin Rikkers. Iemand met wie het prettig samenwerken, patenten schrijven en conferentie's bezoeken is, is natuurlijk Gert Veldhuis. Freek Blom was nooit te beroerd voor een Hexen/Raid sessie of ingenieuze devices te verzinnen en te realiseren. Sami Musa, voor de introductie in de Afrikaanse literatuur. The French connection, Gregory Pandraud. Next-in-line, '40-in-3.40h-en-een-beetje-hoofdpijn-de-volgende-dag' Remco Stoffer, Chris (de goede opmerking op de goede tijd) Roeloffzen, Dion (de foute opmerking op de goede tijd, houden zo) Klunder, Joris 'Frisbee! komt ie..... oh, sorry, mis' van Lith, Israel 'ola, que tal?, muy bien, Buenos!' Rabelo. De ongeveer 30 studenten die de afgelopen 4 jaar in de groep hebben gezeten en voor de goede sfeer zorgden. Melis Jan voor het veroorzaken van veel spierpijn en oplossen van cleanroomprobleempjes. De mensen van die 'andere' vakgroep: Erwin Berenschot (9-6) en Meint de Boer (54-11) voor technologische raad enzo, Han Gardeniers (reisleider in Limburg) Pino (toch een beetje optisch) de micromossels

Stefan (wit met rode stipjes), Edwin, Willem en Jasper. Voor klimfestijnen in oude Belgische kertorens en hoge Britse bergen, Twan Bearda. De korte en lage fietrondjes zouden een stuk ongezelliger zijn zonder een Magnum, een Wilbert en (on)zinnige gesprekken. 'Thuiszorg Twente'. Hoe ik ben en wat ik doe schijnt volgens de laatste theorieen zijn oorsprong te vinden in een combinatie van de genen en de opvoeding, waarvoor in beide gevallen mijn ouders verantwoordelijk waren; Veel dank.

't is nu donker buiten, en ik hou het voor gezien.....

C'ya,

Ton.

Bibliography

G.J.Veldhuis, C.Gui, T.Nauta, T.M.Koster, J.W.Berenschot, P.V.Lambeck, J.G.E. Gardeniers, M. Elwenspoek, *Mechano-optical waveguide on-off intensity modulator*, Optics Letters, vol.23, no.19, pp.1532-4.

C.Gui, G.J.Veldhuis, T.M.Koster, P.V.Lambeck, J.W.Berenschot, J.G.E. Gardeniers, M. Elwenspoek, *Nanomechanical optical devices fabricated with aligned wafer bonding*, Proc. MEMS 98, New York, USA, pp.482-7.

T.M.Koster, P.V.Lambeck, *Realisation and characterisation of a fabrication tolerant passive polarisation converter in SiON technology*, Proc. LEOS Benelux Chapter, 26 november, Gent, Belgium, 1998, pp.117-120.

C.Gui, G.J.Veldhuis, T.M.Koster, P.V.Lambeck, J.W.Berenschot, J.G.E. Gardeniers, M. Elwenspoek, *Fabrication of nanomechanical optical devices with aligned wafer bonding*, Microsystem-Technologies, vol.5, no.3, 1999, p.138-43.

T.M.Koster, V.E.Houtsma, P.V.Lambeck, D.J.W.Klunder, T.J.A.Popma, J. Holleman, *Mode selective coupling structures for monolithic integrated waveguide-detector systems*, Proc. SPIE vol. 3630, Photonics West conference, 22-29 january, 1999, San Jose, USA, pp.9-18.

T.M.Koster, P.V.Lambeck, *Bimodal evanescent field integrated optical sensors for the measurement of chemical concentrations*, National Sensor Workshop, 29-30 March 2000, Zeist, the Netherlands.

T.M.Koster, N.Posthuma, P.V.Lambeck, *Fully integrated optical polarimeter*, Europt(r)ode V, 16-19 April 2000 Lyon, France. (Winner of the Best Poster Award)

G. Pandraud, T.M.Koster, C. Gui, M. Dijkstra, P.V Lambeck, *Evanescent wave sensing: new features for detection in small volumes*, Sensors and Actuators A, vol. 85, 2000, pp. 158-162.

T.M.Koster, P.V. Lambeck, *Thermally tunable polarisation converter for WDM filtering applications*, Accepted for oral presentation at LEOS 2000, Puerto Rico, 11-16 November, 2000

T.M.Koster, P.V.Lambeck *Polarimeter sensor for the determination of chemical concentrations*, Accepted for oral presentation at the LEOS Benelux Chapter conference, 30 October 2000, Delft, The Netherlands.

M. Lohmeyer, T.M.Koster, P.V.Lambeck *Integrated optical polariser based on the cross strip interferometer configuration*, Accepted for poster presentation at the LEOS Benelux Chapter conference, 30 October 2000, Delft, The Netherlands.

T.M.Koster, P.V.Lambeck, *Passive polarisation converter in SiON technology*, submitted to Journal of Lightwave Technology.

T.M.Koster, N.E.Posthuma, V.E.Houtsma, R.Dekker, P.V.Lambeck, *Mode selective waveguide-detector couplers*, submitted to Applied Optics.

T.M.Koster, P.V.Lambeck, *Integrated optical platform for absorptive sensing of chemical concentrations using chemo-optical monolayers*, to be submitted to Measurement, science and technology.

T.M.Koster, P.V.Lambeck, *Fully integrated optical polarimeter*, submitted to Journal of Lightwave Technology.